UNIVERSITY OF CALIFORNIA SAN DIEGO

Neuron navigator 1: a regulator of early neural morphogenesis via the cytoskeleton, the plasma membrane, and endocytosis.

A Dissertation submitted in partial satisfaction of the requirements
for the degree Doctor of Philosophy

in

Biology

by

Regina Powers

Committee in charge:

Professor Shelley Halpain, Chair
Professor Susan Ackerman
Professor Robert Hevner
Professor Karen Oegema
Professor Samara Reck-Peterson

2022

The Dissertation of Regin Powers is approved, and it is acceptable in quality and form for publication on microfilm and electronically.

University of California San Diego

2022

DEDICATION

For you Mom, thank you for everything.

TABLE OF CONTENTS

LIST OF FIGURES

LIST OF TABLES

LIST OF ABBREVIATIONS

+TIP(s) - plus-end tracking protein(s)

AAA - AAA+ ATPase

Abi-1 - abelson kinase interactor 1

ASD - Autism Spectrum Disorder

atRA - all *trans* retinoic acid

BDNF - brain derived neurotrophic factor

CC - coiled coil

CH - calponin homology

DIV - days *in vitro*

DTC - distal tip cell

EB1/3 - end binding protein 1/3

F-actin - filamentous actin

FRAP - fluorescence recovery after photobleaching

GEF - guanine nucleotide exchange factor

MTs - microtubules

Nav1/2/3 - neuron navigator 1/2/3

PI3K - phosphatidylinositol 3-kinase

ACKNOWLEDGEMENTS

Thank you to Shelley Halpain and Barbara Calabrese for guidance and support. Thank you to my committee members for your feedback throughout graduate school. Thank you to past and present Halpain lab members. Thank you to my friends here in San Diego and back in Pennsylvania for your friendship. Thank you to my partner, John, and my family, Mom and Rachel, for your unwavering support and love.

Chapter 1, in part, is currently being prepared for submission for publication of the material. Powers, Regina; Hevner, Robert; Halpain, Shelley. “The Neuron Navigators” (working title). The dissertation author was the primary researcher and author of this material.

Chapter 1, in part, is currently being prepared for submission for publication of the material. Powers, Regina; Halpain, Shelley. “Macropinocytosis in the nervous system” (working title). The dissertation author was the primary researcher and author of this material.

Chapter 2, in full, is a reprint of the material as it appears in Molecular Biology of the Cell 2022. Powers, Regina; Daza, Ray, Koehler, Alanna; Courchet, Julian; Calabrese, Barbara, Halpain, Shelley. The dissertation author was the primary investigator and author of this paper.

Chapter 3, in part, is a reprint of the material as it appears in Molecular Biology of the Cell 2022. Powers, Regina; Daza, Ray, Koehler, Alanna; Courchet, Julian; Calabrese, Barbara, Halpain, Shelley; it is also, in part, is currently being prepared for submission for publication of the material. Powers, Regina; Hevner, Robert; Halpain, Shelley. The dissertation author was the primary investigator and author of this paper.

VITA

2015 Bachelor of Science in Biology, Ursinus College

2022 Doctor of Philosophy in Biology, University of California San Diego

ABSTRACT OF THE DISSERTATION

Neuron navigator 1: a regulator of early neural morphogenesis via the cytoskeleton, the plasma membrane, and endocytosis.

by

Regina Powers

Doctor of Philosophy in Biology

University of California San Diego, 2022

Professor Shelley Halpain, Chair

Neuron Navigator 1 (Nav1) is a cytoskeleton-associated protein expressed during brain development that is necessary for proper neuritogenesis, but the underlying mechanisms are poorly understood. Here we show that Nav1 is present in elongating axon tracts during mouse brain embryogenesis. We found that depletion of Nav1 in cultured neurons disrupts growth cone morphology and neurotrophin-stimulated neuritogenesis. In addition to regulating both F-actin and microtubule properties, Nav1 promotes actin-rich membrane ruffles in the growth cone, and promotes macropinocytosis at those membrane ruffles,

including internalization of the TrkB receptor for the neurotrophin BDNF (brain-derived neurotropic factor). Growth cone macropinocytosis is important for downstream signaling, neurite targeting, and membrane recycling, implicating Nav1 in one or more of these processes. Depletion of Nav1 also induces transient membrane blebbing via disruption of signaling in the Rho GTPase signaling pathway, supporting the novel role of Nav1 in dynamic actin-based membrane regulation at the cell periphery. These data demonstrate that Nav1 works at the interface of microtubules, actin, and plasma membrane to organize the cell periphery and promote uptake of growth and guidance cues to facilitate neural morphogenesis during development.

CHAPTER 1

THE NEURON NAVIGATORS

Introduction

During organismal development, myriad cell types continually integrate extra- and intracellular cues to form functional organs. These cues determine the destination of migrating cells, the morphology of differentiating cells, and the formation of networks, such as the synaptic network of the brain. While nearly all cell types undergo morphogenesis during development, the transformation of spherical neural progenitor cells into polarized, functionally integrated neurons is especially complex and extensive, and critical to neural circuit function. This process includes symmetry breaking for polarization, neurite initiation and elongation, and the formation of the axonal growth cone -- a cytoskeleton-rich structure that directs the axon to its targets. The cytoskeleton, which is comprised of microtubules (MTs), intermediate filaments, and actin filaments, undergoes major morphological rearrangements throughout these events, particularly at the cell periphery. MTs and actin filaments and their interactions have been a major focus of study in the context of early neuronal morphogenesis. During early development neurons respond to attractive and repulsive guidance cues to direct their migration and outgrowth, and cytoskeleton-associated proteins are important signal integrators and regulators of these processes.

Dysregulation of the cytoskeleton underlies many disorders of human neurodevelopment[1-4]. Mutations in multiple tubulin genes have been implicated in a group of neurodevelopmental disorders termed “tubulinopathies”[5, 6]. Moreover, mutations in the microtubule associated proteins, Lis1 and DCX, cause cortical malformations resulting in lissencephaly and heterotopia, respectively, due to aberrant microtubule-dependent neuronal

migration[4, 7]. Actin dysregulation through disruption of RhoGTPases, like Rac1/3 and CDC42, has been associated with autism spectrum disorder (ASD) and intellectual disability. Mutations in SHANK3, a post-synaptic scaffolding protein that links glutamate receptors to the actin cytoskeleton, causes Phelan-McDermid Syndrome, a neurodevelopmental disorder that is co-morbid with ASD and intellectual disability[8, 9]. Additionally, mutations in guidance cues can result in neurodevelopmental disorders via their impact on cytoskeleton-mediated events. For example, *reelin* mutations are associated with various neurodevelopmental conditions, including lissencephaly and ASD[10-12]. Reelin is an extra-cellular matrix molecule that influences actin dynamics via the actin regulating protein cofilin[13], and interacts with the Lis1 signaling pathway via induction of phosphorylation of Dab1, a Lis1 binding partner[14] Loss of reelin results in aberrant neural migration and neurite outgrowth, demonstrating the influence that cytoskeletal dynamics play in early neuron development[13, 15]. Finally, proteins that regulate cytoskeletal function have also been implicated in human neurodevelopmental disorders. For example, the regulatory/adaptor molecules 14-3-3ε, encoded by the YWHAE gene, and the protein Crk, encoded by the CRK gene, function downstream of reelin and regulate Lis1 function in neuronal migration[14]. These genes occur within the same 17p13.3 chromosomal region as the Lis1/PAFAH1B1 that is frequently subject to microdeletion or microduplication events that are causative for the neurodevelopmental disorder Miller-Dieker Syndrome, in which patients exhibit severe lissencephaly[16-18]. Another example is the Rho family guanine nucleotide exchange factor Trio, which controls the actin-regulation activities of Rac1 and Cdc42[19, 20] and is a risk gene for ASD[21].

The growth cone is a specialized cytoskeleton-rich structure that responds to extracellular cues and directs neurite outgrowth. The growth cone has a stereotypical cytoskeletal arrangement

that can be divided into three domains: the central domain is filled with microtubules, the peripheral domain is composed of F-actin that form filopodia and lamellipodia, and the transition zone is in between the central and peripheral domains where actin arcs and actin membrane ruffles form and where F-actin and microtubules can interact[22-24]. The growth cone also contains many guidance cue receptors which signal to the cytoskeleton to direct the neurite outgrowth toward the target with positive cues and away from unwanted targets via repellent cues[25]. While the growth cone has been extensively studied, numerous signaling pathways and mechanisms that underlie growth cone morphology and behavior remain uncharacterized.

Similarly, despite the importance of cytoskeleton-regulating proteins, many details of cytoskeleton regulation during brain development remain unknown. One family of proteins that are critically understudied are called the neuron navigators. These are a family of three proteins (neuron navigator 1, 2, and 3) with potential cytoskeleton-interacting and other functional domains in mammals. Homologs of the neuron navigators are also found in invertebrate species, and are important in the development and morphogenesis of various cell types in different organisms. All known navigator isoforms across species contain a AAA+ ATPase (AAA) domain close to their C-terminus, and, although the function of this domain remains undefined as of this writing, its evolutionary conservation suggests it is likely to represent the defining characteristic of the navigator family. AAA-domain containing proteins are, by definition, ATPases Associated with diverse cellular Activities, and it will be essential to characterize this property of the navigators in order to fully understand their cellular functions.

Neuron navigators 1 and 2 are critical in neurite outgrowth, though the underlying mechanisms are still unclear. Despite the apparent importance of these proteins in early development, there are very few studies addressing their role in the cell. This review will provide

comprehensive information of what is currently known about the neuron navigators and their homologs, and point out crucial gaps in our knowledge. Our group has recently provided evidence that Nav1 functions in macropinocytosis in the growth cone. Macropinocytosis is a form of fluid-phase endocytic uptake that occurs in many cells and regulates cell migration, neurite outgrowth, and synapse formation, among other activities. Here, we will suggest that regulation of macropinocytosis could be a cellular function that explains most of the described morphogenic phenotypes attributed to all the navigators.

Initial discovery of the navigators and their homologs

Invertebrates

Invertebrate homologs of the neuron navigators are *unc-53* and *Sickie* in *Caenorhabditis elegans* (*C. elegans*) and *Drosophila melanogaster* (*D. melanogaster*), respectively. These invertebrate homologs most closely resemble Nav2 according to amino acid sequence. Presumed duplication events in evolution resulted in the three neuron navigators seen in vertebrates[26]. Phenotypes associated with *unc-53* were first described after a screen for cell and axon migration mutants in *C. elegans* in 1987[27], and the function of the protein was described in more detail by Hekimi *et al*[28], and Stringham *et al*[29]. Years later, *Sickie* was identified as a part of an RNAi screen in the fruit fly looking for genes involved in the immune system[30], and later was discovered to be involved in actin regulation in mushroom body development[31]. More details regarding the function of these genes are provided below.

Vertebrates

All three mammalian navigators were identified and cloned in 2002 by various labs[32-34]. Because multiple labs cloned the same genes, there was a brief time that the navigators were

referred to by multiple names, before "neuron navigators" became the consensus name for the protein family. It is important to emphasize, however, that these proteins are expressed in and function in multiple cell types, and here we will refer to them simply as the navigators.

Navigator 3 was first called Pore membrane and/or filament interacting like protein 1 (POMFIL1) by Coy *et al*[33] because after cloning and raising an antibody to the protein, they found it was found in nuclear pores in neurons via immunolabeling and electron microscopy. This group also cloned Nav1 and Nav2, which they called POMFIL3 and POMFIL2, rescpectively[33].

Nav2 was identified as an all-*trans* retinoic acid-responsive gene in the human neuroblastoma line SH-SY5Y, and named retinoic acid inducible in neuroblastoma cells (RAINB1)[34]. That same year, Nav2 was identified in a search for genes that respond to adenomatous polyposis coli (APC), a transcription factor implicated in colorectal cancer[6], and was called helicase APC down-regulated 1 (HELAD1)[32].

The most detailed and complete early study that cloned and described the mammalian navigators was by Maes *et al*[26]. This study cloned human Nav1 and described and compared amino acid sequences, alternative splicing, and tissue expression of all three navigators[26], as well as compared the sequences to navigator/unc-53 proteins in *D. melanogaster* and zebrafish. These authors also investigated the phylogenetic relationships and evolution of the navigator genes, and concluded that navigators/unc-53 are conserved at least through nematodes. *D. melanogaster* and multiple fish species, including zebrafish, all express related genes having a homologous AAA-domain containing C-terminus. The authors demonstrated that Nav2 and Nav3 are more closely related to each other than to Nav1[26]. Nav1, Nav2, and Nav3 are found at chromosomal locations 1q32.1, 11p15.1, and 12q21.1, respectively, and genomic analysis suggested that a duplication

event from the ancestor yielded two branches, both of which underwent a second duplication which yielded Nav2 and Nav3 from one branch and Nav1 from the other. Maes *et al*. also point out that it is likely that Nav1 lost its 5' end during one of these genomic rearrangements[26].

Navigator protein structure

Because of its conservation through evolution and presence in all navigator family members, the AAA+ ATPase (AAA) domain at the C-terminus of the proteins is the apparently defining functional domain of the protein family (Figure 1.1). In general terms, AAA domains are associated with a variety of cellular activities, including proteasome function[35-37], membrane fusion, endosomal trafficking[37, 38], and microtubule severing,[39] to name a few. There has only been one study directly investigating the ATPase activity of this domain in navigators, and the study showed the domain was functional *in vitro* and is necessary for a DNA helicase activity of Nav2[32]. This interesting observation deserves follow up, as it may implicate navigators in transcription or chromatin organization.

The AAA domain may be necessary for the navigators' regulation of neurite outgrowth; expression of Nav1 with a mutated ATPase domain showed reduced ability to induce neurite-like protrusions when ectopically expressed in COS-7 cells[40]. The AAA domain is also necessary for the rescue of axon growth defects in a *D. melanogaster sickie* mutant[31]. How, precisely, nuclease activity contributes to these process remains unexplored.

The invertebrate and vertebrate navigators also contain coiled coil (CC) domains. Unc-53 and Sickie have two while the vertebrate navigators have three (Figure 1.1). CC domains are normally associated with protein-protein interactions, though to date there have been no proteins established that interact with the navigators through this domain.

At the N-terminus, unc-53, Sickie, and Nav2 and Nav3, but notably not Nav1, contain a calponin homology domain (CH) (Figure 1.1). A CH domain is typically associated with actin filament binding[41]. While there are no published observations of direct interaction of the navigators with F-actin through the CH domain, UNC-53 interacts with Abelson kinase interactor 1 (ABI-1), a regulator of actin filaments, through its CH domain[42]. We will elaborate on this pathway later in this review. Interestingly, although Nav1 lacks the CH domain, it has been reported to accumulate in actin-rich areas of the cell[43], and to bind to actin via its microtubule associated domain[43, 44]. This may suggest the navigators may interact with or influence actin dynamics via protein domains other than the CH domain.

Finally, the vertebrate navigators have been characterized as +TIP proteins because of their association with microtubules[40, 44-46], the identification of a microtubule binding domain[45, 46], and the presence of SxIP domains[31]. SxIP motifs typically indicate localization to the microtubule plus ends via association with end binding protein 1 (EB1), a protein known to serve as the anchor for many proteins that localize to the plus end, known as +TIP proteins[47, 48]. Notably, only when both of the N-terminal SxIP motifs are mutated in Nav1, and not each one individually, is Nav1's plus-end localization disrupted[44]. Therefore, the N-terminal microtubule binding domain SxIP motifs appear to be the necessary protein domain for plus-end localization and EB binding[40, 44, 45, 49]. All three navigators localize to the plus end of microtubules[40] and associate with EB1, and the microtubule binding domain is sufficient to perform microtubule bundling when overexpressed[45]. In *D. melanogaster*, the Sickie protein does have two SxIP motifs, however only one is in the putative microtubule binding domain, and there has been no evidence of Sickie localizing to microtubule plus-ends. Moreover, the putative microtubule association region in *D. melanogaster* shows some sequence diversion from that in its closest

mammalian homolog, Nav2. Therefore, at this time it is unclear if Sickie is a +TIP protein or whether this property is exclusive to mammalian navigators.

+TIPs are in a unique position to influence subcellular-domain changes at the cell periphery, because they typically track the rapidly polymerizing plus ends of microtubules by binding directly or indirectly to the growing end, but dissociate when the microtubule pauses or depolymerizes. Microtubules and actin can interact to deliver molecules to the cell periphery and initiate plasma membrane dynamics in response to signals[50, 51]. Moreover, specific +TIPs have been shown to mediate microtubule-actin interactions[51, 52] and such precise cytoskeletal dynamics are especially important in the neuronal growth cone[50, 51]. +TIPS are important in regulating the growth cone response to extracellular cues, and therefore influencing directional neurite outgrowth. Not only can they mediate actin-microtubule interactions, but they are also important in integrating cellular signals to initiate signaling pathways for cytoskeleton rearrangement[44, 52, 53].

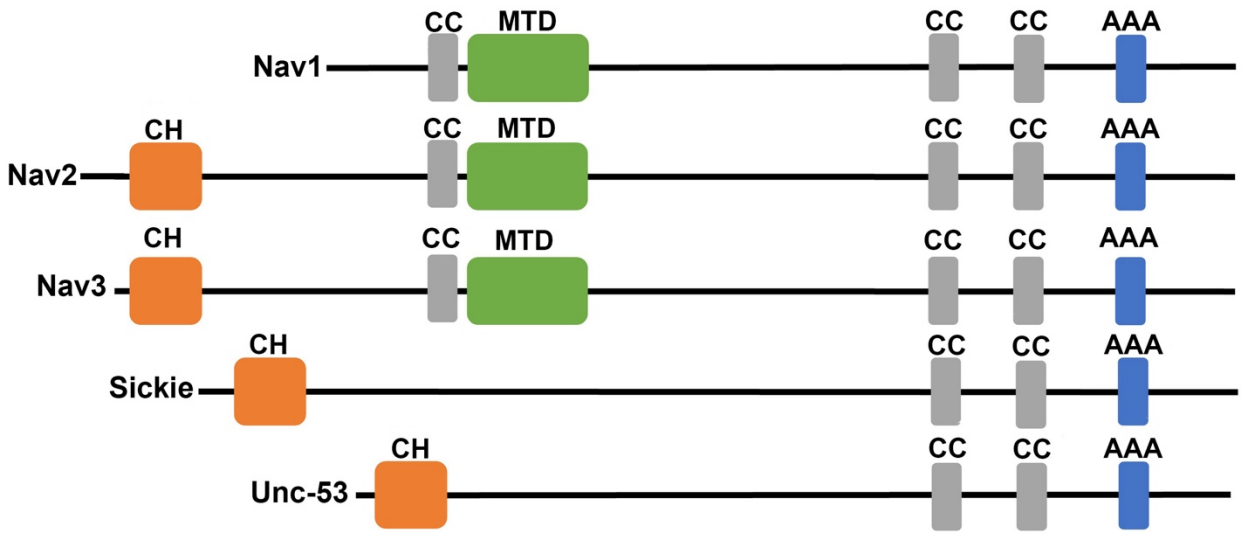

Figure 1.1: Protein domains in the neuron navigator family. CC = coiled coil, MTD = microtubule binding domain, CH = calponin homology domain, AAA = AAA+ ATPase domain.

Navigator expression and localization

Transcriptional regulation

The navigators are expressed in developing tissue, including the central nervous system[26]. However, only limited information is available to date regarding the transcriptional regulation of the Navigator genes. Nav1 and Nav2 have been shown to be regulated by both Tbr1 and Tbr2[54, 55], important early transcription factors that regulate neuronal differentiation[56, 57]. Using ChIPSeq, Tbr1 was found to bind to the Nav1 promotor region[58]. Moreover, Nav1 mRNA was reduced in cerebral cortex from Tbr1KO mice[54], indicating that Tbr1 positively regulates mRNA expression. Conversely, microarray analysis of intermediate progenitor cells indicates that Tbr2 likely suppresses Nav1 transcription in intermediate progenitor cells[55, 59]. Furthermore, Tbr1 and Tbr2 bind the Nav2 promoter region and activate Nav2 gene expression[54, 58-61]. Tbr1 and Tbr2 are essential transcription factors that are expressed in post-mitotic neurons and neural

progenitors, respecitvely[56], which is consistent with data showing that Nav1 is expressed in post-mitotic neurons rather than neural progenitors[43].

Tissue Localization

In invertebrates and vertebrates, the navigators are expressed in multiple tissues, and are most highly expressed during development. In *C. elegans*, UNC-53 is expressed in sex myoblasts, excretory canal cells, and certain neurons[29]. There have been multiple studies with varying results using Northern blot to identify in which tissues the navigators are expressed in vertebrates. Consistently, all three navigators are expressed in the developing brain, but the three molecules are expressed at different levels in different tissues such as the heart, lungs, liver, and skeletal muscle, which may indicate different functions for each navigator[26, 33]; however, their role in non-brain tissues remains largely unexplored. Furthermore, each navigator also has splice variants that may be differentially expressed compared to the full-length transcript. A recent paper by Pook *et al* detailed the expression of Nav2 in the mouse central nervous system during development[62]. They found via *in situ* hybridization that the full-length Nav2 transcript is expressed most abundantly during late embryonic and early-postnatal time periods and is found in the hippocampus, cortex, cerebellum and thalamus[62]. Klein *et al* also characterized *nav3* in zebrafish and found that it is expressed in the endoderm and regulates the developing liver[63], and recently *nav3* was shown to be localized to zebrafish cardiac tissue and is necessary for proper heart development[64]. Many of the tissues in which the navigators are expressed undergo extensive morphogenesis during development, which likely reflects the defining role for the navigators during development. Notably, this information comes from a small number of studies,

and more research is required to further characterize the expression of navigators in different tissues.

Subcellular Localization

The sub-cellular localization of the navigators has been most well-characterized in vertebrate neurons and neuroblastoma and other cancer cell lines. The navigators are +TIP proteins, so a subset of the navigator population is localized to microtubule plus ends[40, 43, 44, 49]. However, the navigators are not exclusively located there; they are also found in throughout the cytoplasm and apparently not associated with any particular cellular structure[40, 43]. Fluorescence recovery after photobleaching (FRAP) experiments in Cos-7 cells showed that GFPNav1 had a slow recovery after photobleaching, indicating that Nav1 is likely to be part of a high molecular weight complex or cellular structure that diffuses slowly through the cytoplasm[40]. Additionally, Nav1 and GFP-Nav2 are reportedly associated with actin-rich areas in neuronal growth cones and Cos-7 cells, respectively[40, 43, 44]

All three navigators are found throughout neurite extensions in neurons and neuroblastoma cells, and Nav1 has been reported to be especially enriched in distal ends of neurites, in growth cones, and at branch points[40, 43-45, 49]. Notably, all three mammalian navigators also show localization to the centrosome[40]. Similarly in *D. melanogaster*, Sickie is highly expressed in the mushroom body neuronal axon[31]. Furthermore, Sickie was also localized to regions of high F-actin in the mushroom body[31].

The localization of the navigators and the invertebrate homologs to cell types that undergo morphogenesis during development, as well as their sub-cellular localization to cytoskeletal structures, implicates these proteins as regulators of the cytoskeleton during

development. The next section will review the literature for the cellular processes and molecular pathways in which UNC-53, Sickie, and the navigators participate.

Functions of the navigators

Insights from Mouse Models

There are few published studies using vertebrate models of the navigators in the whole organism, nevertheless some studies have provided insight into the important role of these proteins *in vivo*. For example, Nav2 hypomorphic mice have been used to uncover its role in the brain[65]. Mice hypomorphic for Nav2 (hypomorphic because the dominant large transcript was abolished, but the shorter transcript was not), showed reduced body weight and smaller organs, as well as various sensory phenotypes compared to control mice. These sensory defects included deficits in olfaction and pain sensitivity revealed by behavioral tests, as well as a smaller optic nerve. Another pair of studies found defects in cranial nerve development and blood pressure regulation, as well as cerebellar abnormalities and ataxic behavior in Nav2 hypomorphic mice[66, 67]. Specifically, most Nav2 hypomorphic cerebella were smaller, and had fewer lobes and foliation compared to WT. Furthermore, granule cell migration was impaired in hypomorphic cerebella *in vivo*, and migration and neurite outgrowth defects were observed in cerebellar explants from the knockout mice[67]. All of these phenotypes demonstrate that Nav2 plays an essential role in migration and morphogenesis of developing neurons.

Navigators in neurodevelopmental disorders: insights from patient case studies

Nav1 is located on chromosome 1q32.1, a region of the chromosome for which duplications or deletions are associated with instances of neurodevelopmental disorders in

human patients[68, 69]. Symptoms include developmental delays and impairments in cognitive and motor function. Nav1 is not the only central nervous system-expressed gene at this chromosomal location; KIF21b and KDM5B are also contained within these regions. KIF21b is a kinesin motor protein, and KDM5B is histone lysine demethylase. Kif21b recently has been implicated in a neurodevelopmental disorder characterized by microcephaly and brain malformations[70]. While KDM5B has not been implicated in any disorders, other histone lysine demethylases have been implicated in neurodevelopmental and neurodegenerative disorders[71]. Therefore, it is unlikely the loss or duplication of Nav1 is the sole reason for the symptoms of the disorder. However the brain malformations and apparent migration defects observed in these case studies suggest that Nav1 may contribute to the disease phenotypes.

Recently, two compound Nav2 variants were identified as the disease-causing mutations for a patient with neurodevelopmental delay and diagnoses of cerebellar dysplasia and hypoplasia[72]. Researchers detected almost no full-length Nav2 mRNA or protein in patient fibroblasts compared to age-matched controls, though they did identify in immunoblots bands of lower molecular weight, likely from truncated or degraded fragments of the protein, consistent with Nav2 mRNA undergoing nonsense-mediated decay. The patient displayed microcephaly and motor and language delays, and patient fibroblasts had deficient migration[72]. This case study marks the first described human disorder caused by mutation in and presumptive loss of a navigator protein, and highlights the importance of understanding the cellular mechanisms underlying the role of the navigators in CNS development.

Cellular studies: cell migration, morphogenesis & response to extracellular cues

Both the invertebrate and vertebrate navigators are associated with regulating the cytoskeleton during cell migration and morphogenesis. This next section will review the existing literature to highlight how the Navigators regulate the cytoskeleton and how that may influence cellular behavior, namely migration and morphogenesis.

Unc-53

Unc-53 loss of function mutants in *C. elegans* cause defects in multiple systems that are associated with cell migration. *Unc-53* mutants were first described in 1974 to have an uncoordinated body motility phenotype [73], and since that point *unc-53* and its homologues have been implicated in cellular migration in multiple cell types.

During sex myoblast migration, myoblasts are guided to the gonads by guidance cues, namely EGL-17/FGF, and the cue is integrated through a pathway involving Sem-5, whose mammalian homologue is the adaptor protein growth factor bound receptor 2 (GRB2)[29], which functions in the Ras signaling pathway. *Unc-53* mutants showed defects in sex myoblast migration such that their anterior-posterior migration is defective. *Sem*-5 mutants have sex myoblast migration defects similar to *unc-53* mutants[29]. In fact, UNC-53 binds SEM-5 and GRB2 *in vitro*[29].

Unc53 is also necessary for distal tip cell (DTC) migration in *C. elegans*. DTCs are gonad cells that migrate during the larval stages to form the U-shape gonads. In *unc-53* mutants, the DTCs exhibit polarity reversal and pathfinding defects resulting in abnormal gonads[74]. These phenotypes are also seen in *ced-10* and *mig-2* mutants (homologues of Rac and RhoG, respectively), and this paradigm was used to identify other genetic interactors of *unc-53*[74]. Double mutants of *unc-53* and either *ced-10* or *mig-2* partially rescued the DTC defects,

especially the polarity reversal phenotype, indicating a negative relationship between *unc-53* and *ced-10* or *mig-2*. The Rho/Rac pathway is also involved in Nav1-regulated neurite outgrowth, which will be discussed later[49]. *Unc-53* and *abi-1*, a molecule also important in DTC migration, similarly have a negative relationship, as *unc-53:abi-1* double mutants have less severe DTC and gonad phenotypes than either single mutant[74]. Though further experimentation is needed to validate the relationships between these proteins in the signaling pathway, these genetic studies highlight the importance of navigators in cell migration and tissue morphogenesis and demonstrate the interaction of navigators with other cell migration cytoskeleton-associated molecules to influence cell behavior.

Nav3

The role of Nav3 in migrating hepatocytes was explored in zebrafish. Nav3 deficient hepatocytes failed to migrate from the endoderm resulting in smaller livers, and overexpression of Nav3 resulted in increased liver budding[63]. Furthermore, Nav3 associated with lamellipodia and filopodia in migrating zebrafish liver cells *in vitro* and *in vivo*[63]. FRAP analysis of Lifeact-RFP *in vitro* also demonstrated that actin polymerization was reduced when Nav3 was knocked down with shRNA[63]. Interestingly, Nav3 was present in actin protrusions of migrating cells, but this presence was lost upon expression of dominant negative CDC42, and enhanced upon expression of a constitutively active CDC42[63]. CDC42 is a Rho GTPase that helps regulate actin formation via the Arp2/3 complex[75] While there is no evidence thus far of a direct interaction of CDC42 with Nav3 (or any of the navigators), this experiment represents another possible mode of action of regulation of the cytoskeleton by the navigators in migrating cells.

Response to extracellular guidance cues

Extracellular cues are integral to proper development in multiple systems, including the nervous system. Nav1 and Nav2 have both been shown to regulate neurite outgrowth in response to some extracellular cues[43-46], and Nav3 may be activated in response to Wnt2bb in zebrafish[63], as Wnt2bb is established as an early guidance cue for differentiation of liver cells in zebrafish[76]. While there is currently no evidence of Nav3 responding to guidance cues in neurons, those data demonstrate the capacity of Nav3 to regulate responses to extracellular cues in general. Nav1 and Nav2 have indeed been shown to integrate extracellular cues in neurons. In mouse neuron explant culture, Nav1 is necessary for proper directional neurite outgrowth in response to the attractant cue Netrin[44, 45]. Adding to the evidence that Nav1 is important for neural migration *in vivo*, Powers *et al*[43] demonstrated that knock-down of Nav1 disrupts the orientation of the leading process of migrating neurons in the developing cortex[43]; proper leading process orientation is necessary for directional migration[77]. Nav2 mRNA expression is induced in SH-SY-5Y human neuroblastoma cells after all-*trans* retinoic acid (atRA) treatment, and Nav2 expression is lower or higher in the developing rat nervous system with atRA deficiency or excess, respectively[46], demonstrating that Nav2 expression is sensitive to atRA in multiple systems. Furthermore, neurite outgrowth is impaired in atRA treated Nav2 deficient SH-SY-5Y cells[46]. These studies demonstrate that the navigators are important in regulating the cellular and molecular response to extracellular cues to direct cell migration in development in multiple tissues, cellular contexts, and throughout evolution, suggesting this may be a shared and important role among the navigators.

Mechanisms of Neurite Outgrowth

Invertebrate navigators

While expressed in multiple tissues, the navigators, especially Nav1 and Nav2, have been most thoroughly investigated in neurons. The navigators and the invertebrate homologues have been implicated in neurite outgrowth in their respective organisms. Lack of *unc-53* in *C. elegans* results in impaired axon outgrowth in ALN and PLN neurons[29]. The axons in *unc-53* mutants have decreased outgrowth as well as axons growing in the wrong direction. These axons usually travel from the tail to the head of the animal along the anterior-posterior axis, but in the mutant the axon frequently stops before the midbody, and may send axonal branches in the dorsal or ventral direction, rather than the anterior[29].

While few binding partners and underlying mechanisms of UNC-53 have been identified in *C. elegans*, it was shown that ABI-1 directly interacts with UNC-53 at the N-terminus[74]. ABI-1 is a protein conserved through vertebrates that is a part of the WAVE complex that regulates actin nucleation by the Arp2/3 complex, which is important in neurite outgrowth and growth cone formation and behavior[78, 79], further pointing to cytoskeleton regulation as the mode of action for UNC-53 (Figure 1.2). ABI-1 also regulates responses to the Abelson tyrosine kinase (Abl), and forms complexes with EPS8 and SOS1, all of which are implicated in various types of trophic factor signaling[80, 81]. UNC-53 and ABI-1 have mostly overlapping expression patterns in the organism, and mutants of each gene display similar phenotypes[42]. These phenotypes include deficient migration and outgrowth of excretory cells, and defects in axon growth of mechanosensory neurons[29]. Additionally, they are both expressed in motoneurons, and the mutants of either gene result in dysregulated branching and dorsal outgrowth, and impaired

development of a proper neuronal network, suggesting both proteins are important in motoneuron development[29].

Interestingly, 14-3-3ε was identified as a binding partner of mammalian Nav2, and a *C. elegans* mutants of its homolog, *ftt-2*, also displays defects in PLM neuron outgrowth like the *unc-53* mutant[82]. These phenotypes described in *C. elegans* highlight that UNC-53 is important for integrating guidance cues, as the migrating cells and outgrowth are directed by these cues. Investigations into Sickie and the vertebrate navigators give further insight into these molecular processes, as well as the role of the navigators as integrators of extracellular cues.

Abe *et al*[31] examined the role of Sickie in the formation of the mushroom body, a neuronal structure in the central brain of *D. melanogaster*[31]. As with *unc-53*, *sickie* is most similar to Nav2. Flies without Sickie had smaller mushroom body axonal lobes, shorter axon branches, and defective ellipsoid bodies in mutant flies[31]. These phenotypes and further experiments revealed that Sickie acts upstream of cofilin and contributes to axon growth by regulating the dephosphorylation of cofilin through slingshot[31]. This pathway helps balance cofilin activity alongside the Pak LIM kinase pathway, and subsequently balances actin dynamics, aids in actin recycling, and regulates axon extension[31]. The loss of Sickie in this context results in less active cofilin and therefore less cofilin-mediated actin reorganization, which is necessary for proper axon growth[31]. This demonstrates the critical role that navigators can play in regulating cytoskeleton dynamics during development.

Mammalian navigators

Investigation into the mammalian navigators further reveal neurite outgrowth defects as well as insights into the cellular mechanisms underlying the role of the navigators in neurons.

Exogenous expression of all three mammalian navigators can induce neurite-like extensions in normally non-polarized cells, such as COS-7 cells, demonstrating their capacity to re-organize cytoskeleton and cell periphery and create extensions[40], Nav2 is necessary for neuritogenesis in SH-SY5Y cells[46, 82], and Nav1 is necessary for neuritogenesis in multiple systems, including neuroblastoma cells and primary neurons[43, 49]. However, there are only a few studies that have looked at the underlying mechanisms of the navigators' involvement in these processes. The rest of this section will outline our knowledge to this point of the cellular and molecular mechanisms of the navigators' involvement in neurite outgrowth.

A yeast two-hybrid screen and subsequent biochemical experiments identified 14-3-3ε and 14-3-3β as binding partners via amino acids 761-960 of Nav2[82]. 14-3-3ε as a Nav2 binding partner is especially interesting because it has been established as important in early neuron development. In fact, Miller-Dieker Syndrome, a neurodevelopmental disorder characterized by lissencephaly, can be caused by a loss of 14-3-3ε[17]. The multiple 14-3-3 family proteins are essential regulatory and adaptor proteins in a variety of signaling pathways, and 14-3-3ε has been shown to regulate the degradation of δ-catenin to promote neural migration[17, 83]. Co-expression of exogenous Nav2 and 14-3-3ε yielded overlapping localization along microtubules in the cell body and the neurite, and reduction of 14-3-3ε in SH-SY-5Y cells resulted in impaired atRA-induced neurite outgrowth, similar to silencing of Nav2[82].

The identification of the navigators as microtubule binding proteins, and +TIP proteins specifically, led to interest in their influence on microtubules (MTs) and how that may affect their role in neuritogenesis. Overexpression of all three navigators in non-neuronal cells induced neurites and promoted microtubule bundling[40]. A recent study revealed MTs in LLCPK-α cells overexpressing Nav1 had shorter depolymerization events compared to control cells, and MTs

also spent more time pausing[44]. Furthermore, Nav1 promoted MT persistence in the growth cone periphery[44], consistent with observations from our own lab demonstrating Nav1 is more highly concentrated on plus ends that are in the periphery of the growth cone compared to the central domain of the growth cone[43]. These data together suggest Nav1 prevents MT catastrophes, preferentially associates with plus ends in the growth cone periphery and demonstrate that navigators affect MT dynamics in the neuronal growth cone.

The binding partners and molecular mechanisms underlying the regulation of the cytoskeleton by Nav1 is of particular interest as it lacks the actin-associated calponin homology domain present in Nav2 and Nav3. One binding partner identified in N1E mouse neuroblastoma cells is Trio[23], a RhoGEF that regulates actin dynamics via the Rho/Rac pathway and is important in neurite outgrowth[19, 20] (Figure 1.2). Nav1 associates with Trio at the microtubule plus end via the Nav1 microtubule binding domain, and this interaction is necessary for neurite outgrowth via activation of Rac1[49]. Interestingly, the authors showed that GFPNav2 also binds Trio and EB1, and that GFPNav2-induced neurite outgrowth was abolished after addition of a dominant-negative Trio that binds EB1 but has no GEF activity[49]. These data suggest that Nav1 and Nav2 may operate in the same pathway(s) to promote neuritogenesis.

A recent study offered evidence that Nav1 may directly bind F-actin despite its lack of a CH domain. Sanchez *et al*[44] found that Nav1 can mediate cross-linking to microtubules and F-actin *in vitro*, and tracks with retrograde F-actin flow in the growth cone. Depletion of Nav1 caused increased growth cone area and a higher density of filopodia with more extension events, though there was no change in filopodia length. These data suggest Nav1 influences actin dynamics in the growth cone (Figure 1.2).

Nav1 in macropinocytosis

Adding further evidence to the regulation of F-actin by Nav1, Powers *et al*[43] demonstrated that Nav1 promotes F-actin rich membrane ruffles in the growth cone, which gather within the transition zone. Membrane ruffles are patches of concentrated F-actin whose role in the growth cone is not well defined but are involved in cell migration, endocytosis, and morphogenesis in other cell types[84-86], as well as membrane recycling in growth cones[87]. We demonstrated that Nav1 promotes macropinocytosis at these F-actin ruffles. Furthermore, Nav1 promotes membrane accumulation at the membrane ruffles, demonstrating a novel connection of Nav1 and the plasma membrane[43]. Interestingly, loss of Nav1 in SH-SY5Y cells induces membrane blebbing representing a disconnection between the plasma membrane and cortical actin, further supporting a role for Nav1 in regulating the dynamics of the cytoskeleton and the plasma membrane[43]. Notably, Nav1 also promoted the internalization of TrkB in the growth cone, the receptor for the neurotrophin brain-derived neurotrophic factor (BDNF)[43] (Figure 1.2). The endocytosis of the BNDF-TrkB complex leads to downstream signaling events that promote cell survival and neurite growth[88-91], and so the observation that Nav1 promotes internalization of this receptor provides new insight into why Nav1 is necessary for proper neuritogenesis. This observation also demonstrates that Nav1 is involved with multiple extracellular cues during neuron development, and suggests that integrating a variety of extracellular cues may be a general characteristic of the navigator molecules.

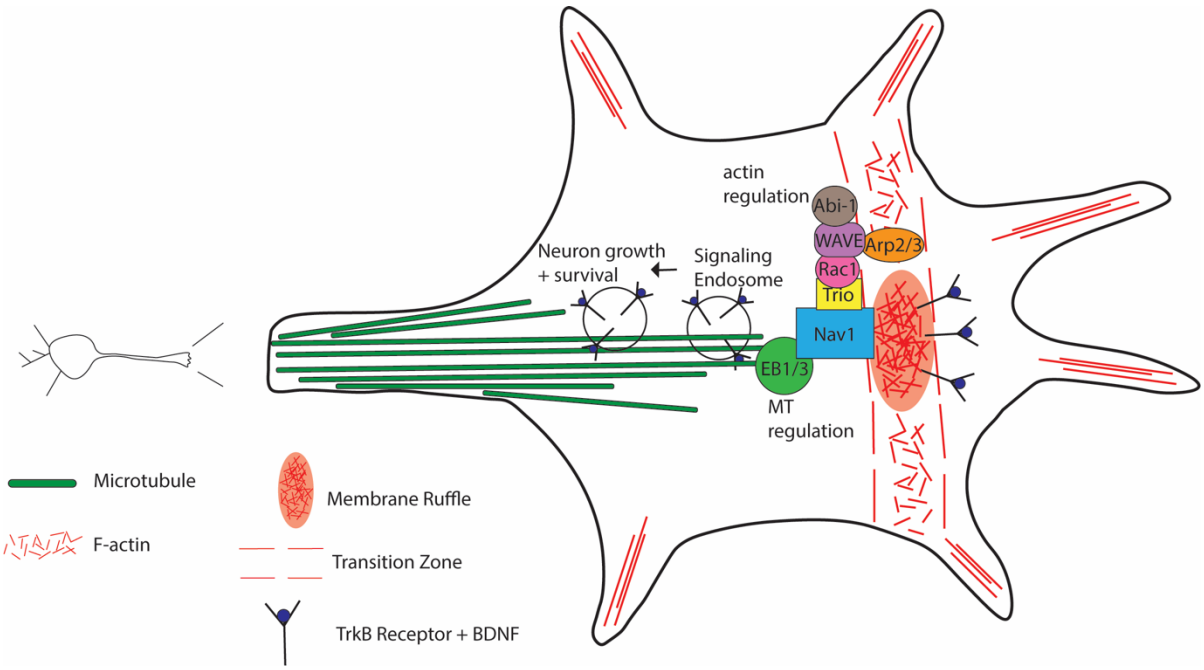

Figure 1.2: Navigators in the growth cone. Summary figure indicating relevant signaling pathways, binding partners, and downstream functions of Nav1 in the growth cone.

MACROPINOCYTOSIS

Introduction

In general terms, there exist two categories of endocytosis: clathrin-dependent and clathrin-independent endocytosis. Clathrin-dependent endocytosis has been extensively studied, but the different kinds of clathrin-independent endocytosis haven been more recently defined, and their mechanisms and downstream functions are still being elucidated. One type of clathrin-independent endocytosis is macropinocytosis, an ancient, fluid-phase form of endocytosis that internalizes extracellular fluids and solute via formation of large (>200nm diameter) vesicles called macropinosomes. Macropinocytosis is hypothesized to have evolved as a means for unicellular organisms and, later, cells within multicellular organisms to ingest nutrients. Eventually became employed for cell-specific functions like immune surveillance and cell signaling[92]. The term “bulk

endocytosis", or "bulk transport" has also been used to describe the internalization of large extracellular material as well as cellular membrane, and includes macropinocytosis as well as phagocytosis[87, 93]. The term bulk endocytosis has also been used to describe processes that resemble macropinocytosis but either do not share an established characteristic of macropinocytosis or when the process was not extensively characterized to yield a definitive identification of macropinocytosis[87, 94]. "Macroendocytosis" has also been used as a term to describe a bulk endocytosis that shares some but not all characteristics with macropinocytosis[95, 96]. It is possible that some features of macropinocytosis are cell type-, or context-dependent; it is also possible that some bulk uptake mechanisms are distinct enough to define them as unique endocytosis processes. Mechanisms for the regulation of macropinocytosis have been most extensively studied in the amoeba *Dictyostelium* and in mammalian antigen-presenting immune cells. These cells display especially high levels of macropinocytosis[97, 98]. However, emerging evidence suggests macropinocytosis underlies specific cellular processes of a variety of cells, including cancer cells and neurons. This section will address some general mechanisms of macropinocytosis and present evidence that for its importance in neuronal and synaptic development.

Markers of Macropinocytosis

Historically, fluid-phase markers like dextrans have been used to visualize macropinocytosis because those with a sufficiently large molecular weight (≥40kDa) are excluded from smaller vesicles generated by non-bulk endocytosis like CME. Uptake of large dextrans are often used as a specific assay for macropinocytosis. Fluorescent lipophilic dyes like the FM series (e.g., FM1-43, FM4-64)[87, 99, 100] can also be used to visualize macropinocytosis if

they are incubated for short periods (~one minute), because longer incubation allows incorporation into internal organelle membranes[101]. These dyes bind directly to the outer leaflet of the plasma membrane and are readily internalized, and thus can be visualized for bulk internalization, and used in conjunction with inhibitors of macropinocytosis for macropinocytosis identification[87].

Multiple forms of fluid-phase uptake that resemble macropinocytosis have been described. For example, caveolae-mediated endocytosis occurs at cholesterol-concentrated membrane domains[102], and circular dorsal ruffle endocytosis has been linked to receptor tyrosine kinase uptake in some cancer cell lines[103, 104]. These are non-clathrin mediated endocytosis processes that are distinct from macropinocytosis; caveolae-mediated endocytosis excludes high-molecular weight dextran[105], and circular dorsal ruffle endocytosis, as will be described later, requires distinct signaling molecules from macropinocytosis[106]. *In vivo*, while there have been a few studies looking macropinocytosis, namely in invertebrates[107, 108] but also in mammalian macrophages[109], it remains unclear how the constraints and geometry of the 3-dimensional environment shape the morphology and mechanics of macropinocytosis, especially in different cell types.

Mechanisms and inhibitors of macropinocytosis

Macropinocytosis is actin-dependent, and macropinosomes form as a result of intense membrane ruffling, in which actin-based protrusions emerge from the cell surface and then curve to form spherical macropinosomes[97, 98, 110, 111]. Macropinocytosis is often constitutive, though certain growth factors, like the commonly used epidermal growth factor (EGF), can evoke macropinocytosis[112]. Actin polymerization and active Rac1[84], a major inducer of membrane-

associated actin polymerization, are both necessary for membrane ruffling and therefore macropinocytosis. Interestingly, in macrophages Rac1 activation is necessary to initiate macropinocytosis, but must be de-activated for endosomes to form from the macropinosomes[113].

The macropinocytosis inhibitor amiloride and its derivatives (such as the more specific and more potent ethylisopropylamiloride [EIPA])[114], which reduce Na+/H+ exchange via blockage of Na+/H+ exchange channels (NHEs)[112, 114], inhibit macropinocytosis via acidification of intracellular area adjacent to the plasma membrane[115]. At low concentrations amilorides do not interfere with CME[115], so these compounds are useful tools in probing the pathways for fluid-phase uptake. The acidification and resulting inhibition of macropinocytosis by amilorides are attributable to the inhibition of Rac1 and Cdc42 activity[115]. However, caution must be applied in interpretation of amiloride experiments, as disruption of Rac1 and Cdc42 activity is likely to affect other non-CME endocytosis processes such as GPI-enriched endocytic compartment endocytosis (which requires CDC42)[116] and interleukin-2 receptor uptake (which requires Rac1)[117]. The precise biophysical basis for the requirement of acidification is yet to be determined, and represents an important area for future studies.

Besides its reliance on actin, macropinocytosis is also dependent on phosphatidylinositol (3,4,5)-trisphosphate (PIP3), and therefore on the enzyme phosphatidylinositol 3-kinase (PI3K)[98, 118], which generates PIP3 from phosphoinositol 4,5-bisphosphate. Circular dorsal ruffle (CDR)-dependent endocytosis, which functions in receptor tyrosine kinase internalization[103], is a more recently described form of bulk endocytosis. CDR-dependent endocytosis relies on PI3-kinase activity, like macropinocytosis. However, CDR reportedly requires WAVE, and not N-WASP (two Wiskott-Aldrich Syndrome protein family members involved in actin regulation[119]), while the converse was reportedly true of macropinocytosis[106]. These observations reinforce the need

for further studies to clarify the relationships among various types of macropinocytosis-like uptake.

Other factors important in signaling mechanisms for the initiation, maintenance, and termination of macropinocytosis and the subsequent trafficking of macropinosomes include Arf6[120], dynamin[121], and microtubules[120, 122], among others, but their exact roles in macropinocytosis and whether they are consistent across all cell types and organisms remains unclear. Here again, more research is needed to fully elucidate the signaling pathways necessary for macropinocytosis and its regulation. Moreover, because of mechanistic crossover with other clathrin-independent uptake pathways, it is generally necessary to use multiple inhibitors to probe the mechanisms of any endocytosis observed, and to use high molecular weight dextran to distinguish macropinocytosis from other modes of uptake. Finally, studies of macropinocytosis *in vivo*, or in more physiologically relevant 3-dimensional environments such as explants or organoids, are needed to solidify our understanding of this critical aspect of cell biology.

Macropinocytosis in neural development

Growth cone macropinocytosis

The first indication of macropinocytosis at the growth cone comes from a 1999 paper that reported a population of endosomes created during constitutive endocytosis using the lipophilic dye FM1-43 in chick ciliary ganglion neuron growth cones[99]. The authors postulated that constitutive endocytosis might be useful for membrane recycling and rearrangement of the plasma membrane components of the growth cone, such as receptors, pumps, and channels[99].

Indeed, almost 10 years later, using a similar lipophilic dye, FM4-64, Bonanomi et al. observed macropinocytosis in mammalian growth cones[87] of cultured rat hippocampal neurons.

Importantly, FM4-64 uptake was concentrated in the transition zone of the growth cone where intense membrane ruffling occurred, and endocytosis was positively correlated with increased motility as measured by changes in growth cone area[87]. Furthermore, uptake was PI3-kinase, cholesterol, and Rac1-dependent -- all features of macropinocytosis -- and uptake of high-molecular weight dextran, was observed[87].

Interestingly, the chaperone protein Pincher was shown in this study to regulate macropinocytosis in a concentration-dependent manner. Overexpression of Pincher or expression of a dominant-negative Pincher inhibited growth cone macropinocytosis as well as disrupted axon elongation[87]. Pincher has also been shown to be regulate the internalization of the neurotrophin receptors TrkA/B in developing neurons, highlighting the potential impact of Pincher-regulated macropinocytosis on neurodevelopment[96].

Finally, growth cone macropinocytosis may be developmentally regulated. Bonanomi *et al* showed that, while macropinocytosis was readily observed in hippocampal cultures prepared from day 18 embryos at 2-3 days *in vitro* (DIV), endocytosis in the growth cone displayed mostly receptor-mediated endocytosis by 7 DIV[87], rather than macropinocytosis, This suggests that macropinocytosis might be specific to early pathfinding axons. The data from my thesis work, which will be described later, adds to this body of work by demonstrating that a cytoskeleton-associated protein, neuron navigator 1, promotes membrane ruffles and macropinocytosis, including internalization of growth factor receptors, in the growth cone[43].

Growth cone collapse and macropinocytosis

Several studies demonstrate that endocytosis can be evoked in the growth cone by negative guidance cues that mediate growth cone collapse[123-125]. Negative guidance cues (also

called “repulsive cues”) such as sonic hedgehog (Shh)[125], ephrin A2[125], or Semaphorin3A (Sema3A)[123, 124] play critical roles in circuit wiring by directing outgrowing axons to pause, stop, or change direction. Repulsive cues such as these induce growth cone collapse and thus aid in the directional outgrowth of axons, as collapse can happen in a local, sub-cellular manner[25]. It is possible, however, that the cue-induced endocytosis investigated in these papers share similar mechanisms to macropinocytosis but are a unique process, as one study showed that repulsive cue-induced growth cone endocytosis was not PI3-kinase dependent, and therefore possibly inconsistent with macropinocytosis as described elsewhere[125]. One of the studies demonstrated that the macropinocytosis inhibitor ethylisopropylamiloride (EIPA) disrupted dextran uptake and growth cone collapse in response to Sema3A[124] suggesting a mechanistic similarity to macropinocytosis. However multiple other studies investigating this phenomenon only used 10kda dextran to assay macropinocytosis[123, 125], and because this molecule is small enough to be taken up by other endocytic processes like micropinocytosis[105], the conclusions of these studies as they pertain to macropinocytosis are hard to interpret. However, these studies do offer useful insight into other mechanisms regulating macropinocytosis-mediated growth cone collapse.

Synapse development and macropinocytosis

Macropinocytosis has also been shown to be important in the formation of *Drosophila* neuro-muscular junction (NMJ) synapses[122], as inhibition of macropinocytosis (via the PI3kinase inhibitor LY29400 or the N+/H+ exchanger inhibitor EIPA) resulted in excess synapse formation[122]. NMJ synapse formation is regulated by retrograde bone morphogenetic protein (BMP) signaling, with BMP receptors (BMPRs) expressed on the presynaptic terminal that respond to BMP released from the post-synaptic muscle cell[126]. A recent study demonstrated that

BMP signaling is downregulated via macropinocytosis and subsequent degradation of BMPRs after BMP stimulation[122]. BMP-induced macropinocytosis was dependent on Abi, Abl, and Rac1. Interestingly, it was also associated with downstream microtubule regulation, since synapses deficient in macropinocytosis had higher MAP1B expression, and the synaptic overgrowth phenotype was abrogated with treatment of vinblastine[122] which disrupts the microtubule network[127]. This study demonstrates that regulating growth cone dynamics is not the only neurodevelopmental process that requires macropinocytosis and draws attention to the fact that there is still much to discover about the downstream functions of macropinocytosis in the nervous system.

Summary

There is still much unknown about growth cone macropinocytosis, but it seems clear that it is an essential process during neurodevelopment. Furthermore, it is likely that even more connections between macropinocytosis, the cytoskeleton, and growth cone dynamics and guidance will be discovered. Growth cone membrane content and tension are maintained by a balance of exo- and endocytosis, and so it is likely that macropinocytosis contributes to this balance, and the relationship between the two processes and their effects on growth cone dynamics and axon outgrowth should be researched further[128, 129]. Furthermore, as alluded to above, microtubules seem to be involved in macropinocytosis. While a link to microtubules downstream of macropinocytosis in response to BMP at the NMJ[122] has been implicated, it has also been shown in non-neuronal cells that microtubules are necessary for macropinocytosis to occur[120]. A prime candidate, then, for involvement in macropinocytosis in the growth are +TIP proteins, like Nav1, that localize to the plus-end of microtubules. +TIPs often associate with

actin[51], and are an important group of proteins for growth cone dynamics and axon outgrowth[50, 53].

ACKNOWLEDGEMENTS

Chapter 1, in part, is currently being prepared for submission for publication of the material. Powers, Regina; Hevner, Robert; Halpain, Shelley. “The Neuron Navigators” (working title). The dissertation author was the primary researcher and author of this material.

Chapter 1, in part, is currently being prepared for submission for publication of the material. Powers, Regina; Halpain, Shelley. “Macropinocytosis in the nervous system” (working title). The dissertation author was the primary researcher and author of this material.

CHAPTER 2

INTRODUCTION

Mammalian brain development requires a series of steps coordinated by intra- and extra-cellular cues. Integration of these cues by developing neurons results in morphological changes guiding the maturation of newborn neurons and their ultimate integration into neuronal networks. Actin and microtubules (MTs) of the neuronal cytoskeleton, regulated by cytoskeleton-associated proteins, undergo major rearrangements to drive neuronal morphogenesis throughout development.

One group of critical cytoskeleton-associated proteins are microtubule plus-end tracking proteins (+TIPs). +TIPs localize to the dynamic, growing end of MTs and form complexes there, many anchored by end-binding proteins (EBs), which bind directly to the microtubule plus end [130]. In addition, actin filaments and MTs can interact to deliver molecules to and from the cell periphery and initiate membrane remodeling in response to signals, and +TIPs have been shown to mediate certain types of MT-F-actin interactions [52, 131, 132]. Such precisely regulated cytoskeleton dynamics are especially important in the neuronal growth cone, a specialized cytoskeleton-rich structure that responds to extracellular cues and directs neurite outgrowth [52, 131, 133-135].

The growth cone comprises cytoskeletal structures containing both MTs and actin, including microtubule arrays, filopodia, actin arcs, and F-actin membrane ruffles [135, 136], and their regulated dynamics are essential for growth cone responses to external cues and proper neurite outgrowth and guidance [53, 135, 137-139]. The role of growth cone F-actin membrane ruffles in growth cone behavior, however, remains largely unexplored. In non-neuronal cells, membrane ruffles influence cell migration, morphogenesis, and endocytosis [85, 86, 111]. Notably, Bonanomi *et*

al found that growth cone membrane ruffles are sites of bulk-endocytosis, and that this endocytosis is important for neuritogenesis [87]. However, the mechanisms that regulate growth cone membrane ruffles and their functional impact are largely unexplored.

The neuron navigators (Nav1, Nav2, and Nav3) are a group of +TIP proteins functioning in development and tissue morphogenesis. All three proteins are large (>200kDa), and contain multiple domains including a microtubule binding domain and a AAA ATPase domain whose function is poorly understood [26]. Nav1 is enriched in the developing nervous system [45], and concentrates at neurite tips [49]. Both Nav1 and Nav2 have been implicated in neuritogenesis [40, 46, 49, 82, 140]. Nav1 regulates neuritogenesis in neuroblastoma cells via binding to the Rho GEF Trio [49]. Nav1 might also facilitate MT-actin crosstalk via direct F-actin binding [44]. While these studies provide insight into the role of Nav1 in neural development, many of the underlying mechanisms remain to be elucidated. In this paper, we investigate the critical role of Nav1 in neuritogenesis in multiple model systems, describe its selective enrichment in and function in growth cone membrane ruffles, and identify two novel roles of Nav1 in regulating the cytoskeleton. These novel roles include the regulation of cortical actin-plasma membrane connections via the Rho/Rac pathway, and a key role in macropinocytic uptake of neurotrophin receptors in the nascent growth cone via regulation of membrane ruffles.

Nav1 is enriched in pathfinding axons *in vivo*

Nav1 mRNA is enriched in the developing CNS [45], but thus far the *in vivo* localization of Nav1 protein regionally within the brain has not been described. We characterized Nav1 immunoreactivity in embryonic mice at E12.5 and E14.5. As expected, Nav1 mRNA was enriched throughout the developing brain and enriched in the majority of neuronal cell bodies of

differentiated neurons [141] (Figure 2.1 A,B). Within the developing neocortex, immunoreactivity for Nav1 was low in the progenitor-containing ventricular zone (VZ) and subventricular zone (SVZ) (Figure 2.1 C). However, Nav1 immunoreactivity was abundant in the intermediate zone (IZ) and cortical plate (CP) (Figure 2.1 C). In addition to enrichment in cell bodies (Figure 2.1 D,E), Nav1 immunoreactivity was enriched in several developing axon tracts, including the lateral olfactory tract, the stria medullaris thalami, and the internal capsule (Figure 2.1C). Within these axon tracts and within the IZ, Nav1 colocalized with multiple axonal markers, including antibody SMI-31, which labels neurofilaments (Figure 2.1 F-K), antibody to growth associated protein-43 (GAP-43) (Figure 2.1 L-N), and antibody TuJ1, which labels neuron-selective βIII-tubulin [142] (Figure 2.1 O,P). Enrichment of Nav1 in these axon tracts is consistent with a role in axon outgrowth or pathfinding *in vivo*.

Figure 2.1: Nav1 is localized in neuronal cell bodies and growing axons in developing mouse brain. (A, B) Nav1 mRNA, detected by in situ hybridization (ISH) on E14.5 (Genepaint, set ID EH1164), was widely expressed in differentiating neurons, but not in progenitor cells around the ventricles. In cerebral cortex (boxed area in A, shown at higher magnification in B), Nav1 mRNA was not detected in the progenitor-containing ventricular zone (VZ) and subventricular zone (SVZ), but was highly expressed in the intermediate zone (IZ) and cortical plate (CP), where postmitotic neurons are located (Genepaint, set ID EH1164). (C-E) Nav1 protein on E14.5 was expressed in neuronal cell bodies, but was also highly enriched in axon tracts including the stria medullaris thalami (smt), lateral olfactory tract (lot), and internal capsule (ic). Higher magnification views of the CP in D and E demonstrate Nav1 protein in many cell bodies (arrows in E). (F-K) Double immunofluorescence for Nav1 and neurofilament heavy chain (antibody SMI-31), a marker of axons, confirmed the presence of Nav1 in axons coursing through the IZ. (L-N) On E12.5, double immunofluorescence for Nav1 and GAP-43, a marker of growth cones, demonstrated extensive colocalization, notably in growing axons of the smt, shown at higher magnification in M-N. (O, P) Double immunofluorescence for Nav1 and class III b-tubulin (antibody TuJ1), a marker of neurons and their processes, confirmed the presence of Nav1 in smt axons. Plane of section: sagittal for A, B; coronal for C-P. Scale bars: A, 500 μm; B, 100 μm; C, 500 μm; D, 20 μm; E, 10 μm; F-H, 100 μm; I-K, 20 μm; L, 200 μm; M-P, 50 μm. Cx = Cortex, LV = Lateral Ventricle, Th = Thalamus, OB = Olfactory Bulb, Cb = Cerebellum. Images represent observations from 3 individual culture preparations.

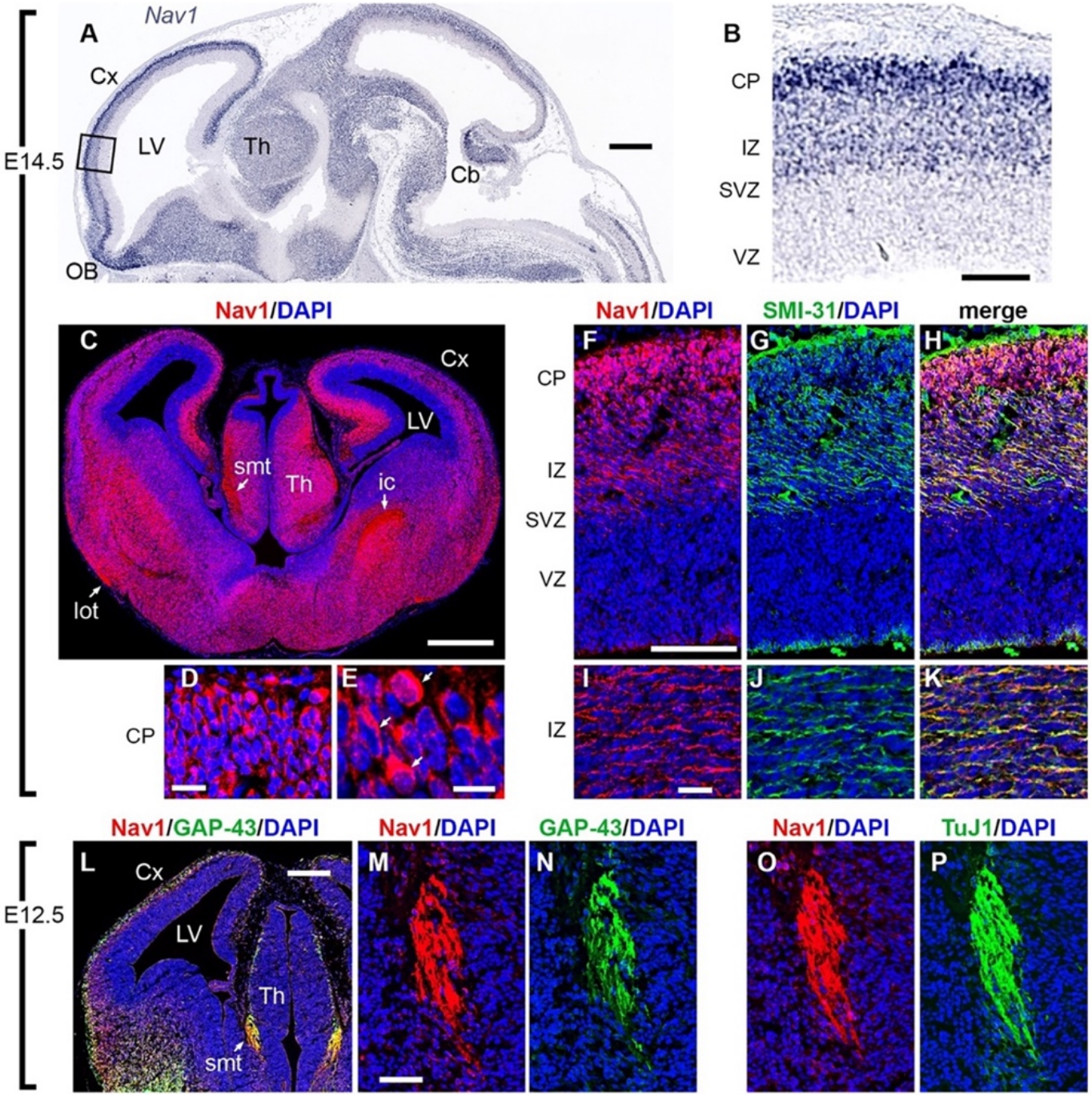
E14.5
A
Nav1
Cx
LV
Th
Cb
OB
B
CP
IZ
SVZ
VZ
Nav1/DAPI
C
Cx
LV
smt
Th
ic
lot
D
E
CP
Nav1/DAPI
SMI-31/DAPI
merge
F
G
H
CP
IZ
SVZ
VZ
I
J
K
IZ
E12.5
Nav1/GAP-43/DAPI
L
Cx
LV
Th
smt
Nav1/DAPI
M
GAP-43/DAPI
N
Nav1/DAPI
O
TuJ1/DAPI
P

Nav1 accumulates in subcellular regions of morphological change

Together with previous studies [40, 44, 45, 49], the observation of Nav1 expression in axonal tracts during the phase of outgrowth and cue-driven guidance *in vivo* suggests that Nav1 is involved in neurite development. We therefore assessed the localization of endogenous Nav1 in multiple neural cell types. We used dissociated hippocampal neurons cultured from embryonic rat brain, SH-SY5Y human neuroblastoma cells, and human iPSC-derived neurons as model systems to further investigate the functional role of Nav1 in developing neurons. These cell models recapitulate in culture many of the key morphological changes that neurons undergo during neuritogenesis *in vivo*, and are amenable to detailed sub-cellular studies and time-lapse observation [34, 46, 143].

In newly-plated primary hippocampal neurons that had yet to extend processes, endogenous Nav1 was distributed in a punctate pattern throughout the cell. Clusters of Nav1 puncta were especially enriched at peripheral locations (Figure 2.2 A, Stage 1.1), which are often sites of symmetry breakage where *in vitro* growth cone formation and neurite initiation commonly occur in this model [133, 144]. Neurons transfected with GFP-Nav1 displayed an even greater clustering of GFP-Nav1 in growth cones and their precursors, and time-lapse imaging confirmed that GFP-Nav1 was concentrated within subcellular domains that are presumptive sites of neurite initiation (Figure 2.3). Regions enriched with Nav1 redistributed as the cell margin dynamically segmented and coalesced into nascent growth cones (Figure 2.2 A, Stage 1.2-1.3). Nav1 enrichment was evident in all identified growth cones of minor neurites (Figure 2.2 A, Stage 2). Growth cone enrichment of Nav1 continued throughout the early stages of neurite elongation, and persisted as one of the minor neurites began differentiating into a presumptive axon (Figure 2A, Stage 3). This pattern of Nav1 localization is consistent with a

potential role in directing multiple stages of neuritogenesis, including neurite initiation, elongation, and axon guidance. Experiments demonstrated that clusters of Nav1 were present in growth cone sub-regions containing enriched immunoreactivity to the actin binding protein drebrin (Figure 2B), which we used as an F-actin marker compatible with the methanol fixation method that optimizes Nav1 immunoreactivity. In addition, many Nav1 puncta colocalized with tyrosinated tubulin, which labels newly polymerized microtubules [145] (Figure 2.2 C).

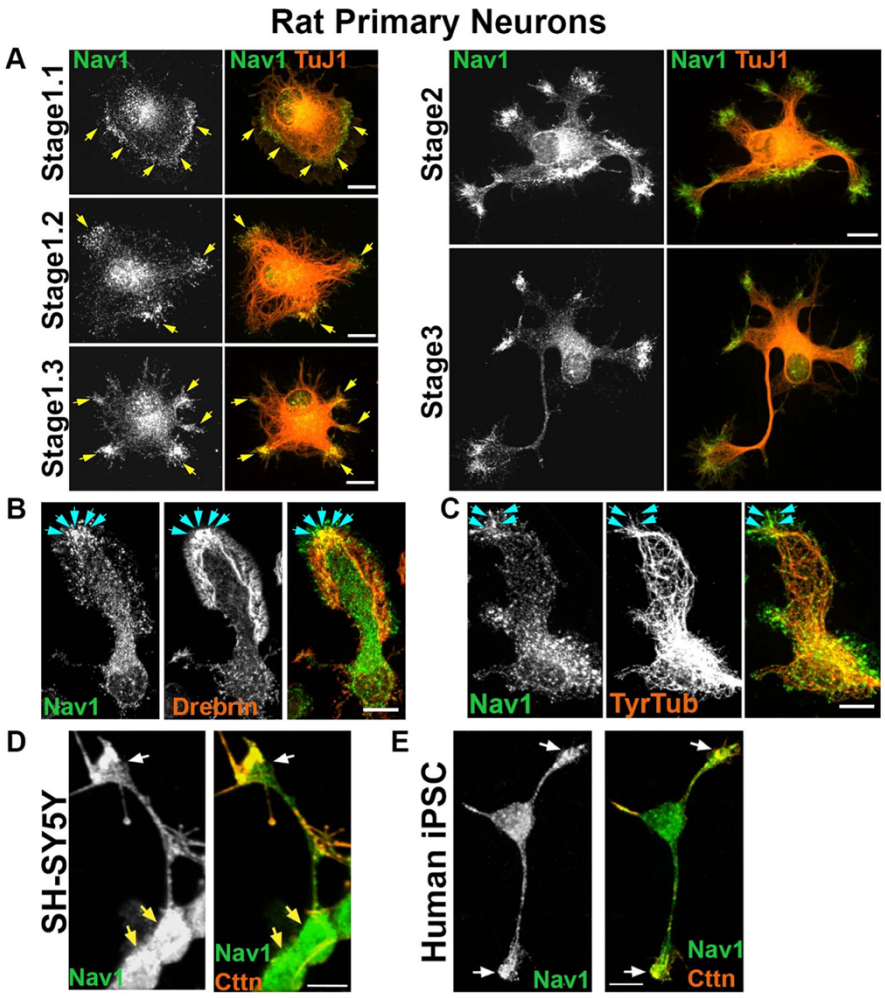

Figure 2.2: Nav1 is expressed in areas of morphological change. (A) Primary cultures from rat hippocampus were fixed after 3 DIV and immunostained for Nav1 and neuron-specific ß-III tubulin (antibody TuJ1). Representative images of neurons at different stages of neuritogenesis are shown. In Stage 1.1 neurons have a lamellipodia surrounding the cell body and Nav1 is enriched close to the membrane in this area. As the lamellipodium undergoes segmentation (Stage 1.2), Nav1 remains enriched in this location. The segments coalesce into nascent growth cones as the microtubules adopt a parallel organization behind them (Stage 1.3). Nav1 remains similarly clustered in nascent growth cones as minor neurites become established in Stage 2, and one neurite is specified as the presumptive axon in Stage 3. (B) Representative image of a growth cone immunostained for Nav1 and the actin binding protein drebrin, highlighting the transition zone of the growth cone. (C) Representative image of growth cone immunostained for Nav1 and tyrosinated tubulin shows that newly-polymerized microtubules are present together with Nav1. (D) Representative image of 3 day BDNF-differentiated SH-SY5Y cells showing enriched Nav1 puncta in distal ends of neurite (white arrow indicate growth cone, yellow arrows indicate cell bodies). (E) Representative image of human iPSC-derived neuron showing enriched Nav1 in distal ends of neurites (white arrows indicate growth cones). All scale bars = 10µm. Images represent observations from 3 individual culture preparations.

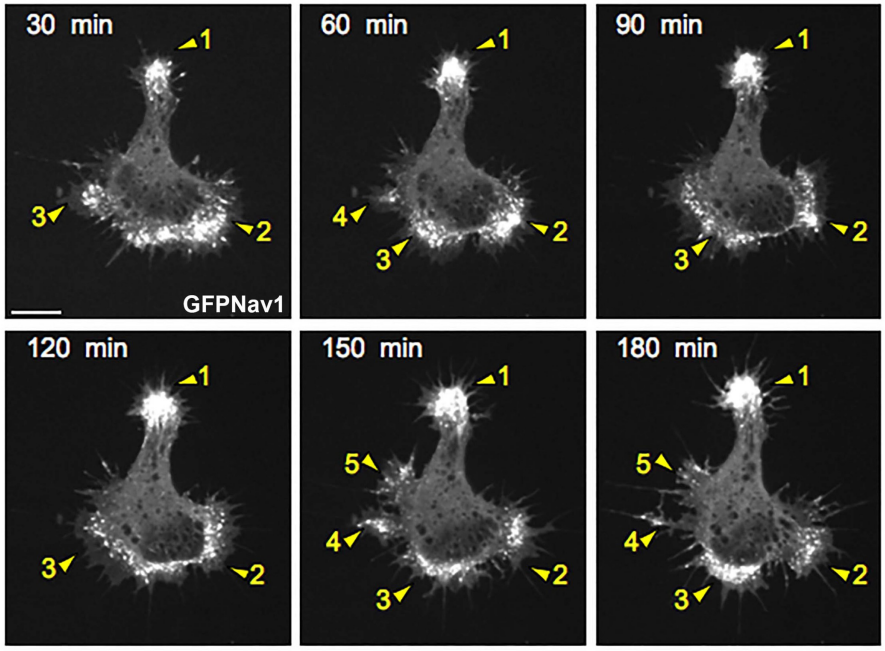

Figure 2.3: GFP-Nav1 subcellular dynamics during neuritogenesis. Selected frames from a time-lapse sequence showing that Nav1 is enriched in subcellular regions (arrowheads) that extend from the cell body and might commit to becoming neurites. Arrowheads show the appearance of these nascent growth cones over neuronal morphogenesis. Cells presented the characteristic filopodial activity and segmentation of the initial lamellipodia surrounding the soma. Such membrane segmentation commonly precedes the selection of a neurite initiation site in cultured hippocampal neurons. Scale bar = 20μm. Images represent observations from 3 individual culture preparations.

Human SH-SY5Y cells stop dividing, differentiate into neuronal-like cells, and emit neurites after sequential stimulation with retinoic acid and brain-derived neurotrophic factor (BDNF) [146]. Similar to the rat hippocampal neurons, differentiated SH-SY5Y cells displayed enriched clusters of Nav1 puncta in the distal ends of neurites (Figure 2.2 D), although the relative degree of enrichment was lower than what was observed in hippocampal neurons. Finally, we also observed enriched Nav1 in growth cones of human iPSC-derived neurons (Figure 2.2 E). Taken together, these data show that Nav1 is present in developing human and rodent neurons and accumulates in areas of morphological change as the nascent neurites are forming.

Nav1 deficiency disrupts neuritogenesis

Previous studies have shown that knockdown of Nav1 in a mouse neuroblastoma cell model disrupts neuritogenesis [49]. To address whether Nav1 plays a similar role in primary neurons, we performed knockdown experiments in freshly dissociated hippocampal neurons (Figure 2.4 A). Cells were electroporated with control vector or Nav1-shRNA just prior to plating, and examined at 3 days in vitro (3DIV). Nav1 shRNA induced a ~50% reduction in neuronal Nav1 expression compared to control shRNA (Figure 2.5 A). First, we analyzed the effect of Nav1 silencing on early morphogenesis by classifying neurons into three stages [147]: stage 1 cells have no identifiable neurites; stage 2 cells have one or more minor neurites but lack a defined axon; stage 3 cells have one or more axons. The proportion of cells in stage 1 was significantly higher in Nav1-depleted neurons, with no significant effect on the proportions of cells in stages 2 and 3 (Figure 2.4 B). This indicates that Nav1 directs neuronal morphology from the earliest morphological steps.

Figure 2.4: Nav1 deficiency disrupts neuritogenesis. (A) Hippocampal neurons were electroporated on the day of plating to express GFP as transfection marker and either Control shRNA (Ctrl shRNA) or Nav1 shRNA. Neurons were fixed after 3 DIV and stained for GFP and ß-III-tubulin to specifically identify neurons. Representative GFP images are shown; blue arrowheads indicate the cell body. Scale bar = 100µm (B) Quantification of neurite growth in Ctrl and Nav1 shRNA electroporated dissociated hippocampal neurons: Neurons were classified into different stages as described in Methods. Stacked histogram showing that knock-down of Nav1 increases the percentage of cells in stage 1. Statistical analysis: Two-way ANOVA with Bonferroni post hoc comparisons, *$p<0.05$.; n = 3 experiments; Control shRNA = 240 cells, Nav1 shRNA = 352 cells (C) Nav1-supressed neurons show a decrease in the number of primary neurites per cell. Statistical analysis: Mann-Whitney test ****$p<0.0001$. Same n as (B). (D) Nav1-suppressed neurons show decreased mean neurite length. Mann-Whitney test ****$p<0.0001$. Same n as (B). (E) Representative images showing WT and Nav1KO SH-SY5Y cells after 2 days of BDNF differentiation as described in Methods. Scale bar = 50µm (F) Nav1KO cells have reduced neurite growth over time. Neurite length quantified as described in Methods. Statistical analysis: Kruskal-Wallis, Dunn's multiple comparisons ****$p<0.0001$; n = 3 experiments; Undiff WT = 226 images, Undiff Nav1KO = 238 images, 2 day diff WT = 234 images, 2 day diff Nav1KO = 193 images, 5 day diff WT = 232 images, 5 day diff Nav1KO = 175 images; (G) Typical example of neuronal morphology and orientation of cells electroporated on E15.5 with mVenus (detected using antibody to GFP; green) and either Ctrl shRNA or Nav1 shRNA. Tissue was fixed and counterstained with anti-nestin antibody (red) on E18.5. Scale bar = 100µm. (H) Representative images of Control shRNA and Nav1 shRNA-expressing neurons (green) illustrating the vector (red) used to measure the angle to the pial surface (blue). Tbr1 antibody was used to label the cortical plate (CP). Scale bar = 10µm. (I) Quantification of the effect of Nav1 shRNA on the percentage of cells in the multipolar stage within the intermediate zone (IZ)/subventricular zone (SVZ). Statistical analysis: t-test, two tailed, *$p<0.05$; Control shRNA vector, n = 3 experiments with 6 embryos, 527 neurons; Nav1 shRNA vector, n = 3 experiments with 7 embryos, 635 neurons. (J) Quantification of the effect of Nav1 shRNA on neuron orientation in the lower IZ and SVZ. Angle of orientation in control vs. shRNA expressing neurons was quantified as described in Methods. Statistical analysis: t-test, two-tailed, *$p<0.05$; Control shRNA vector, n = 3 experiments with 6 embryos, 966 neurons; Nav1 shRNA vector, n = 3 experiments with 7 embryos, 717 neurons All data are expressed as mean +/- SEM.

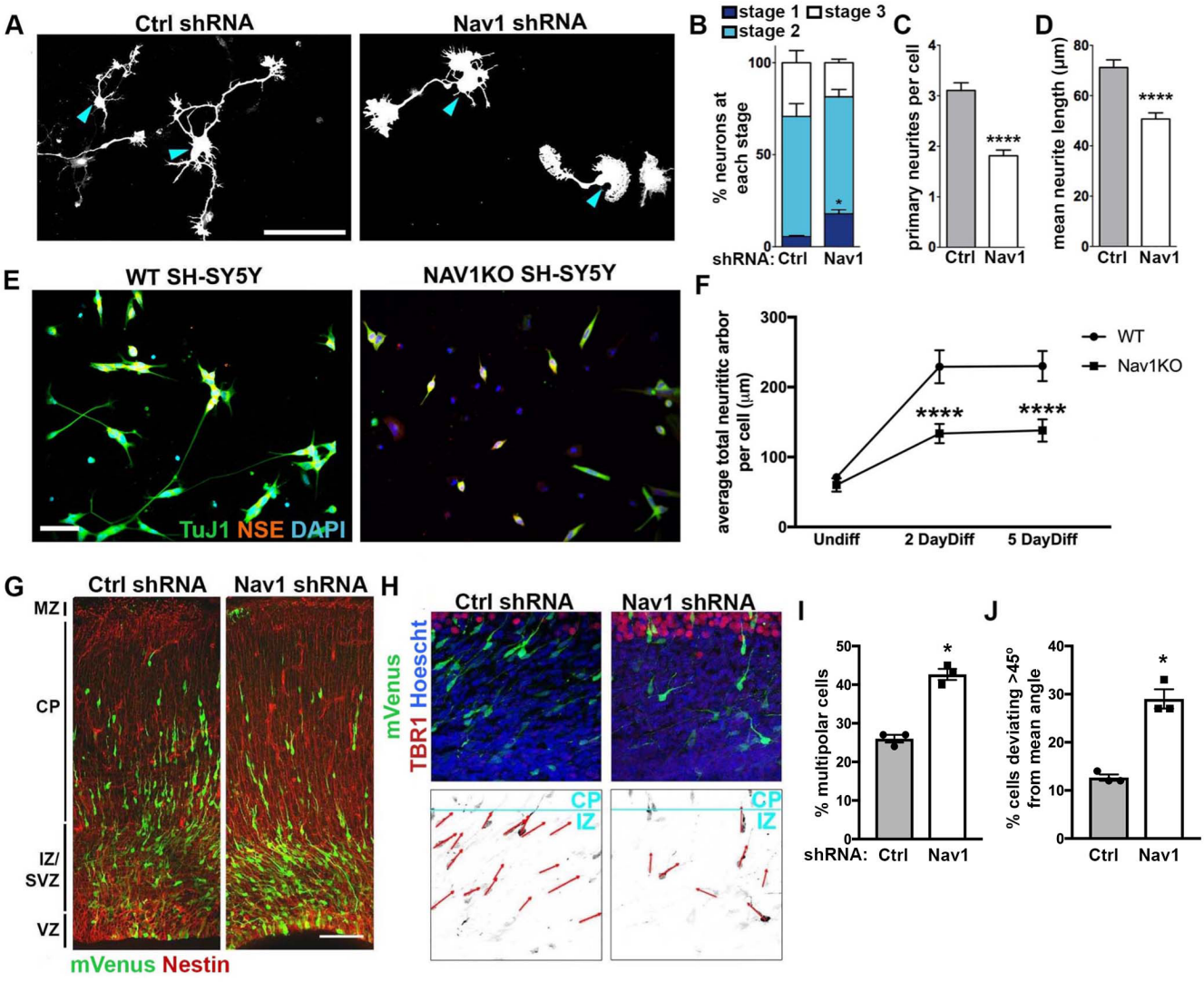
A
Ctrl shRNA
Nav1 shRNA
B
stage 1
stage 3
stage 2
% neurons at each stage
shRNA: Ctrl Nav1
C
primary neurites per cell
****
Ctrl Nav1
D
mean neurite length (µm)
****
Ctrl Nav1
E
WT SH-SY5Y
NAV1KO SH-SY5Y
TuJ1 NSE DAPI
F
average total neurititc arbor per cell (µm)
WT
Nav1KO
****
****
Undiff
2 DayDiff
5 DayDiff
G
Ctrl shRNA
Nav1 shRNA
MZ
CP
IZ/ SVZ
VZ
mVenus Nestin
H
Ctrl shRNA
Nav1 shRNA
mVenus
TBR1 Hoescht
CP
IZ
I
% multipolar cells
shRNA: Ctrl Nav1
J
% cells deviating >45° from mean angle
Ctrl Nav1

Consistent with a role in neurite initiation we observed that the average number of primary neurites per cell was significantly reduced by the partial Nav1 knockdown (Figure 2.4 C). The total length of neurite arbor was also modestly but significantly reduced, an effect that could result from reduced neurite initiation, reduced elongation, or both. Because the average neurite length was reduced in the knockdown condition (Figure 2.4 D), and the number of primary neurites was also reduced, it seems likely that Nav1 affects neurite elongation as well as neurite initiation.

Many primary hippocampal neurons begin emitting neurites within 4-6 hours of plating, making it difficult to ensure that genetic silencing is uniformly effective prior to the initiation of neuronal morphogenesis. Therefore, we created a Nav1knockout (Nav1KO) line using CRISPR/Cas9 in SH-SY5Y cells to examine the effect of complete Nav1 silencing on differentiation and neuritogenesis (Figure 2.5 B,C). As described above, differentiated SH-SY5Y cells emit neurites that grow longer over time. We differentiated WT and Nav1KO SH-SY5Y cells, and fixed and assessed them at various times post-differentiation. Nav1KO cells stopped dividing and displayed small neurites positive for TuJ1. However, they showed a significantly lower total neuritic arbor length at both differentiated time points measured, and no difference when undifferentiated (Figure 2.4 E, F).

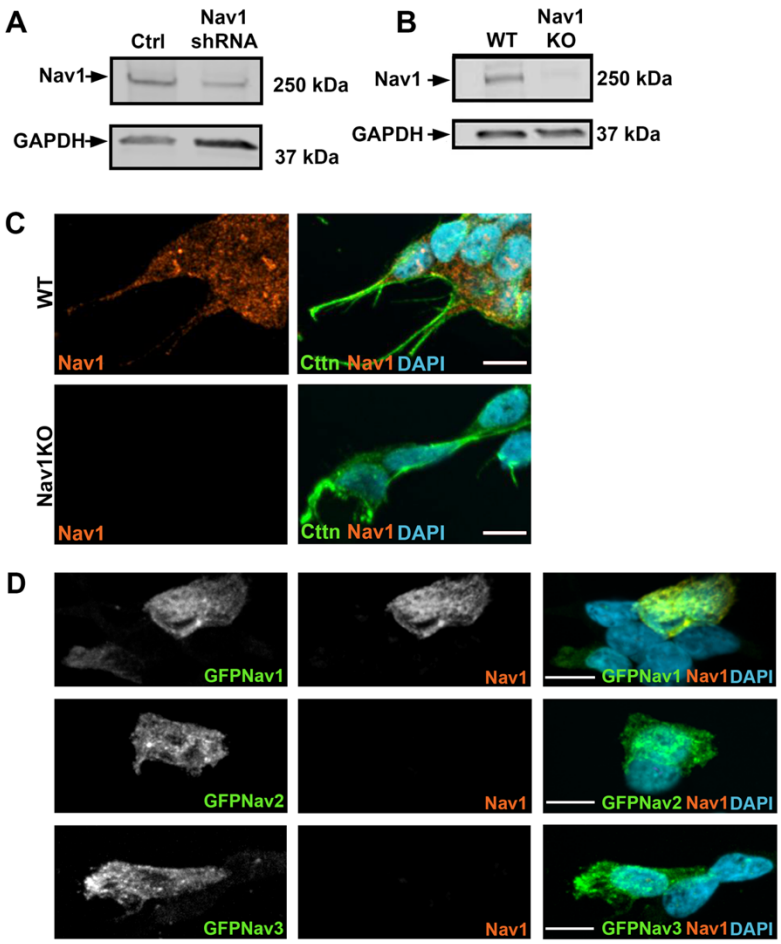

Figure 2.5: Validation of Nav1 gene silencing and antibody specificity. (A) Immunoblot demonstrating the partial knockdown of Nav1 by shRNA in N1E cells. Arrows indicate band at indicated size. (B) Immunoblot of WT and Nav1KO SH-SY5Y cells demonstrating the lack of detectable expression of Nav1 expression in cells where the Nav1 gene was silenced via CRISPR/Cas9 gene editing. Arrows indicate band at indicated size. (C) Representative images of undifferentiated WT and Nav1KO SH-SY5Y demonstrating the lack of detectable Nav1 fluorescence signal in the Nav1KO cells using identical image collection and display settings. (D) Representative images demonstrating Nav1 antibody recognizes only GFPNav1, not GFPNav2 or GFPNav3 that were nucelofected into Nav1KO SH-SY5Y cells. Scale bar = 10μm. Images represent observations from 3 individual culture preparations.

Nav1 deficiency disrupts neuronal morphogenesis *in vivo*

To corroborate the above observations that Nav1 depletion disrupts neuronal morphogenesis, we utilized *in utero* electroporation to introduce Nav1 shRNA and control shRNA constructs co-transfected with mVenus into neural progenitor cells in mouse neocortex at embryonic day E15.5. Labeled cells in the developing cortex were examined 3 days later, at E18.5. In brains of embryos treated with control shRNA, approximately two-thirds of the labeled cells had a bipolar morphology, and the remainder had a multipolar morphology. In contrast, the brains of knockdown embryos showed a significant increase in the fraction of multipolar cells, and a corresponding decrease in bipolar cells (Figure 2.4 G,I). When Nav1 knockdown neurons did display a bipolar morphology, they often appeared to be misoriented. In controls, labeled bipolar neurons within the SVZ and lower IZ had a prominent leading process that was oriented toward the pial surface, roughly perpendicular to the plane of the pial surface toward which it is expected to migrate. Instead, the leading process of Nav1-silenced neurons deviated substantially from the perpendicular angle and were not consistently oriented in similar directions (Figure 2.4 H,J). These data suggest that Nav1 is important for the proper orientation of neuronal morphology during cortical cell migration, possibly reflecting a failure to respond to external directional cues. Taken together, the disruption of neural morphogenesis with Nav1 depletion *in vitro* and *in vivo* demonstrate the importance of Nav1 in regulating early neuronal morphogenesis, but the question remained of the role of Nav1 at the growth cone and its influence during development.

Nav1 and EBs have distinct distributions within the growth cone

We more closely examined the distribution of Nav1 in the growth cone to gain insight into the role of Nav1 there. Where possible we took advantage of the occasional examples of especially large, well-spread growth cones in rat hippocampal cultures, where we could more readily distinguish sub domains of the growth cone, such as the central domain (C-domain) occupied by microtubules, and the F-actin rich peripheral domain (P-domain) [22]. Previous research shows that Nav1 is a +TIP protein that is frequently found on growing microtubule ends containing EB1 and/or EB3, and that Nav1 and EB binding is mediated by the Nav1 microtubule binding domain [40, 44]. Within neuronal growth cones, advancing microtubules often extend from the C-domain and frequently invade filopodia in the P-domain [52, 134, 148]. We observed that Nav1 immunoreactivity was often (but not always) associated with the tip of filopodial microtubules, as expected for a +TIP protein (Figure 2.6 A; yellow arrowheads). Such microtubules were recently polymerized and presumably dynamic, since they were immunopositive for tyrosinated tubulin (Figure 4B). However, Nav1 puncta could also be observed along the length of some microtubules (Figure 2.6 A; cyan arrowheads), as well as in filopodia that were devoid of detectable microtubules (Figure 2.6 A; white arrowheads). Thus, it appears that Nav1 is neither an obligatory nor an exclusive member of +TIP complexes in the growth cone.

Figure 2.6: Nav1 is a +TIP protein that associates with EB1 in the growth cone. (A) Growth cone stained for Nav1 and neuron-specific marker TuJ1 (ß -III tubulin). The white box indicates the region enlarged in three panels to the right. Note that Nav1 puncta are present at the tips of microtubules in the periphery of the growth cone. Yellow arrowheads indicate Nav1 puncta at the tips of individual microtubules; blue arrowheads indicate Nav1 puncta arrayed along microtubules; white arrowheads indicate Nav1 puncta not colocalized with detectable microtubules. (B) Nav1 localizes to the tips of newly polymerized microtubules (arrowheads) labeled with antibody to tyrosinated tubulin. (C) Growth cone immunostained for Nav1 and EB1. Note that the overall distribution of Nav1 is different from that of EB1; Nav1 puncta accumulate in the growth cone periphery, while EB1 puncta distribute more uniformly. Boxed regions are shown at higher magnification in (D). (D) Box 1 is zoomed region outlined by white rectangle, Box P (P-domain) and Box C (C-domain) outlined in yellow rectangles in (C). Note that of the three Nav1 puncta in box 1 (arrowheads) only one detectably colocalizes with EB1 (yellow arrowhead). Arrowheads in Box P indicate two intense Nav1 puncta that colocalize with intense EB1 puncta. Single arrowhead in Box C indicates a faint Nav1 punctum that colocalizes with an intense EB1 punctum. (Note that the display settings in zoomed regions are enhanced from those in b.) (E) Quantification of the relative concentration of endogenous EB1 and Nav1 at microtubule tips in the P-domain versus the C-domain. This assay indicates that Nav1 concentration at plus ends is greater in the P-domain compared to the C-domain. Statistical analysis: Mann-Whitney test; ***$p<0.001$; n = 3 experiments; P-domain = 234 comets; C-domain = 243 comets. a.u. = arbitrary units. All scale bars = 10μm. All data are expressed as mean +/- SEM. Images represent observations from 3 individual culture preparations.

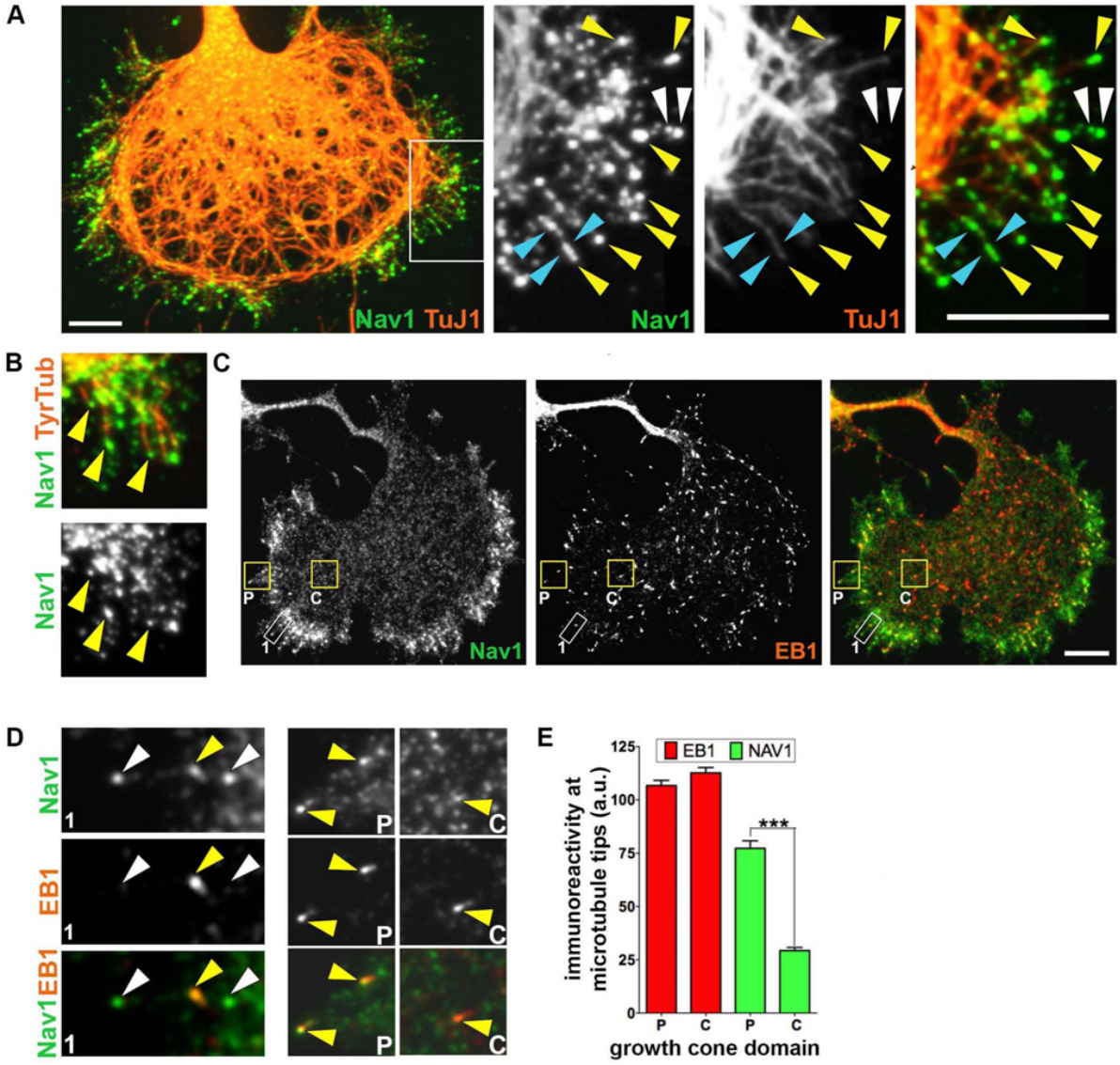
A
Nav1 TuJ1
Nav1
TuJ1
B
Nav1 TyrTub
Nav1
C
P
C
1
Nav1
EB1
D
Nav1
EB1
Nav1 EB1
E
EB1
NAV1
immunoreactivity at microtubule tips (a.u.)
125
100
75
50
25
0
***
P
C
P
C
growth cone domain

Indeed, endogenous Nav1 showed a distribution pattern in growth cones that was overall very different from that of EB1 and EB3. EB1 immunoreactivity was present as small, often comet-shaped puncta that were uniformly distributed throughout all domains of the growth cone (Figure 2.6 C). In contrast, endogenous Nav1 puncta were relatively enriched in the periphery of the growth cone (Figure 2.6 C). Similarly, the overall distribution of puncta of ectopic EB3-mCherry was fairly uniform throughout the growth cone, and distinct from that of ectopic GFP-Nav1 (Figure 2.7 A). In time-lapse imaging EB3-mCherry showed the dynamic, comet-like behavior that is characteristic of +TIP proteins [149]. Individual puncta that contained both EB3-mCherry and GFP-Nav1 moved in concert, and GFP-Nav1 puncta often invaded growth cone filopodia, as described previously for the EBs (Figure 2.7 B). Quantitative image analysis in fixed specimens revealed that endogenous Nav1 displayed a significantly higher coefficient of variation (CV) for its distribution profile across the growth cone compared to that for endogenous EB1 in the same cells (CV for Nav1 = 1.17 ± 0.02; CV for EB1 = 0.57 ± 0.02, n = 91 cells; Mann-Whitney test, $p<0.0001$), thereby confirming the distinct localization patterns of the two proteins. Despite their overall differences in distribution, endogenous EB1 and Nav1 frequently co-localized at specific puncta. Some puncta were positive for both EB1 and Nav1, while other Nav1 puncta in close proximity showed no detectable EB1 (Figure 2.6 C,D). It is possible these Nav1 puncta represent microtubules plus ends that have stalled and EB1 has fallen off, since Sanchez-Huertas *et al* [44] observed that Nav1 stays associated with plus ends after microtubule stalling. We also observed, though rarely, EB1 puncta without Nav1 (Figure 2.7 A cyan arrow). Taken together, these data suggest that Nav1 is selectively targeted to structures within the periphery of the growth cone, and are not exclusively found on growing microtubule ends.

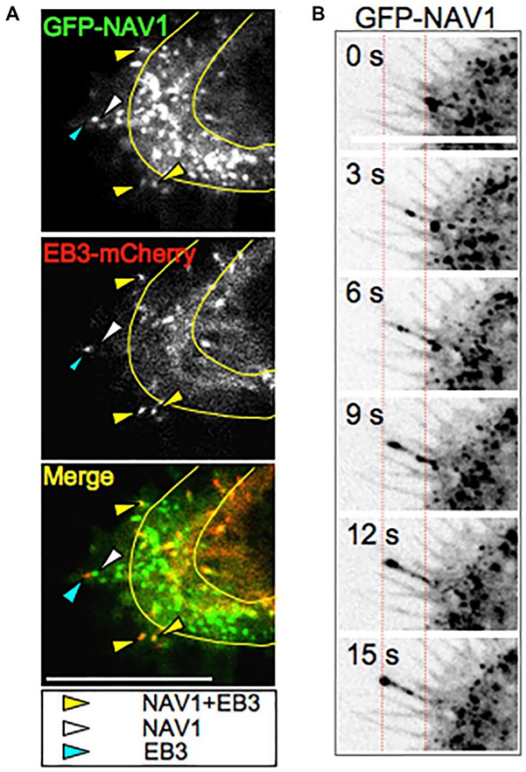

Figure 2.7: Nav1 associates with some EB3 puncta in the growth cone periphery. (A) Representative frame from a time-lapse sequence of a nascent growth cone cotransfected with GFP-Nav1 and EB3-mCherry. Yellow arrowheads indicate colocalized puncta of GFP-Nav1 and EB3-mCherry; white arrowhead indicates a GFP-Nav1 positive motile punctum lacking detectable EB3-mCherry; cyan arrowhead indicates an EB3-mCherry positive punctum lacking detectable GFP-Nav1. Transition zone (T-zone) is highlighted with a yellow line. Scale bar = 10μm (B) Time-lapse sequence of GFP-Nav1 in a nascent growth cone. Red dashed lines indicate the position in the first and last time points of a GFP-Nav1 motile punctum advancing from the T-zone and entering a filopodium in the peripheral domain. Scale bar = 10μm. Images represent observations from 3 individual culture preparations.

Differential Nav1 stoichiometry on growing microtubule ends in the growth cone

Specific targeting might enhance Nav1 association with the +TIP complex when polymerizing microtubules pass from the C-domain to the P-domain. We therefore quantified the mean intensity of Nav1 and EB1 immunofluorescence at individual microtubule plus ends in the C- and P-domain, which we presume reflects concentration of each molecule. We observed a nearly three-fold higher concentration of Nav1 on the P-domain localized plus ends compared to

the C-domain localized plus ends (Figure 2.6 E). In contrast, immunofluorescence intensity for EB1 on these same individual puncta did not differ between the two domains. These data suggest that the stoichiometry of Nav1 interaction with plus ends can vary, and that Nav1 is preferentially associated with plus ends in the periphery of the growth cone.

Nav1KO SH-SY5Y cells display transient membrane blebs that stem from dysregulation of the Rho/Rac pathway

Further observation of undifferentiated Nav1KO SH-SY5Y cells revealed that a portion of the cells displayed membrane blebs (Figure 2.8 A). These membrane blebs were surrounded by a ring of F-actin and contained immunoreactivity for tubulin, reminiscent of non-apoptotic membrane blebs described elsewhere [150-152]. Membrane blebs such as these occur when cortical F-actin disconnects from the plasma membrane, and the F-actin ring surrounding the blebs is thought to draw the plasma membrane back into the cell [150-152]. Observations of SH-SY5Y Nav1 KO cells via live imaging showed that blebs dynamically extended and retracted from the plasma membrane, and that periods of membrane blebbing were transient in any given cell. Time-lapse imaging over 24 hours indicated that, on average, 51% of Nav1KO cells displayed transient membrane blebs for periods of time (Figure 2.8 B, black arrows point to blebs). In contrast, blebbing cells were never observed in the WT line. In fixed samples we found that, on average, 12 percent of Nav1KO cells displayed membrane blebs (Figure 2.8 C). This suggests that the majority of cells undergo membrane blebs at some point over the course of time, and that fixed cells capture only a small portion of blebbing cells at any given moment. Together, these data suggest that Nav1 may be important for the proper connection of cortical actin and the plasma membrane, which is a previously undescribed role for Nav1.

A balance in the activities of RhoA and Rac1 is important for maintaining the cell cortex. Specifically, over-active RhoA or under-active Rac1 can lead to membrane blebbing [153, 154]. Therefore, we investigated the role of RhoA and Rac1 in the Nav1KO membrane blebs. To test the role of RhoA, we incubated Nav1KO cells with the Rho-kinase (a primary RhoA effector molecule) inhibitor Y-27632, and found it completely rescued the membrane blebs compared to DMSO-treated Nav1KO cells (Figure 2.8 D). To test the role of Rac1, we expressed an eGFP control or a constitutively active form of Rac1 (Rac1CA) in Nav1KO cells, and found that Rac1CA also completely rescued the membrane bleb phenotype (Figure 2.8 E). To ensure that the membrane blebs are attributable to the loss of Nav1 we performed a rescue experiment. Reintroduction of GFP-Nav1 to Nav1KO cells significantly decreased the number of cells with membrane blebs (Figure 2.8 F). These results collectively suggest that Nav1 promotes a proper balance in the Rho/Rac pathway, and that a Nav1 deficit results in overactive Rho-kinase and/or under-active Rac1, resulting in membrane blebs.

Figure 2.8: Nav1 KO cells reveal membrane blebs that indicate Nav1 regulates cortical actin dynamics via RhoA and Rac1 pathway. (A) Representative image of SH-SY5Y Nav1KO cells displaying membrane blebs. Arrows indicate peripheral blebs. Scale bar = 10μm (B) Representative montage of a transiently blebbing cell expressing GFP-Ftractin for a portion of a 24 hour live imaging experiment. Cell imaged every 30 minutes; time signature = hours:minutes. Scale bar = 10μm. (C) Nav1KO SH-SY5Y cells display significantly more membrane blebs than WT SH-SY5Y. Statistical analysis: Mann-Whitney, *$p<0.05$. n = 4 experiments, WT = 304 cells, KO = 310 cells. (D) 2 hour ROCK Inhibitor (RI) treatment prevents blebbing in Nav1KO cells compared to Nav1KO cells treated with DMSO. Statistical analysis: Mann-Whitney,***$p<0.001$. n = 6 coverslips from 3 experiments, DMSO = 634 cells, RI = 607 cells (E) Nav1KO cells transfected with constitutively active Rac1 (Rac1CA) do not display membrane blebs compared to eGFP transfected Nav1KO cells. Statistical analysis: Mann-Whitney, ***$p<0.001$; n = 7 coverslips from 3 experiments, eGFP = 230 cells, Rac1CA = 198 cells. (F) Electroporation of Nav1KO cells with GFP-Nav1 significantly reduced blebbing cells. Statistical analysis: Mann-Whitney, **$p<0.01$. n = 6 coverslips from 3 experiments, GFP = 343 cells, GFPNav1 = 259 cells. All data are expressed as mean +/- SEM. Images represent observations from 3 individual culture preparations.

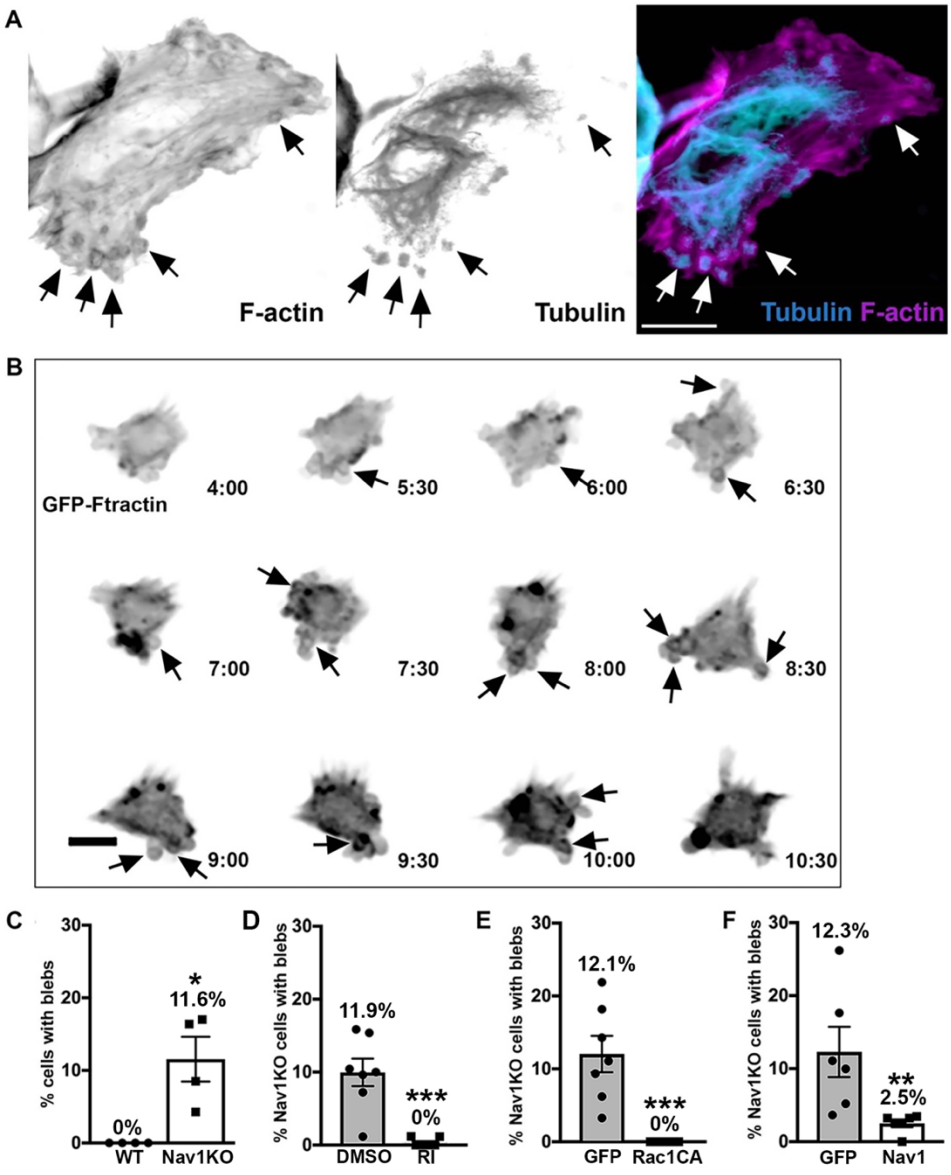
A
F-actin
Tubulin
Tubulin F-actin
B
GFP-Ftractin
4:00
5:30
6:00
6:30
7:00
7:30
8:00
8:30
9:00
9:30
10:00
10:30
C
% cells with blebs
0%
*
11.6%
WT
Nav1KO
D
% Nav1KO cells with blebs
11.9%
***
0%
DMSO
RI
E
% Nav1KO cells with blebs
12.1%
***
0%
GFP
Rac1CA
F
% Nav1KO cells with blebs
12.3%
**
2.5%
GFP
Nav1

Nav1 accumulates in and promotes F-actin rich membrane ruffles

Because we observed that a substantial portion of Nav1 puncta in the growth cone are not resident on growing microtubule ends and that Nav1 plays a role in actin organization in the cell periphery, we investigated in further detail the localization of Nav1 puncta in relation to actin-rich growth cone structures in hippocampal neurons. Immunoreactivity for endogenous Nav1 displayed a highly punctate pattern throughout the growth cone. However, Nav1 clusters of various sizes and shapes were usually enriched within the so-called transition zone (T-zone) (Figure 2.9 A,B), a growth cone region that lies between the microtubule-filled C-domain and the filopodia-filled P-domain [22, 155, 156]. The T-zone is less well studied than the other two; however, in addition to containing actin arcs [148] it is enriched in cortactin (Figure 2.9 B) and drebrin, which are actin binding proteins concentrated in active membrane ruffles [22, 136, 157, 158]. Ectopic GFP-Nav1 strongly co-localized with phalloidin labeled F-actin in sub-domains within the growth cone (Figure 2.9 C). With higher magnification we observed that, although there was not a perfect spatial overlap between GFP-Nav1 and phalloidin-labeled F-actin, clearly the most intense accumulations of GFP-Nav1 puncta corresponded to regions where phalloidin staining was similarly most intense (Figure 2.9 C, see zoomed region depicted in lower panels). In neurons co-transfected with GFP-Nav1 and mRFP1-actin, we observed that such regions dynamically changed size, shape, and location in a coordinated manner. In dynamic behavior these Nav1 and F-actin enriched regions were reminiscent of actin–rich membrane ruffles (Figure 2.10). We therefore conclude that Nav1 is highly enriched in membrane ruffles, and use this term to refer to these structures throughout this study.

Growth cones in SH-SY5Y cells are typically small, and we did not succeed in finding culture conditions to facilitate the development of large, well-spread growth cones. However, in

larger size growth cones in human iPSC-derived neurons where a T-zone could be discerned we observed clusters of Nav1 puncta enriched in the T-zone of the growth cone colocalized with cortactin (Figure 2.9 D), suggesting that T-zone accumulation of Nav1 puncta is a general feature.

Figure 2.9: Nav1 associates with and regulates F-actin membrane ruffles in the transition zone (T-zone) in the growth cone. (A) Cultured rat embryonic neurons were fixed on 3DIV and double labeled for endogenous Nav1 and ß-III tubulin (TuJ1). Growth cone domains borders are highlighted in solid yellow lines. Note the accumulation of endogenous Nav1 puncta within clusters in the T zone. Scale bar = 10µm. (B) Growth cone stained for endogenous Nav1 and the actin binding protein cortactin (Cttn), which is a marker of actin-rich membrane ruffles. Scale bar = 20µm (C) Growth cone from a stage 2 hippocampal neuron expressing GFP-Nav1, labeled for F-actin by Alex568-conjugated phalloidin. Boxed region is enlarged in panel directly below. Note that clusters of GFP-Nav1 puncta are enriched within the T-zone, and their concentration correlates with that of F-actin. Orange and blue solid lines indicate regions of moderate and intense concentrations, respectively, of F-actin, which correspond to membrane ruffles. Scale bars: upper panel 20µm, lower panel, 10µm (D) Differentiated human iPSC-derived neurons were fixed and double labeled for endogenous Nav1 and Cttn. Yellow lines indicate growth cone domain borders. Boxed region is enlarged in panel directly below. Black solid lines indicate membrane ruffle where both Cttn and Nav1 are enriched. Scale bar = 10µm. (E) GFP-Nav1 over-expression increases the number of F-actin ruffles per neuron. Mann-Whitney test, ****$p<0.0001$. n = 3 experiments; GFP transfected = 29 cells; GFP-Nav1 transfected = 30 cells. (F) Knockdown of endogenous Nav1 using shRNA decreases the number of F-actin rich membrane ruffles per neuron. Mann-Whitney test, ****$p<0.0001$. n = 3 experiments; Control and Nav1 shRNA = 70 cells each. (G) Two stage 1 neurons stained with Alexa568- conjugated phalloidin. Note that the cell transfected with GFP-Nav1 (“T”) shows large accumulations of F-actin within the periphery compared to the adjacent untransfected neuron (”U”). Scale bar = 20µm. All data are expressed as mean +/- SEM. Images represent observations from 3 individual culture preparations.

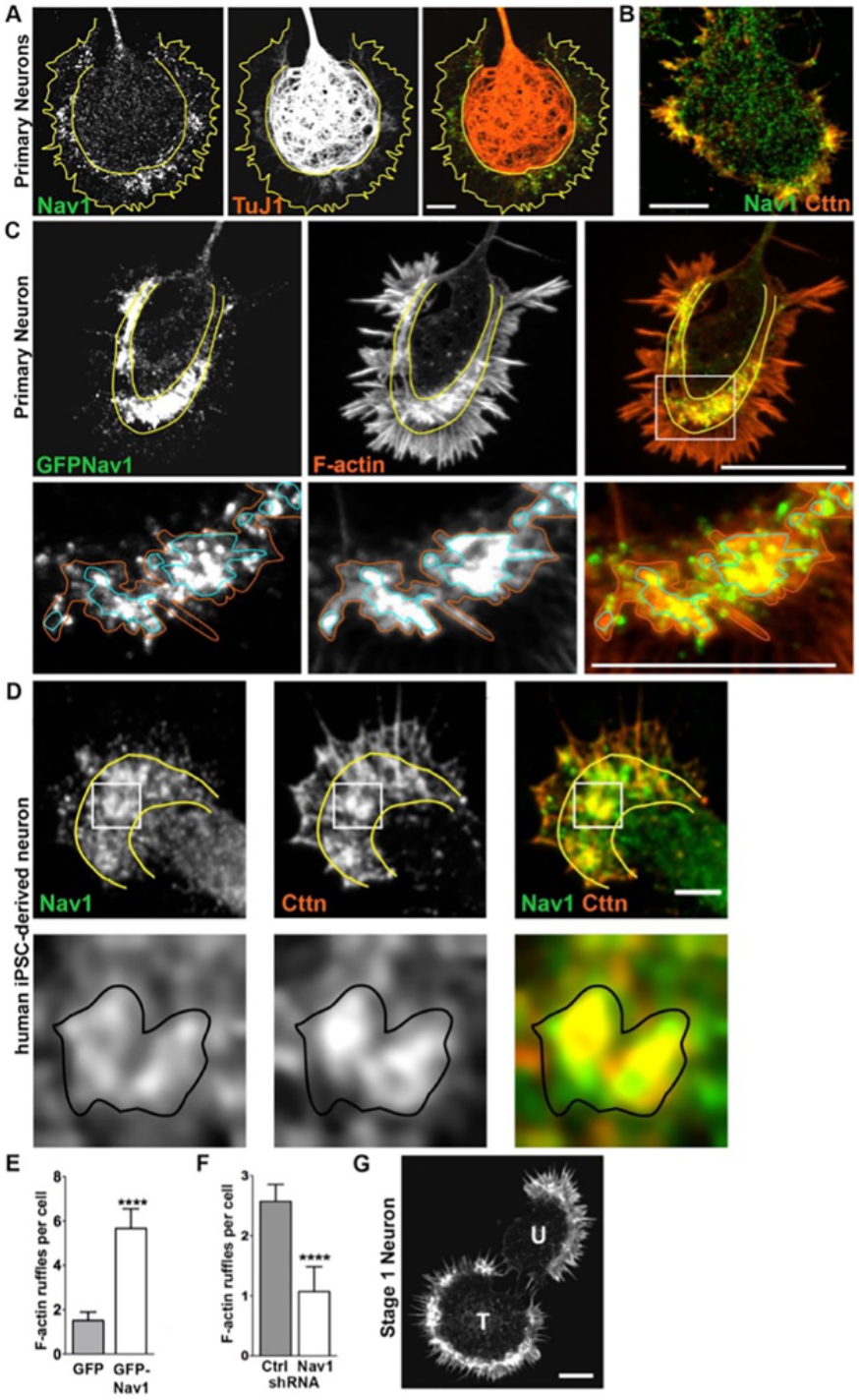
A
Primary Neurons
Nav1
TuJ1
B
Nav1 Cttn
C
Primary Neuron
GFPNav1
F-actin
D
human iPSC-derived neuron
Nav1
Cttn
Nav1 Cttn
E
F-actin ruffles per cell
****
GFP
GFP-Nav1
F
F-actin ruffles per cell
****
Ctrl shRNA
Nav1
G
Stage 1 Neuron
U
T

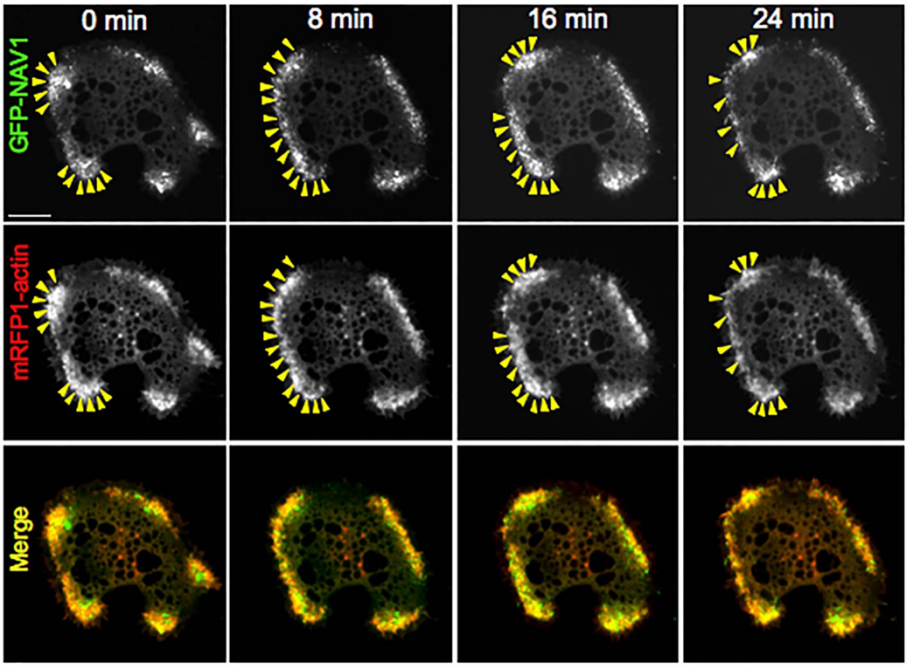

Figure 2.10: Nav1 and actin colocalize in stage 1 neurons. Time-lapse sequence from a neuron cotransfected with GFP-Nav1and mRFP1-actin; images were acquired every 8 minutes. Note that mobile clusters (arrowheads) containing GFP-Nav1 and mRFP1-actin reorganize in coordinated fashion. Scale bar = 20μm. Images represent observations from 3 individual culture preparations.

Strikingly, Nav1 not only accumulated in membrane ruffles in the T-zone but also regulated their presence. Expression of GFP-Nav1 in hippocampal neurons (which on average resulted in ~2.5- fold increase over endogenous levels) induced a significant increase in the number of actin-rich ruffles per cell (Figure 2.9 E). Endogenous Nav1 similarly regulates membrane ruffles, since shRNA against Nav1 induced a significant decrease in membrane ruffles compared to control neurons (Figure 6F). Interestingly, we also observed that stage 1 neurons (i.e., pre-neurite initiation) that expressed GFP-Nav1 displayed enriched F-actin in the lamellipodial region in membrane ruffles (Figure 2.9 G), suggesting that lamellipodial regions from which growth cones presumably emerge also display these Nav1-associated structures.

Collectively, these data indicate that Nav1 has a concentration-dependent effect on the presence of membrane ruffles in the developing growth cone.

Nav1-rich membrane ruffles are sites of bulk endocytosis

While growth cone membrane ruffles and similar dynamic actin-rich structures have been described previously [87, 159-161], their specific function at the growth cone is not well-defined. One function proposed for growth cone membrane ruffles in the early growth cone is non-clathrin mediated bulk endocytosis [87, 99]. We therefore used the lipophilic dye FM4-64 to examine endocytosis at the growth cone (Bonanomi *et al.*, 2008). This dye is readily endocytosed in a non-specific manner after attaching to the membrane [162]. As expected, we observed that FM4-64 is taken up in areas of the growth cone with F-actin membrane ruffles. To test whether enriched clusters of Nav1 puncta in the growth cone are sites of bulk endocytosis, we electroporated GFP-Nav1 and pcs-CeruleanMembrane-FP (to visualize the whole growth cone) into rat primary neurons, and repeated the FM4-64 experiments. Indeed, we found that FM4-64 uptake at the growth cone occurs where GFP-Nav1 and F-actin are enriched (Figure 2.11 A). Furthermore, we compared growth cones expressing GFP-Nav1 and pcs-CeruleanMembrane-FP to growth cones expressing pcs-CeruleanMembrane-FP alone, and found that growth cones expressing ectopic Nav1 showed significantly more FM4-64 uptake (Figure 2.11 B).

Figure 2.11: Nav1 promotes endocytosis at F-actin membrane ruffles. (A) Representative image of 3DIV hippocampal neurons transfected with GFP-Nav1 (green), pcs-CeruleanMembrane-FP (used to make yellow cell outline), incubated with FM4-64 (red), and incubated with Alexa647 conjugated Phalloidin (blue) demonstrates Nav1-enriched F-actin ruffles are sites of FM4-64 uptake. Arrow points to region enriched in GFP-Nav1, F-actin and FM4-64. Scale bar = 10µm (B) Growth cones expressing GFP-Nav1 and pcs-CeruleanMembrane-FP have significantly more FM4-64 uptake than growth cones just expressing pcs-CeruleanMembrane-FP. Statistical analysis: Mann-Whitney, **$p<0.01$. n = 4 experiments; Control = 69 growth cones GFP-Nav1 = 69 growth cones (C) Representative image of 3DIV stage 1 hippocampal neuron transfected with GFP-Nav1 (green) and incubated with FM4-64 (red) demonstrating that FM4-64 is taken up in GFPNav1 enriched areas (white arrows). Scale bar = 10µm (D) Representative image of 3DIV hippocampal neurons transfected with GFP-Nav1 (green) and pcs-CeruleanMembrane-FP (blue) and incubated with 568-conjugated transferrin (red). Scale bar = 10µm (E) There is no difference in transferrin intensity between GFP-Nav1 expressing and control growth cones. Statistical Analysis: Mann-Whitney test, n.s. = not significant. n = 4 experiments; Control = 34 growth cones, GFP-Nav1 = 42 growth cones (F) Representative image of 7 day differentiated WT and Nav1KO SH-SY5Y cells with phalloidin-labeled F-actin (green) and incubated with FM4-64 (red). Scale bar = 10µm, 5µm for zoomed image. (G) Nav1KO SH-SY5Y growth cones have less FM4-64 uptake than WT cells, as measured by FM4-64 intensity. Statistical analysis: Mann-Whitney, ***$p<0.001$. n = 4 experiments; WT = 185 growth cones, KO = 116 growth cones. (H) Representative images of 7 day differentiated WT and Nav1KO SH-SY5Y cells with phalloidin-labeled F-actin (red) and incubated with transferrin (red). Scale bar = 10µm, 5µm for zoomed image. (I) There is no significant difference in transferrin intensity between WT and Nav1KO SH-SY5Y cells. Statistical analysis: Mann-Whitney, n.s. = not significant. n = 4 experiments; WT = 83 growth cones, KO = 59 growth cones. All data are expressed as mean +/- SEM. Images represent observations from 3 individual culture preparations.

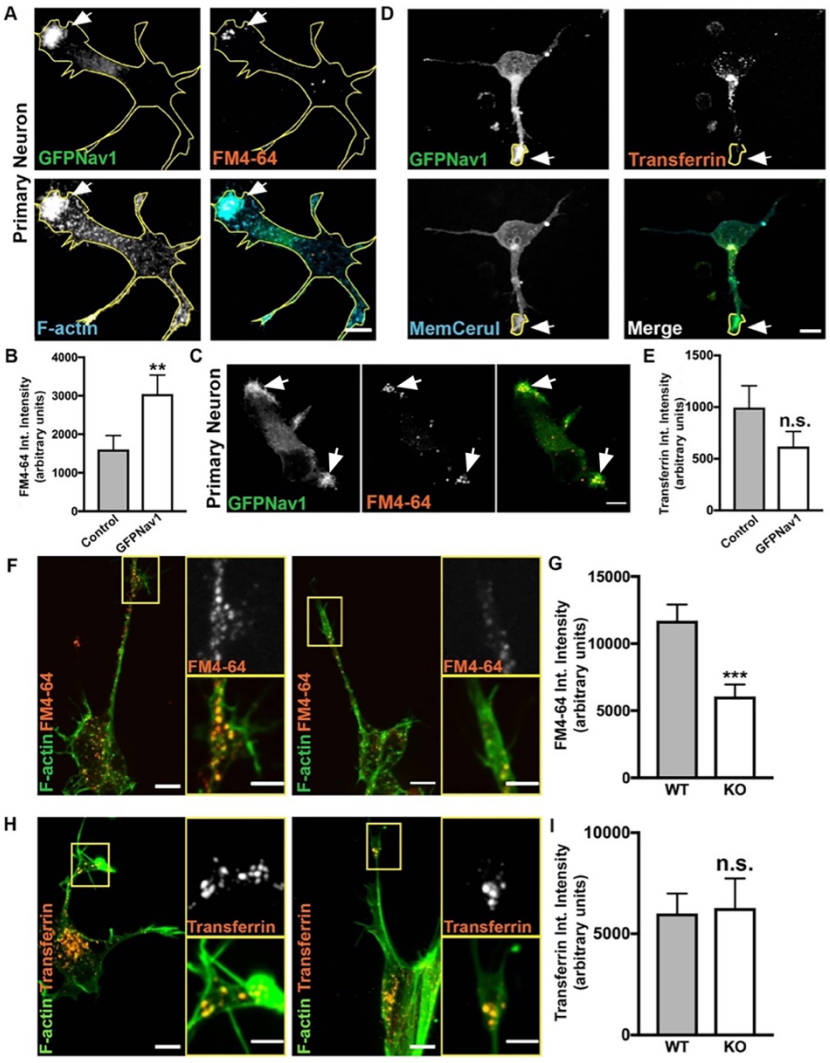
A
Primary Neuron
GFPNav1
FM4-64
F-actin
D
GFPNav1
Transferrin
MemCerul
Merge
B
FM4-64 Int. Intensity (arbitrary units)
4000
3000
2000
1000
0
**
Control
GFPNav1
C
Primary Neuron
GFPNav1
FM4-64
E
Transferrin Int. Intensity (arbitrary units)
1500
1000
500
0
n.s.
Control
GFPNav1
F
F-actin FM4-64
FM4-64
F-actin FM4-64
FM4-64
G
FM4-64 Int. Intensity (arbitrary units)
15000
10000
5000
0
***
WT
KO
H
F-actin Transferrin
Transferrin
F-actin Transferrin
Transferrin
I
Transferrin Int. Intensity (arbitrary units)
10000
5000
0
n.s.
WT
KO

When we observed stage 1 neurons, we found that they, too, had FM4-64 uptake at Nav1 enriched peripheral membrane ruffles (Figure 2.11 C), suggesting that Nav1-promoted endocytosis occurs from the earliest stages of neuronal development. We also found that GFP-Nav1 expressing growth cones displayed significantly higher intensity of pcs-CeruleanMembrane-FP, suggesting that Nav1 may promote membrane accumulation (Figure 2.12 A,B). These data suggest a novel role of Nav1 in regulating bulk endocytosis and membrane recycling at the growth cone.

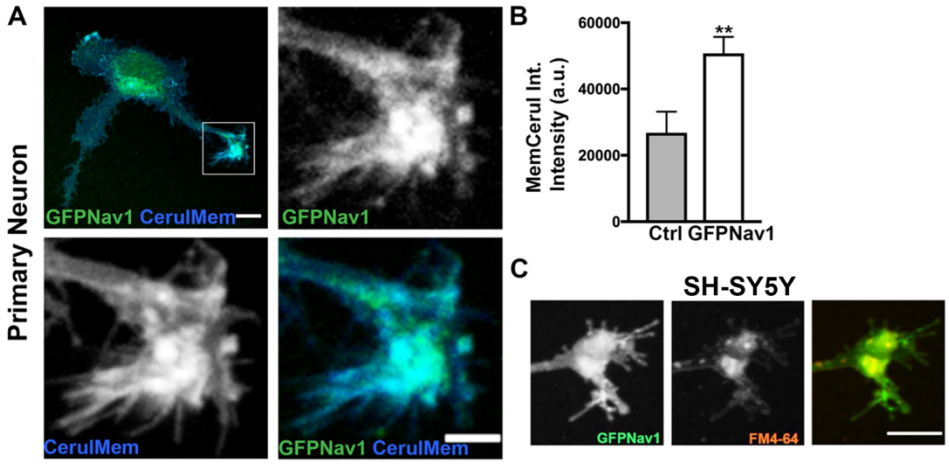

Figure 2.12: GFP-Nav1 promotes endocytosis and membrane accumulation. (A) Representative image of growth cone showing enriched pcs-membrane-cerulean-FP in the same growth cone areas where GFP-Nav1 is enriched. White box indicates growth cone. Scale bars = 10µm for large image, 5µm for zoomed image. (B) GFP-Nav1expressing growth cones have significantly higher intensity of pcs-CeruleanMembrane-FP than control growth cones. Statistics: Mann-Whitney, **p<0.01, n = 4 experiments; Control = 52 growth cones, GFP-Nav1 = 142 growth cones GFP-Nav1. (C) Representative image showing FM4-64 is taken up in GFP-Nav1-expressing WT SH-SY5Y growth cone. Scale bar = 10µm. Images represent observations from 3 individual culture preparations.

To test whether Nav1 promotion of endocytosis is specific to non-clathrin mediated endocytosis, we tested uptake of transferrin in primary neurons, as transferrin is taken up exclusively by clathrin-mediated endocytosis [163]. We found no difference in transferrin uptake in

GFP-Nav1 expressing neurons compared to control (Figure 2.11 D,E). Furthermore, there were substantially fewer GFP-Nav1-transfected or untransfected growth cones with any detectable transferrin uptake compared to growth cones exhibiting FM4-64 uptake (GFP-Nav1 transfected growth cones: 60% FM4-64 uptake, 26% transferrin uptake; untransfected growth cones: 40% FM4-64 uptake, 14% transferrin uptake). Our results are consistent with the previous conclusion that clathrin-mediated endocytosis is not a predominant means of endocytosis in the neuronal growth cone during early morphogenic stages [87].

We also confirmed that endocytosis occurs in F-actin rich and GFP-Nav1 enriched membrane ruffles in differentiated SH-SY5Y cell growth cones (Figure 2.12 C), and found that a significantly lower amount of FM4-64 was taken up in growth cones in the Nav1KO cells compared to WT controls (Figure 2.11 F,G). This directly implicates endogenous Nav1 in endocytosis at the growth cone. We also compared transferrin uptake in growth cones of WT versus Nav1KO SH-SY5Y cells, and found no difference between the two lines (Figure 2.11 H,I). Altogether, our Nav1 gene silencing and overexpression data demonstrate that Nav1 specifically promotes non-clathrin-mediated endocytosis in growth cones.

Nav1 promotes macropinocytosis

We hypothesized that the Nav1-regulated endocytosis occurring at the growth cone is the same form of micropinocytosis identified by Bonanomi *et al* [87]. To test this hypothesis, we first ectopically expressed GFP-Nav1 in primary neurons, and incubated them with high molecular weight (70kDa) dextran, uptake of which is a marker of macropinocytosis [164]. We found that 70kDa dextran is indeed taken up in Nav1-enriched growth cones membrane ruffles (Figure 2.13 A). Next, we blocked some reported molecular components of macropinocytosis to test whether

that would decrease GFP-Nav1-mediated FM4-64 uptake. First, we used methyl-β-cyclodextrin (MβCD) to deplete cholesterol and found that this treatment significantly decreased FM4-64 uptake in GFP-Nav1-expressing neurons (Figure 2.13 B). Macropinocytosis is also reliant on phosphoinositide-3 kinase (PI3K) [118, 165], and indeed we observed that the PI3K inhibitor LY294002 significantly decreased the percentage of growth cones that had FM4-64 uptake (Figure 2.13 C). Together, the uptake of 70kDa dextran at GFP-Nav1-enriched growth cones, along with the requirement of cholesterol and PI3K for FM4-64 uptake in the presence of GFP-Nav1 strongly supports the conclusion that Nav1 promotes a macropinocytosis form of bulk internalization at the growth cone.

Figure 2.13: Nav1 promotes macropinocytosis and growth factor internalization at the growth cone. (A) Representative image of 3DIV hippocampal neurons transfected with GFP-Nav1 (green) and pcs-CeruleanMembrane-FP (blue) and incubated with 70kDa Dextran (red) showing high molecular weight dextran is taken up in Nav1-enriched growth cones. Scale bar = 10μm and 5μm for zoomed images. (B) MβCD treatment of GFP-Nav1 transfected primary neurons decreases FM4-64 uptake in growth cones. Statistical analysis: Mann-Whitney, **$p<0.01$. n = 3 experiments; Control = 46 growth cones, MβCD = 53 growth cones. (C) PI3 kinase inhibition of GFP-Nav1 transfected primary neurons decreases the number of growth cones with FM4-64 uptake. Statistical analysis: Mann-Whitney, *$p<0.05$, n = 4 experiments, DMSO = 199 growth cones, PI3K Inhib = 179 growth cones. (D) Growth cones of primary neurons expressing GFP-Nav1 have significantly more TrkB internalization by intensity than control growth cones. Statistical analysis: Mann-Whitney, *$p<0.05$. n = 3 experiments; Control = 61 growth cones, GFP-Nav1 = 60 growth cones (E) Growth cones of primary neurons expressing GFP-Nav1 have significantly more TrkB internalization by percent area occupied than control growth cones. Statistical analysis: Mann-Whitney, ***$p<0.001$, n same as (D). (F) Representative images of control and GFP-Nav1 primary neurons, expressing pcs-CeruleanMembrane-FP or GFP-Nav1 and pcs-CeruleanMembrane-FP, respectively, after internalization of the TrkB 1D7 antibody. Scale bar = 10μm, 5μm for zoomed images. (G) Representative western blot of 4 day retinoic acid differentiated WT and Nav1KO SH-SY5Y cells showing a double band (arrows indicate each band of doublet) for TrkB. GAPDH included as a loading control. All data are expressed as mean +/- SEM. Images represent observations from 3 individual culture preparations.

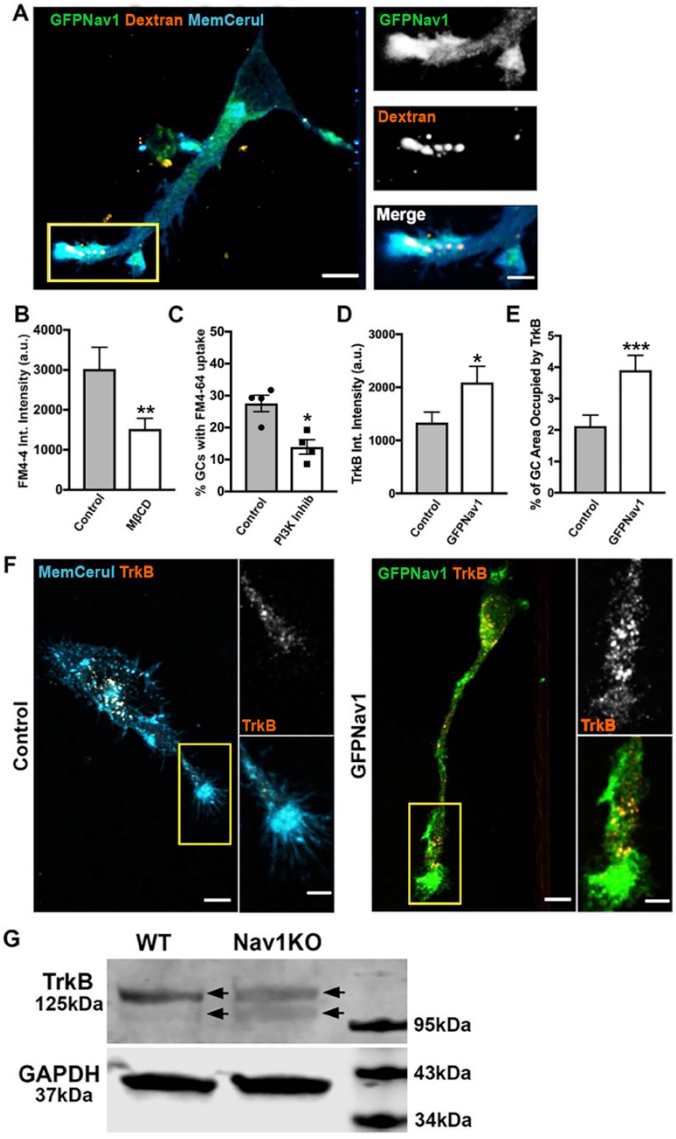
A
GFPNav1 Dextran MemCerul
GFPNav1
Dextran
Merge
B
FM4-4 Int. Intensity (a.u.)
4000
3000
2000
1000
0
**
Control
MβCD
C
% GCs with FM4-64 uptake
50
40
30
20
10
0
*
Control
PI3K Inhib
D
TrkB Int. Intensity (a.u.)
3000
2000
1000
0
*
Control
GFPNav1
E
% of GC Area Occupied by TrkB
5
4
3
2
1
0
***
Control
GFPNav1
F
MemCerul TrkB
Control
TrkB
GFPNav1 TrkB
GFPNav1
TrkB
G
WT
Nav1KO
TrkB
125kDa
95kDa
GAPDH
37kDa
43kDa
34kDa

Nav1 regulates internalization of TrkB in growth cones

The function of endocytosis within growth cone membrane ruffles remains poorly characterized. Previous studies showed that Nav1 is critical for the neurite outgrowth response to the guidance cue netrin [44, 45]. Netrin is one of many guidance cues that direct axon outgrowth and neuronal migration via signaling to the cytoskeleton. Such cues activate a variety of receptors, and some are internalized via endocytosis while others are not [166]. TrkB is a receptor for the growth factor BDNF, is taken up to influence cell growth and differentiation, and can be internalized via macropinocytosis [96, 166, 167]. Because of this, we hypothesized that Nav1 might promote internalization of the BDNF receptor TrkB, which provides critical signals for neuronal morphogenesis and function. To test this hypothesis, we used the 1D7 TrkB antibody, which can be applied to live cells, internalized, then visualized via imaging [168]. We found that ectopic expression of GFP-Nav1 lead to a significant increase in TrkB uptake at hippocampal growth cones (Figure 2.13 D-F). These data demonstrate that Nav1 promotes endocytosis of growth factors important for neuritogenesis.

To test whether this internalization difference could be due to altered expression of TrkB, we performed western blots in differentiated SH-SY5Y cells. We found no quantitative difference in TrkB expression levels, but, interestingly, we observed that while TrkB immunoreactive signal appeared as a doublet in lysates from both WT and Nav1KO cells, the lower band from the WT cells was notably fainter than that in the Nav1KO cells (Figure 2.13 G).

DISCUSSION

Nav1 is enriched in pathfinding axons and areas of morphological change to promote neuritogenesis and growth cone formation

Previous research and the data presented in this paper demonstrate that Nav1 is a cytoskeleton-associated protein, able to influence actin dynamics in multiple settings, including neural development [26, 40, 44, 49]. Dysregulation of the cytoskeleton is implicated as an underlying mechanism associated with many neurodevelopmental disorders, including lissencephalies, ASD, and intellectual disability [1, 3, 169, 170], underscoring the complex and precise cytoskeletal regulation necessary for early brain development.

Here we show that Nav1 is enriched in areas where rapid cell morphogenesis occurs, including pathfinding axons *in vivo* as well as in the cell periphery and distal neurites in multiple neural cell types: primary rodent neurons, differentiated SH-SY5Y cells, and human iPSC-derived neurons. Additionally, we show that reduction of Nav1 via shRNA-knockdown or complete knockout inhibits neuritogenesis in primary neurons and SH-SY5Y cells, respectively. Defective neuritogenesis after Nav1 knockdown was demonstrated previously in neuroblastoma cells [49], and defective neurite outgrowth in response to netrin was also shown [44, 45]. However, our study is the first to show that neurite initiation, in addition to elongation, is affected in neurons with Nav1 depletion. We also provide evidence for altered morphology and guidance after Nav1 knockdown *in vivo*. A growing body of evidence thus implicates an integral role for Nav1 in the cell's ability to organize the cytoskeleton to properly produce, elongate, and guide functional neurites during differentiation.

Nav1 promotes cortical actin-membrane association via Rho-GTPase signaling

We demonstrated that Nav1-knockdown induces non-apoptotic transient membrane blebbing that denotes a disruption in the cortical actin-membrane association. Membrane blebs in the Nav1KO cells were rescued by either Rho-kinase inhibitor or introduction of a constitutively active Rac1, suggesting that disrupted Rac1 and Rho-kinase signaling contribute to membrane blebbing in the Nav1KO cells. Nav1 has been shown to promote Rac1 activation in the context of neuritogenesis via the guanine nucleotide exchange factor (GEF) Trio [49], a gene that has been implicated in autism [171]. It is therefore logical that a total knockout of Nav1 would disrupt Rac1 signaling. Furthermore, Rac1 and Rho-kinase often have opposite effects on cytoskeleton dynamics in a variety of cellular processes [153, 172-174], and disruption of Rho signaling has been shown to cause membrane blebs in other cell types [47, 152, 175, 176]. These data suggest that Nav1 may have a larger influence on Rho signaling than previously known, and suggest a novel connection among Nav1, the cytoskeleton, and regulation of the plasma membrane. Furthermore, a recent paper demonstrated that RhoA signaling in tuberous sclerosis patient-derived iPSCs regulates cue-guided axon extension downstream of the causative gene TSC2 [177]. This highlights the necessity of proper regulation of Rho signaling in the growth cone during neural development, and our data suggests Nav1 may contribute to this regulation.

Nav1 is associated with +TIPs in the growth cone

In accordance with previous studies, we confirm that Nav1 tracks growing microtubule ends in association with EB in the growth cone [40, 44, 45, 49]. Importantly, we observe a significantly higher concentration of Nav1 on individual microtubule plus ends in the P-domain versus the C-domain. This suggests that Nav1 stoichiometry can potentially vary on microtubule plus ends, an

observation that warrants further study. Our observations are consistent with the hypothesis that the T-zone serves as a reservoir for Nav1 and thereby enhances Nav1's binding to the +TIP complex as microtubules polymerize toward the growth cone periphery, and suggest that microtubules could be one of the Nav1 effectors that regulate subcellular reorganization during growth cone morphogenesis. Microtubules and +TIP proteins can aid in delivery of necessary molecules for growth factor response signaling to the growth cone periphery, and can also influence a diversity of cellular processes [53, 130, 178]. For example, neurotrophin receptors are incorporated into early endosomes in the growth cone and then retrogradely transported on microtubules [179]. Thus, we speculate that the peripheral Nav1-occupied microtubule plus ends may represent a subset poised for endosomal transport at sites of uptake.

Nav1 accumulates in and regulates T-zone F-actin rich membrane ruffles and endocytosis

The transition zone of the growth cone is of potential importance for multiple functions for growth cone guidance. The T-zone may act as a microtubule barrier, permitting only a select set of pioneering microtubules to advance to the growth cone periphery [50, 180]. This "gatekeeper" function may represent a key regulator of signaling to influence growth cone morphological changes [50, 180]. The T-zone is also a site of membrane recycling, ensuring that membrane is available for dynamic changes in the growth cone [87, 99]. We observed that clusters of Nav1 puncta are enriched specifically in the actin-rich regions of the T-zone, and that these actin-rich accumulations resemble membrane ruffles. Furthermore, we demonstrated that Nav1 promotes actin ruffles in the T-zone, indicating that Nav1 may promote the formation or persistence of the ruffles.

The function of growth cone membrane ruffles is relatively uncharacterized, but in non-neuronal cell types, membrane ruffles are associated with actin-remodeling and cell migration [139, 181, 182]. Prior evidence suggests that growth-cone membrane ruffles are sites of bulk endocytosis, and that the endocytosis is necessary for neurite outgrowth [87]. We observed patches of enriched F-actin as sites of non-clathrin mediated, but not clathrin-mediated, endocytosis in our rat primary neuron cultures, and we demonstrated that Nav1 promotes endocytosis in these regions. This is a novel mechanism by which Nav1 may influence neuritogenesis. There are several mechanisms by which Nav1 might promote endocytosis, and this presents an opportunity for further research. For example, as described above, Nav1 promotes Rac1 activation through its activation of the GEF Trio [49], and Rac1 promotes membrane ruffles [84], as well as bulk endocytosis [84, 87, 174]. Moreover, Rac1, along with other Rho-family proteins, plays an important role in endocytosis regulation. Therefore, we postulate that one key function of Nav1 is to influence non-clathrin mediated endocytosis via its interaction with Trio. It is also possible that Nav1 influences endocytosis by promoting actin polymerization at the membrane, which in turn promotes endocytosis. A recent study reported that Nav1 and actin may interact directly via the +TIP binding domain [44]. Thus, Nav1 might stimulate endocytosis through direct binding to F-actin as an additional or an alternative means to its regulation of Rac1. Furthermore, microtubule polymerization has been shown to be important for macropinosome function; nocodazole treatment in HeLA cells and HT1080 cells, a human fibrosarcoma cell line, blocks fluid-uptake by macropinocytosis [120]. Therefore, we postulate that Nav1 is in a unique position to influence both actin and microtubules during macropinocytosis, and may serve as a cross-linker between the two molecules to regulate macropinocytic uptake.

Other dynamic actin-rich structures have been described in the growth cone literature. Inductapodia are dynamic actin-rich structures that form in *Aplysia* growth cones as localized sites where the growth cone plasma membrane engages integrin-dependent cell adhesion molecules [24, 159, 160], and their formation is dependent upon Rac1 activity [159]. Intrapodia are described in rodent sensory neurons as actin-rich structures of unknown function that form spontaneously in the growth cone membrane at microtubule tips [161]. Further research is required to determine what relationship, if any, such structures have to the actin-rich membrane ruffles described here and in Bonanomi *et al* [87].

The function of membrane ruffle-associated macropinocytosis is not well understood, but our data suggest a novel connection to neurotrophin signaling. Macropinocytosis reportedly facilitates growth cone collapse during negative guidance cue-induced axon repulsion [123-125]. We found that ectopic expression of Nav1 significantly increased the growth cone uptake of TrkB, the receptor for the positive growth and guidance cue BDNF. TrkB is endocytosed via both clathrin mediated endocytosis [90, 183], and clathrin-independent macropinocytosis [88, 96]. Our study implicates Nav1 in non-clathrin mediated macropinocytic TrkB uptake as a mechanism by which Nav1 promotes neuronal responses to growth and guidance cues. Indeed, we found that SH-SY5Y Nav1 KO cells were defective in BDNF-stimulated neuritogenesis. Our data adds to the body of evidence that the navigators are key regulators of cellular response to extracellular guidance cues. UNC-53, the *Caenorhabditis elegans* navigator homolog, has been implicated in pathfinding of motor neuron axons and migration of multiple other cell types, including an interaction with the GRB2 adaptor homolog SEM-5 that mediates FGF signaling in migrating sex myoblasts [29], Furthermore, Nav1 has been shown to mediate directionality of axon outgrowth

in response to Netrin [44, 45]. These data together with our observations suggest the navigators play an important role in multiple guidance cue response pathways.

Our immunoblot results suggest that Nav1 gene silencing causes an alteration in the molecular properties of the BDNF receptor TrkB. The observed alteration in the relative mobility of TrkB in SDS-PAGE suggests that one or more transcriptional, translational, or post-translational modifications is somehow under Nav1's control, which is an interesting topic for further investigation. As a receptor tyrosine kinase, TrkB becomes autophosphorylated on multiple tyrosine residues upon ligand engagement and activation [184], a step that is essential for recruitment of downstream effectors to mediate cell signaling for neuronal survival and growth [185]. Additionally, TrkB is phosphorylated by Cdk5 on Serine478, which is essential for BDNF promotion of dendritic growth and long-term potentiation of synaptic plasticity [89, 186]. Phosphorylated TrkB receptor-mediated intracellular signaling is integral to neuronal survival and neurite outgrowth [167], and this therefore represents a potential downstream role for Nav1. Furthermore, it has been shown that endocytosis of TrkB receptors is necessary for directional migration of cerebellar granule cell precursors in response to BDNF [91]. In this manner, disruption of Nav1-mediated TrkB endocytosis may explain the leading-process misorientation phenotype we observed upon Nav1 reduction in developing mouse cortex. The importance of tight regulation of neurotrophin endocytosis for neural morphogenesis during brain development and the role of Nav1 in these processes opens up an exciting avenue of research.

METHODS

Reagents

Pharmacological compounds were obtained from the following sources: Rho Kinase Inhibitor (Tocris). Retinoic Acid (Sigma), Brain-derived neurotrophic factor (BDNF) (Peprotech), Methyl-β-Cyclodextrin (MβCD) (Sigma), phosphoinositide-3 kinase (PI3Kinase) inhibitor LY294002 (Selleck Chemicals).

Table 2.1 Target and primer sequences

Reagent	**Sequence**
Nav1 crRNA	GATATGGCCAAGGCGCCCAA
Forward primer for cut site amplification	CCAACCTGCGCAAGCAGAAGTCA
Reverse primer for cut site amplification	CCTGGAAGAGCGAGTGCTCCG
Nav1 shRNA target	GGATCAAGGTTCATGGACA

Plasmids

mRFP-β-actin [187], GFP-Ftractin (gift from Dr. H. Higgs), GFP-Nav1 [45], GFP-Nav2 and GFP-Nav3, gifts from Dr. N. Galjart [40], mVenus [188], pECFP-Rac1Q61L (gift from Dr. K. Yamada, Addgene #105292), pEGFP-N1 (Clontech), pCS-membrane-ceruleanFP (kind gift from Dr. S. Megason, Addgene #53749), EB3mCherry (kind gift from M. W. Davidson). Nav1 shRNA was inserted into the pSuper vector according to manufacturer's instructions (Oligoengine) (Table 2.1).

Cell Culture and Differentiation

All cell lines and primary neurons were cultured at 37°C and 5% CO_2. N1E-115 cells were cultured in Dulbeco's modified Eagles medium (DMEM; Gibco) supplemented with 10%

(v/v) fetal bovine serum (FBS; Atlanta Biologicals S11150). SH-SY5Y (ATCC CRL-2266) cells were cultured in DMEM/F12 1:1 with 25mM HEPES, 10% heat inactivated FBS, and penicillin/streptomycin. The SH-SY5Y differentiation protocol was modified from Encinas *et al* [146]. Once undifferentiated SH-SY5Y cells reached 90% confluency, they were rinsed once with PBS, and then RA media (DMEM/F12 with 0.5% FBS, and 10μM Retinoic Acid) was added. RA media was changed on day 2 of differentiation, and were replated on day 4 using StemPro accutase (Life Technologies); cells were seeded at 394 cells/mm^2 on ibidi μ-Plate 24 well (82406) coated with 200μg/mL poly-(D)-lysine overnight at room temperature. Cells were cultured in RA media for 24 hours after re-plating, and then media was changed to BDNF media (DMEM/F12 and 50ng/μL BDNF), with half media changes every other day. Nucleofected SH-SY5Y cells were plated into 6 well plates dishes for 24 hours to recover, and then cells were seeded at 394 cells/mm^2 on ibidi μ-Plate 24 well coated with 100μg/mL poly-(D)-lysine, and fixed 24 hours later. Human iPSCs were purchased from Cellular Dynamics (iCell GlutaNeurons R1061), and cultured per the manufacturer's protocol. Primary hippocampal cultures were prepared from embryonic day 19 rat brains as described [189]. For fixed primary neuron experiments (except FM4-64 experiments), cells were plated on coverslips coated with poly-(D)-lysine (Sigma 100ug/mL) at a density of 375 cells/mm^2.

Transfection methods

Nucleofection of cultured cells. Dissociated primary neurons and undifferentiated SH-SY5Y cells were electroporated, prior to plating, using either Lonza Nucleofector 2b, or Lonza 4D-Nucleofector core unit, according to manufacturer's protocol.

Lipofection of cultured cells. N1E-115 cells and SH-SY5Y cells (Rac1Q61L experiment and membrane blebs live imaging) were transfected using either Lipofectamine 2000 or 3000 (ThermoFisher Scientific), respectively, according to the manufacturer's protocol. Nav1 shRNA and control vector were incubated for 3 days, all other constructs were incubated for 24 hrs.

In utero electroporation. Electroporation was performed as previously described [190]. Endotoxin-free plasmid DNA was injected at a concentration of 1 μg/μl in the lateral ventricles. mVenus was co-electroporated at a 2:1 ratio to the pSuper empty vector or Nav1 shRNA to verify that fluorescent neurons were electroporated with the DNA of interest. Electroporation was performed with gold-coated paddles at E15.5 to target cortical layer 2/3. The electroporation settings were: 4 pulses of 45V for 50 ms with 500 ms interval.

Nav1 antibody generation

Anti-Nav1 was produced using the GST-MTD plasmid construct expressed in *E.coli*. Soluble GST-MTD was purified on a glutathione affinity column, eluted with glutathione, and injected into rabbits (antiserum production by COVANCE). Antisera to GST-MTD was affinity purified by pre-absorption on an Affi-Gel (Bio-Rad) column coupled with GST, followed by affinity purification with an Affi-Gel column coupled with GST-MTD. This affinity-purified antibody was used for all experiments to detect endogenous Nav1. Antibody specificity to Nav1 was confirmed as follows: using immunoblot, lack of detectable immunoreactivity for the Nav1 antibody in extracts of Nav1 KO SH-SY5Y cells compared to WT controls (Figure 2.5 B); using immunofluorescence staining, lack of detectable immunoreactivity for the Nav1 antibody in Nav1 KO SH-SY5Y cells compared to WT controls (Figure. Fig. 2.5 C). Antibody specificity was further demonstrated by nucleofecting GFP-Nav1, -Nav2, and -Nav3 in Nav1KO SH-SY5Y

cells, and there was only detectable immunoreactivity for the Nav1 antibody in cells expressing GFP-Nav1.

SH-SY5Y Nav1KO cell line generation

Nav1 knockout (KO) was achieved using CRISPR-Cas9 and the Alt-R system (Integrated DNA Technologies). RNA components (IDT) and purified Cas9 (UCB Macrolab) were nucleofected in the SH-SY5Y cell line (Lonza 4D-Nucleofector core unit; see Transfection methods). crRNA sequence and primers used to evaluate cutting are listed in Table 2.1. Nav1KO clones were identified via sequencing, and the lack of Nav1 in SH-SY5Y cell line was validated via Western Blot and immunofluorescence (Figure 2.5 B,C).

Immunostaining

Immunocytochemistry. Cell cultures were fixed in 3.7% formaldehyde with 120mM sucrose in phosphate buffered saline (PBS) at 37°C for 15 minutes, then permeabilized with 0.2% Triton-X 100 in PBS for 10min, blocked in 1% bovine-serum albumin in PBS for 30min, and incubated for 1hr at RT with the following primary antibodies diluted in PBS: TuJ1 (1:2000 to stain primary neurons, 1:300 to stain SH-SY5Y cells, gift of Dr. A. Frankfurter, or Neuromics MO15013), anti-Nav1 (generation described above, 1:300), anti-GFP (1:200; Invitrogen A-11122), anti-drebrin (1:400 MBL D029-3), anti-EB1 (1:300, BD Biosciences 610535), anti-cortactin (1:300, Millipore 05-180), anti-tyrosinated tubulin (1:2000; Sigma MAB1864-I), anti-neuron specific enolase (1:300; Novus Biologicals NB110-58870), anti-α tubulin (1:1000; abcam ab6161), anti-SMI-31(1:300-1:500; Biolegend 801601), anti-GAP43 1:250; Novus Biological NBP1-92714), anti-nestin (0.5mg/mL; BD Bioscience), anti-GFP (5mg/Ml; Aves Lab

GFP-1010); and anti-Tbr1 (1:500, Santa Cruz sc-48816). Immunostaining against Nav1, EB1, fascin or cortactin required 3min fixation with 100% ice-cold MeOH instead of formaldehyde. Following rinsing we incubated with Alexa-Fluor-488, -568, -647-conjugated secondary antibodies, DAPI (1:2000; Biotium 40011), Hoechst (1:1000; Pierce 33258), or phalloidin (1:250; Invitrogen) in blocking buffer at 37°C for 45min. mVenus or eGFP was used to identify neurons cotransfected with Control or Nav1 shRNA and the mVenus/eGFP signal was enhanced with anti-GFP antibody.

Immunohistochemistry. Brain sections were prepared and immunostained according to Castanza *et al* (2021). Briefly, embryonic mouse brain tissues were dissected, fixed in 4% paraformaldehyde (PFA), and were sectioned in a coronal plane at 7 (E12.5) and 12 microns thickness (E14.5) (Figure 2.1) or 100 mm thickness (E18.5) (Figure 2.4). No heat induced antigen retrieval (H.I.E.R.) was performed. Sections were blocked for 30 min at room temperature in 10% serum (goat or donkey depending on primary antibody origin species), 3% BSA, and 0.1% Triton X-100 in PBS. Primary antibodies were diluted in blocking solution and incubated overnight at 4°C. Sections were washed 3x5 min in PBS in secondary antibodies were diluted 1:400 in blocking solution and incubated for 2 h at room temperature. Tissue was again washed 3x5 min in PBS, incubated briefly in DAPI when indicated and mounted with Southern Biotech Fluoromount-G (Figure 2.1) or Vectashield (Figure 2.4) and allowed to cure before imaging.

Immunoblotting

Cells were lysed in radioimmunoprecipitation assay (RIPA) buffer (150mM NaCl, 0.1% Triton X-100, 0.5% sodium deoxycholate, 0.1% SDS, 50mM Tris-HCl pH 8.0, with 1mM

phenylmethylsulfonyl fluoride in isopropanol added right before lysis) with constant agitation at 4°C for 30 minutes. Lysates were then centrifuged at 12,000 rpm at 4°C for 20min and total protein extracts were boiled in Laemmli sample buffer (BioRad), separated by SDS-PAGE under reducing conditions and transferred to PVDF membranes (Millipore), which were then incubated with the following primary antibodies: anti-GAPDH (1:2000; GeneTex GT239), anti-Nav1 (1:1000), or anti-TrkB (1:500; BD Biosciences 610101). Immunoreactive bands were visualized by the LI-COR Odyssey Imaging System using anti-mouse IRDye 800 and anti-rabbit IRDye 680 (1:5000, LI-COR). To quantify and compare signal intensity, a box was applied to encompass the band of interest, and integrated intensity was determined after background subtraction. In the case of TrkB, we assumed that both bands of the doublet appearing in the WT and SH-SY5Y cell extracts corresponded to TrkB, and were included in the boxed region.

Membrane blebs

Cells were seeded at 263 cells/mm^2 on 100μg/mL poly-(D)-lysine coated glass coverslips. Rho-kinase Inhibitor Y-27632 (5μM) in DMSO or DMSO alone was applied to Nav1KO SH-SY5Y cells for 2 hours before fixation. SH-SY5Y Nav1KO cells were transfected with 1.5μg of Rac1Q61L or eGFP, and fixed 48 hours after transfection. For quantification of membrane blebs in WT vs Nav1KO cells, cells were plated on coverslips and fixed 24 hours later. A cell was considered to be blebbing if it had at least two blebs in the periphery. For live imaging of membrane blebs, cells were seeded at 263 cells/mm^2 on 100μg/mL poly-(D)-lysine coated ibidi μ-Plate 24 well plates, and imaged every 30 minutes for 24 hours in an environmental chamber at 37°C and 5% CO_2.

Endocytosis labeling

FM4-64 (Thermo T13320) dye application protocol was modified from Bonanomi *et al* 2008. For primary neurons, FM4-64 (10μM) was diluted in Krebs-Ringer-Hepes (KRH) solution, the dye was loaded onto the cells for 1 min, and then washed 2 times with KRH for no more than 2 minutes, and immediately fixed in 3.7% MeOH-free paraformaldehyde (PFA) with 120mM sucrose in PBS for 15min at RT. Acute cholesterol extraction was performed using MβCD (5mM, 3 minutes, 37°C), and LY294002 was used to inhibit PI3Kinase (50μm, 30 minutes, 37°C). Images were acquired within 1 week after fixation, as a loss of signal was observed after 1 week. Lysine-fixable dextran (Thermo D1818, 2mg/mL) or transferrin (Invitrogen T23365) was incubated for 10 min at 37°C and immediately fixed according to the MeOH-free PFA protocol. For SH-SY5Y cells, FM4-64 was loaded for 5 minutes, and SH-SY5Y cells were either live imaged or fixed according to the MeOH-free PFA protocol, and fixed cells were incubated with phalloidin (1:100) overnight at 4°C.

TrkB uptake experiments

TrkB 1D7 [168], an agonistic monoclonal antibody, was applied in cold HBSS plus 2mM $CaCl_2$ to primary neurons for 30 minutes. Samples were washed twice in the cold HBSS solution, and then incubated in 37°C HBSS solution for 10 minutes, and immediately fixed with paraformaldehyde for 15 minutes at RT. After fixation, cells were permeabilized with 0.2% Triton-X-100 for 10 minutes, and incubated with Alexa Fluor 568 anti-mouse IgM secondary (1:250, Invitrogen, A-21043).

Image acquisition

Histological tissue sections. For the *in utero* electroporation experiments, images were acquired in 1024 x 1024 mode with a Nikon Ti-E microscope equipped with the A1 laser scanning confocal microscope. We used the following objective lenses (Nikon): 10x PlanApo, NA 0.45 (for images of cortical slices), 60x Apo TIRF, NA 1.49 (analyses the leading process and morphometric analyses of multipolar and bipolar cells). Images were acquired using Nikon software NIS-Elements (Nikon Corporation, Melville, NY). The immunohistochemistry performed for Nav1 localization was acquired with Zeiss LSM780 confocal microscope, and digital images were adjusted for brightness and contrast in Photoshop (Adobe).

Primary neurons. Excluding the endocytosis experiments, fluorescence imaging was carried out using a CSU-X1 spinning disk confocal (Yokogawa) mounted onto an Olympus IX70 microscope and a 20x 0.8 NA Plan APO for shRNA experiments and 60x 1.42 NA Plan APO oil immersion objective for the rest. Fluorescent specimens were excited using a laser launch equipped with the following 50mW solid-state lasers: 405nm, 488nm, 561nm and 640nm. Fluorescence emission was selected through the following band-pass filters: 460/50nm, 525/50nm, 595/50, 700/75. A stack of images was acquired in the z dimension using optical slice thickness of 0.2 using a CoolSNAP HQ2 digital CCD camera (Photometrics) with pixel size of 91 nm.

Primary neuron endocytosis and SH-SY5Y experiments. Fluorescence imaging was carried out CSU-X1 spinning disk confocal (Yokogawa) mounted onto a Ti-E microscope with perfect focus system (Nikon) and a 60x 1.4 NA Plan APO oil immersion objective. For the SH-SY5Y neuritogenesis experiment, we used a 20x 0.75 NA objective. Fluorescent specimens were excited using a laser launch equipped with the following 50mW solid-state lasers: 405nm,

488nm, 561nm and 640nm. Fluorescence emission was selected through the following band-pass filters: 460/50nm, 525/50nm, 595/50, 700/75. A stack of images was acquired in the z dimension using optical slice thickness of 0.2 μm using an Photometrics Prime 95B cMOS camera. For the SH-SY5Y neuritogenesis experiment, automatic acquisition was used using the MetaMorph high content screening module.

Image Analysis

Primary neuron neuritogenesis. Morphometric analysis was performed using MetaMorph software (Molecular Devices or Fiji (NIH). Neurons were identified by immunostaining for the neuronal marker ß-III tubulin and neurite length was measured manually using the eGFP signal and computer-assisted analysis from MetaMorph. Neurons without neurites were classified as stage 1, neurons with at least one neurite were considered stage 2 and neurons with one neurite at least twice the length of the other ones was considered the axons and the cells in stage 3.

SH-SY5Y neuritogenesis. The length of neurites was measured per field using a custom cell profiler pipeline (available upon request). Briefly, TuJ1 and neuron-specific enolase were used to identify neurogenic cells, expanded DAPI was used to exclude cell bodies in measurements, and a high phalloidin signal was used to exclude non-neurogenic cells that also expressed TuJ1 at low levels. We then calculated total neurite length in the image field divided number of cells (as measured by number of cells identified using DAPI).

In utero Nav1 shRNA experiments. The length of the leading process of migrating neurons in the cortical plate and the angle of migration in the Intermediate Zone was measured using Nikon Software NISElements (Nikon Corporation, Melville, NY). The orientation of each leading process was defined as that of a line connecting the cell body center and the base of the

leading process and its angle was measured with respect to the pial surface. An average of all angles was used to calculate the deviation of each individual angle to the average. The quantification of bipolar and multipolar neurons was performed by morphological criteria. Briefly, for each neuron in the IZ we quantified the number of non-axon processes (axon was identified by thickness, length and orientation). Neurons were considered bipolar when they presented one axon and one process. Neurons were considered multipolar when they displayed more than one non-axonal process.

Nav1 and EB1 analysis. For estimation of the amount of the Nav1 proteins bound to the outer most MT tips; mean integrated fluorescence intensities within a box of four pixels on a side (outer tip) were measured for each channel after subtracting external background. EB1 centroid was used to position the region of interest.

Membrane Ruffles. The F-actin channel was thresholded to encompass the structures. The resulting mask was used to generate a manual selection that would include the F-actin membrane ruffles within the transition zone, identified as the actin-rich region adjacent to the central zone microtubules. From this double selection the area and intensity of the F-actin signal was measured.

Endocytosis. Growth cones were identified by their morphology, and a mask was created using the pcs-membrane-ceruleanFP signal for primary neurons, or phalloidin-labeled F-actin for the SH-SY5Y cells. Intensity of endocytosis probes (FM4-64, transferrin, TrkB1D7) was measured within that mask after background subtraction and thresholding. A growth cone was considered to have uptake if there were at least two FM4-64 puncta within the growth cone. For the PI3Kinase treatment, we quantified the percentage of growth cones with FM4-64 uptake, instead of integrated signal intensity, because we unexpectedly observed that LY294002 caused

FM4-64 to be taken up all over the cell, not just at growth cones as in controls, thereby complicating intensity measurements.

Statistical Analysis & Experimental Rigor

All results reported have been observed reproducibly in at least 3 experiments; specific replicate values are indicated in figure legends. Prior to quantitative analysis, sample identity was encoded for blinding of the experimental group. Statistical significance was set at the 95% confidence level (two tailed) and calculated using Prism (Graphpad Software). Values are presented as the mean ± S.E.M.

To assess the normality of the data, we used the D'Agostino-Pearson test to determine deviation or kurtosis. When normality was not met either the Mann-Whitney or Kruskal-Wallis test with Dunn's multiple comparisons was chosen as described in the figure legends. Otherwise, two-way ANOVA with Bonferroni post-hoc comparisons were used. Pharmacological and genetic experiments were statistically compared to their corresponding control or wild-type counterparts.

ACKNOWLEDGEMENTS

Chapter 2, in full, is a reprint of the material as it appears in Molecular Biology of the Cell 2022. Powers, Regina; Daza, Ray, Koehler, Alanna; Courchet, Julian; Calabrese, Barbara, Halpain, Shelley. The dissertation author was the primary investigator and author of this paper.

CHAPTER 3

CONCLUSIONS

In summary, the data presented in this dissertation suggest a novel concept regarding the function of Nav1 in the regulation of neuronal development. Nav1 not only associates selectively with and regulates both the microtubule and actin cytoskeletons, but may play a general role in mediating uptake of and signaling by neurotrophins and other growth and guidance cues. This is especially important in developing neurons, where Nav1 is highly expressed, and allows newly extending axons to quickly respond to extra- and intracellular signals to facilitate tightly-regulated morphogenesis and brain circuit establishment.

From *C. elegans* to humans, the navigators and their homologs have been shown to be essential for proper development of multiple tissues, including the mammalian nervous system where they are expressed during development. The navigators integrate the cellular responses to multiple extracellular guidance cues in different cell types, and likely coordinate the cytoskeletal response to these cues. The work in this dissertation has offered insight into the mechanism of the regulation of neuritogenesis by Nav1 via macropinocytosis[43]. This work in combination with other recent studies that shed light on the cytoskeleton interacting properties of Nav1[44], offer interesting avenues of research for the other navigators. It is also likely that the navigators influence morphogenesis and migration via interaction to other signaling molecules that may indirectly affect cytoskeleton dynamics[49, 82]. The recent identification of a patient with a neurodevelopmental disorder attributable to the loss of Nav2[72] underscores the urgency to characterize the molecules and the cellular processes in which they participate to not only further our understanding of brain development but also for human health and disease.

ACKNOWLEDGEMENTS

Chapter 3, in part, is a reprint of the material as it appears in Molecular Biology of the Cell 2022. Powers, Regina; Daza, Ray, Koehler, Alanna; Courchet, Julian; Calabrese, Barbara, Halpain, Shelley; it is also, in part, currently being prepared for submission for publication of the material. Powers, Regina; Hevner, Robert; Halpain, Shelley. The dissertation author was the primary investigator and author of this paper.

REFERENCES

1. Bellenchi GC, Gurniak CB, Perlas E, Middei S, Ammassari-Teule M, Witke W. N-cofilin is associated with neuronal migration disorders and cell cycle control in the cerebral cortex. Genes Dev. 2007;21(18):2347-57. Epub 2007/09/19. doi: 10.1101/gad.434307. PubMed PMID: 17875668; PMCID: PMC1973148.

2. des Portes V, Pinard JM, Billuart P, Vinet MC, Koulakoff A, Carrie A, Gelot A, Dupuis E, Motte J, Berwald-Netter Y, Catala M, Kahn A, Beldjord C, Chelly J. A novel CNS gene required for neuronal migration and involved in X-linked subcortical laminar heterotopia and lissencephaly syndrome. Cell. 1998;92(1):51-61. Epub 1998/03/07. doi: 10.1016/s0092-8674(00)80898-3. PubMed PMID: 9489699.

3. des Portes V, Francis F, Pinard JM, Desguerre I, Moutard ML, Snoeck I, Meiners LC, Capron F, Cusmai R, Ricci S, Motte J, Echenne B, Ponsot G, Dulac O, Chelly J, Beldjord C. doublecortin is the major gene causing X-linked subcortical laminar heterotopia (SCLH). Hum Mol Genet. 1998;7(7):1063-70. Epub 1998/06/09. doi: 10.1093/hmg/7.7.1063. PubMed PMID: 9618162.

4. Pilz DT, Matsumoto N, Minnerath S, Mills P, Gleeson JG, Allen KM, Walsh CA, Barkovich AJ, Dobyns WB, Ledbetter DH, Ross ME. LIS1 and XLIS (DCX) mutations cause most classical lissencephaly, but different patterns of malformation. Hum Mol Genet. 1998;7(13):2029-37. Epub 1998/11/18. doi: 10.1093/hmg/7.13.2029. PubMed PMID: 9817918.

5. Gonçalves FG, Freddi TAL, Taranath A, Lakshmanan R, Goetti R, Feltrin FS, Mankad K, Teixeira SR, Hanagandi PB, Arrigoni F. Tubulinopathies. Top Magn Reson Imaging. 2018;27(6):395-408. doi: 10.1097/RMR.0000000000000188. PubMed PMID: 30516692.

6. Romaniello R, Arrigoni F, Fry AE, Bassi MT, Rees MI, Borgatti R, Pilz DT, Cushion TD. Tubulin genes and malformations of cortical development. Eur J Med Genet. 2018;61(12):744-54. Epub 20180717. doi: 10.1016/j.ejmg.2018.07.012. PubMed PMID: 30016746.

7. Jheng GW, Hur SS, Chang CM, Wu CC, Cheng JS, Lee HH, Chung BC, Wang YK, Lin KH, Del Alamo JC, Chien S, Tsai JW. Lis1 dysfunction leads to traction force reduction and cytoskeletal disorganization during cell migration. Biochem Biophys Res Commun. 2018;497(3):869-75. Epub 2018/02/23. doi: 10.1016/j.bbrc.2018.02.151. PubMed PMID: 29470990.

8. Wilson HL, Wong AC, Shaw SR, Tse WY, Stapleton GA, Phelan MC, Hu S, Marshall J, McDermid HE. Molecular characterisation of the 22q13 deletion syndrome supports the role of

haploinsufficiency of SHANK3/PROSAP2 in the major neurological symptoms. J Med Genet. 2003;40(8):575-84. doi: 10.1136/jmg.40.8.575. PubMed PMID: 12920066; PMCID: PMC1735560.

9. Durand CM, Perroy J, Loll F, Perrais D, Fagni L, Bourgeron T, Montcouquiol M, Sans N. SHANK3 mutations identified in autism lead to modification of dendritic spine morphology via an actin-dependent mechanism. Mol Psychiatry. 2012;17(1):71-84. Epub 2011/05/25. doi: 10.1038/mp.2011.57. PubMed PMID: 21606927; PMCID: PMC3252613.

10. Hong SE, Shugart YY, Huang DT, Shahwan SA, Grant PE, Hourihane JO, Martin ND, Walsh CA. Autosomal recessive lissencephaly with cerebellar hypoplasia is associated with human RELN mutations. Nat Genet. 2000;26(1):93-6. doi: 10.1038/79246. PubMed PMID: 10973257.

11. Chang BS, Duzcan F, Kim S, Cinbis M, Aggarwal A, Apse KA, Ozdel O, Atmaca M, Zencir S, Bagci H, Walsh CA. The role of RELN in lissencephaly and neuropsychiatric disease. Am J Med Genet B Neuropsychiatr Genet. 2007;144B(1):58-63. doi: 10.1002/ajmg.b.30392. PubMed PMID: 16958033.

12. Fatemi SH. The role of Reelin in pathology of autism. Mol Psychiatry. 2002;7(9):919-20. doi: 10.1038/sj.mp.4001248. PubMed PMID: 12399938.

13. Chai X, Förster E, Zhao S, Bock HH, Frotscher M. Reelin stabilizes the actin cytoskeleton of neuronal processes by inducing n-cofilin phosphorylation at serine3. J Neurosci. 2009;29(1):288-99. doi: 10.1523/JNEUROSCI.2934-08.2009. PubMed PMID: 19129405; PMCID: PMC6664910.

14. Assadi AH, Zhang G, Beffert U, McNeil RS, Renfro AL, Niu S, Quattrocchi CC, Antalffy BA, Sheldon M, Armstrong DD, Wynshaw-Boris A, Herz J, D'Arcangelo G, Clark GD. Interaction of reelin signaling and Lis1 in brain development. Nat Genet. 2003;35(3):270-6. Epub 20031026. doi: 10.1038/ng1257. PubMed PMID: 14578885.

15. Frotscher M, Zhao S, Wang S, Chai X. Reelin Signaling Inactivates Cofilin to Stabilize the Cytoskeleton of Migrating Cortical Neurons. Front Cell Neurosci. 2017;11:148. Epub 2017/06/08. doi: 10.3389/fncel.2017.00148. PubMed PMID: 28588454; PMCID: PMC5440592.

16. Cardoso C, Leventer RJ, Ward HL, Toyo-Oka K, Chung J, Gross A, Martin CL, Allanson J, Pilz DT, Olney AH, Mutchinick OM, Hirotsune S, Wynshaw-Boris A, Dobyns WB, Ledbetter DH. Refinement of a 400-kb critical region allows genotypic differentiation between isolated lissencephaly, Miller-Dieker syndrome, and other phenotypes secondary to deletions of 17p13.3.

Am J Hum Genet. 2003;72(4):918-30. Epub 20030305. doi: 10.1086/374320. PubMed PMID: 12621583; PMCID: PMC1180354.

17. Toyo-oka K, Shionoya A, Gambello MJ, Cardoso C, Leventer R, Ward HL, Ayala R, Tsai LH, Dobyns W, Ledbetter D, Hirotsune S, Wynshaw-Boris A. 14-3-3epsilon is important for neuronal migration by binding to NUDEL: a molecular explanation for Miller-Dieker syndrome. Nat Genet. 2003;34(3):274-85. doi: 10.1038/ng1169. PubMed PMID: 12796778.

18. Yingling J, Toyo-Oka K, Wynshaw-Boris A. Miller-Dieker syndrome: analysis of a human contiguous gene syndrome in the mouse. Am J Hum Genet. 2003;73(3):475-88. Epub 20030805. doi: 10.1086/378096. PubMed PMID: 12905154; PMCID: PMC1180674.

19. Estrach S, Schmidt S, Diriong S, Penna A, Blangy A, Fort P, Debant A. The Human Rho-GEF trio and its target GTPase RhoG are involved in the NGF pathway, leading to neurite outgrowth. Curr Biol. 2002;12(4):307-12. doi: 10.1016/s0960-9822(02)00658-9. PubMed PMID: 11864571.

20. Briançon-Marjollet A, Ghogha A, Nawabi H, Triki I, Auziol C, Fromont S, Piché C, Enslen H, Chebli K, Cloutier JF, Castellani V, Debant A, Lamarche-Vane N. Trio mediates netrin-1-induced Rac1 activation in axon outgrowth and guidance. Mol Cell Biol. 2008;28(7):2314-23. Epub 20080122. doi: 10.1128/MCB.00998-07. PubMed PMID: 18212043; PMCID: PMC2268419.

21. Tian C, Paskus JD, Fingleton E, Roche KW, Herring BE. Autism Spectrum Disorder/Intellectual Disability-Associated Mutations in Trio Disrupt Neuroligin 1-Mediated Synaptogenesis. J Neurosci. 2021;41(37):7768-78. Epub 20210805. doi: 10.1523/JNEUROSCI.3148-20.2021. PubMed PMID: 34353896; PMCID: PMC8445058.

22. Forscher P, Smith SJ. Actions of cytochalasins on the organization of actin filaments and microtubules in a neuronal growth cone. J Cell Biol. 1988;107(4):1505-16. doi: 10.1083/jcb.107.4.1505. PubMed PMID: 3170637; PMCID: PMC2115246.

23. Lin CH, Forscher P. Cytoskeletal remodeling during growth cone-target interactions. J Cell Biol. 1993;121(6):1369-83. doi: 10.1083/jcb.121.6.1369. PubMed PMID: 8509456; PMCID: PMC2119712.

24. Forscher P, Lin CH, Thompson C. Novel form of growth cone motility involving site-directed actin filament assembly. Nature. 1992;357(6378):515-8. doi: 10.1038/357515a0. PubMed PMID: 1608453.

25. Kalil K, Dent EW. Touch and go: guidance cues signal to the growth cone cytoskeleton. Curr Opin Neurobiol. 2005;15(5):521-6. doi: 10.1016/j.conb.2005.08.005. PubMed PMID: 16143510.

26. Maes T, Barcelo A, Buesa C. Neuron navigator: a human gene family with homology to unc-53, a cell guidance gene from Caenorhabditis elegans. Genomics. 2002;80(1):21-30. doi: 10.1006/geno.2002.6799. PubMed PMID: 12079279.

27. Hedgecock EM, Culotti JG, Hall DH, Stern BD. Genetics of cell and axon migrations in Caenorhabditis elegans. Development. 1987;100(3):365-82. PubMed PMID: 3308403.

28. Hekimi S, Kershaw D. Axonal guidance defects in a Caenorhabditis elegans mutant reveal cell-extrinsic determinants of neuronal morphology. J Neurosci. 1993;13(10):4254-71. PubMed PMID: 8410186; PMCID: PMC6576365.

29. Stringham E, Pujol N, Vandekerckhove J, Bogaert T. unc-53 controls longitudinal migration in C. elegans. Development. 2002;129(14):3367-79. PubMed PMID: 12091307.

30. Foley E, O'Farrell PH. Functional dissection of an innate immune response by a genome-wide RNAi screen. PLoS Biol. 2004;2(8):E203. Epub 20040622. doi: 10.1371/journal.pbio.0020203. PubMed PMID: 15221030; PMCID: PMC434151.

31. Abe T, Yamazaki D, Murakami S, Hiroi M, Nitta Y, Maeyama Y, Tabata T. The NAV2 homolog Sickie regulates F-actin-mediated axonal growth in Drosophila mushroom body neurons via the non-canonical Rac-Cofilin pathway. Development. 2014;141(24):4716-28. doi: 10.1242/dev.113308. PubMed PMID: 25411210.

32. Ishiguro H, Shimokawa T, Tsunoda T, Tanaka T, Fujii Y, Nakamura Y, Furukawa Y. Isolation of HELAD1, a novel human helicase gene up-regulated in colorectal carcinomas. Oncogene. 2002;21(41):6387-94. doi: 10.1038/sj.onc.1205751. PubMed PMID: 12214280.

33. Coy JF, Wiemann S, Bechmann I, Bachner D, Nitsch R, Kretz O, Christiansen H, Poustka A. Pore membrane and/or filament interacting like protein 1 (POMFIL1) is predominantly expressed in the nervous system and encodes different protein isoforms. Gene. 2002;290(1-2):73-94. doi: 10.1016/s0378-1119(02)00567-x. PubMed PMID: 12062803.

34. Merrill RA, Plum LA, Kaiser ME, Clagett-Dame M. A mammalian homolog of unc-53 is regulated by all-trans retinoic acid in neuroblastoma cells and embryos. Proc Natl Acad Sci U S A. 2002;99(6):3422-7. doi: 10.1073/pnas.052017399. PubMed PMID: 11904404; PMCID: PMC122539.

35. Glickman MH, Rubin DM, Coux O, Wefes I, Pfeifer G, Cjeka Z, Baumeister W, Fried VA, Finley D. A subcomplex of the proteasome regulatory particle required for ubiquitin-conjugate degradation and related to the COP9-signalosome and eIF3. Cell. 1998;94(5):615-23. doi: 10.1016/s0092-8674(00)81603-7. PubMed PMID: 9741626.

36. Köhler A, Cascio P, Leggett DS, Woo KM, Goldberg AL, Finley D. The axial channel of the proteasome core particle is gated by the Rpt2 ATPase and controls both substrate entry and product release. Mol Cell. 2001;7(6):1143-52. doi: 10.1016/s1097-2765(01)00274-x. PubMed PMID: 11430818.

37. Meyer HH, Shorter JG, Seemann J, Pappin D, Warren G. A complex of mammalian ufd1 and npl4 links the AAA-ATPase, p97, to ubiquitin and nuclear transport pathways. EMBO J. 2000;19(10):2181-92. doi: 10.1093/emboj/19.10.2181. PubMed PMID: 10811609; PMCID: PMC384367.

38. Misura KM, May AP, Weis WI. Protein-protein interactions in intracellular membrane fusion. Curr Opin Struct Biol. 2000;10(6):662-71. doi: 10.1016/s0959-440x(00)00151-2. PubMed PMID: 11114503.

39. McNally FJ, Vale RD. Identification of katanin, an ATPase that severs and disassembles stable microtubules. Cell. 1993;75(3):419-29. doi: 10.1016/0092-8674(93)90377-3. PubMed PMID: 8221885.

40. van Haren J, Draegestein K, Keijzer N, Abrahams JP, Grosveld F, Peeters PJ, Moechars D, Galjart N. Mammalian Navigators are microtubule plus-end tracking proteins that can reorganize the cytoskeleton to induce neurite-like extensions. Cell Motil Cytoskeleton. 2009;66(10):824-38. doi: 10.1002/cm.20370. PubMed PMID: 19396870.

41. Yin LM, Schnoor M, Jun CD. Structural Characteristics, Binding Partners and Related Diseases of the Calponin Homology (CH) Domain. Front Cell Dev Biol. 2020;8:342. Epub 20200514. doi: 10.3389/fcell.2020.00342. PubMed PMID: 32478077; PMCID: PMC7240100.

42. Schmidt KL, Marcus-Gueret N, Adeleye A, Webber J, Baillie D, Stringham EG. The cell migration molecule UNC-53/NAV2 is linked to the ARP2/3 complex by ABI-1. Development. 2009;136(4):563-74. doi: 10.1242/dev.016816. PubMed PMID: 19168673.

43. Powers RM, Daza R, Koehler AE, Courchet J, Calabrese B, Hevner RF, Halpain S. Growth cone macropinocytosis of neurotrophin receptor and neuritogenesis are regulated by Neuron Navigator 1. Mol Biol Cell. 2022:mbcE21120623. Epub 20220330. doi: 10.1091/mbc.E21-12-0623. PubMed PMID: 35352947.

44. Sanchez-Huertas C, Bonhomme M, Falco A, Fagotto-Kaufmann C, van Haren J, Jeanneteau F, Galjart N, Debant A, Boudeau J. The +TIP Navigator-1 is an actin-microtubule crosslinker that regulates axonal growth cone motility. J Cell Biol. 2020;219(9). Epub 2020/06/05. doi: 10.1083/jcb.201905199. PubMed PMID: 32497170; PMCID: PMC7480110.

45. Martinez-Lopez MJ, Alcantara S, Mascaro C, Perez-Branguli F, Ruiz-Lozano P, Maes T, Soriano E, Buesa C. Mouse neuron navigator 1, a novel microtubule-associated protein involved in neuronal migration. Mol Cell Neurosci. 2005;28(4):599-612. doi: 10.1016/j.mcn.2004.09.016. PubMed PMID: 15797708.

46. Muley PD, McNeill EM, Marzinke MA, Knobel KM, Barr MM, Clagett-Dame M. The atRA-responsive gene neuron navigator 2 functions in neurite outgrowth and axonal elongation. Dev Neurobiol. 2008;68(13):1441-53. doi: 10.1002/dneu.20670. PubMed PMID: 18726912; PMCID: PMC4409142.

47. Honnappa S, Gouveia SM, Weisbrich A, Damberger FF, Bhavesh NS, Jawhari H, Grigoriev I, van Rijssel FJ, Buey RM, Lawera A, Jelesarov I, Winkler FK, Wüthrich K, Akhmanova A, Steinmetz MO. An EB1-binding motif acts as a microtubule tip localization signal. Cell. 2009;138(2):366-76. doi: 10.1016/j.cell.2009.04.065. PubMed PMID: 19632184.

48. Vaughan KT. TIP maker and TIP marker; EB1 as a master controller of microtubule plus ends. J Cell Biol. 2005;171(2):197-200. doi: 10.1083/jcb.200509150. PubMed PMID: 16247021; PMCID: PMC2171192.

49. van Haren J, Boudeau J, Schmidt S, Basu S, Liu Z, Lammers D, Demmers J, Benhari J, Grosveld F, Debant A, Galjart N. Dynamic microtubules catalyze formation of navigator-TRIO complexes to regulate neurite extension. Curr Biol. 2014;24(15):1778-85. doi: 10.1016/j.cub.2014.06.037. PubMed PMID: 25065758.

50. Bearce EA, Erdogan B, Lowery LA. TIPsy tour guides: how microtubule plus-end tracking proteins (+TIPs) facilitate axon guidance. Front Cell Neurosci. 2015;9:241. Epub 2015/07/16. doi: 10.3389/fncel.2015.00241. PubMed PMID: 26175669; PMCID: PMC4485311.

51. Cammarata GM, Bearce EA, Lowery LA. Cytoskeletal social networking in the growth cone: How +TIPs mediate microtubule-actin cross-linking to drive axon outgrowth and guidance. Cytoskeleton (Hoboken). 2016;73(9):461-76. Epub 2016/01/20. doi: 10.1002/cm.21272. PubMed PMID: 26783725; PMCID: PMC4955630.

52. Geraldo S, Khanzada UK, Parsons M, Chilton JK, Gordon-Weeks PR. Targeting of the F-actin-binding protein drebrin by the microtubule plus-tip protein EB3 is required for

neuritogenesis. Nat Cell Biol. 2008;10(10):1181-9. doi: 10.1038/ncb1778. PubMed PMID: 18806788.

53. Lowery LA, Van Vactor D. The trip of the tip: understanding the growth cone machinery. Nat Rev Mol Cell Biol. 2009;10(5):332-43. Epub 2009/04/17. doi: 10.1038/nrm2679. PubMed PMID: 19373241; PMCID: PMC2714171.

54. Bedogni F, Hodge RD, Elsen GE, Nelson BR, Daza RA, Beyer RP, Bammler TK, Rubenstein JL, Hevner RF. Tbr1 regulates regional and laminar identity of postmitotic neurons in developing neocortex. Proc Natl Acad Sci U S A. 2010;107(29):13129-34. Epub 20100706. doi: 10.1073/pnas.1002285107. PubMed PMID: 20615956; PMCID: PMC2919950.

55. Bedogni F, Hevner RF. Cell-Type-Specific Gene Expression in Developing Mouse Neocortex: Intermediate Progenitors Implicated in Axon Development. Front Mol Neurosci. 2021;14:686034. Epub 20210712. doi: 10.3389/fnmol.2021.686034. PubMed PMID: 34321999; PMCID: PMC8313239.

56. Englund C, Fink A, Lau C, Pham D, Daza RA, Bulfone A, Kowalczyk T, Hevner RF. Pax6, Tbr2, and Tbr1 are expressed sequentially by radial glia, intermediate progenitor cells, and postmitotic neurons in developing neocortex. J Neurosci. 2005;25(1):247-51. doi: 10.1523/JNEUROSCI.2899-04.2005. PubMed PMID: 15634788; PMCID: PMC6725189.

57. Bulfone A, Wang F, Hevner R, Anderson S, Cutforth T, Chen S, Meneses J, Pedersen R, Axel R, Rubenstein JL. An olfactory sensory map develops in the absence of normal projection neurons or GABAergic interneurons. Neuron. 1998;21(6):1273-82. doi: 10.1016/s0896-6273(00)80647-9. PubMed PMID: 9883721.

58. Notwell JH, Heavner WE, Darbandi SF, Katzman S, McKenna WL, Ortiz-Londono CF, Tastad D, Eckler MJ, Rubenstein JL, McConnell SK, Chen B, Bejerano G. TBR1 regulates autism risk genes in the developing neocortex. Genome Res. 2016;26(8):1013-22. Epub 20160620. doi: 10.1101/gr.203612.115. PubMed PMID: 27325115; PMCID: PMC4971772.

59. Sessa A, Ciabatti E, Drechsel D, Massimino L, Colasante G, Giannelli S, Satoh T, Akira S, Guillemot F, Broccoli V. The Tbr2 Molecular Network Controls Cortical Neuronal Differentiation Through Complementary Genetic and Epigenetic Pathways. Cereb Cortex. 2017;27(6):3378-96. doi: 10.1093/cercor/bhw270. PubMed PMID: 27600842.

60. Elsen GE, Hodge RD, Bedogni F, Daza RA, Nelson BR, Shiba N, Reiner SL, Hevner RF. The protomap is propagated to cortical plate neurons through an Eomes-dependent intermediate map. Proc Natl Acad Sci U S A. 2013;110(10):4081-6. Epub 20130219. doi: 10.1073/pnas.1209076110. PubMed PMID: 23431145; PMCID: PMC3593833.

61. Elsen GE, Bedogni F, Hodge RD, Bammler TK, MacDonald JW, Lindtner S, Rubenstein JLR, Hevner RF. The Epigenetic Factor Landscape of Developing Neocortex Is Regulated by Transcription Factors Pax6→ Tbr2→ Tbr1. Front Neurosci. 2018;12:571. Epub 20180822. doi: 10.3389/fnins.2018.00571. PubMed PMID: 30186101; PMCID: PMC6113890.

62. Pook C, Ahrens JM, Clagett-Dame M. Expression pattern of Nav2 in the murine CNS with development. Gene Expr Patterns. 2020;35:119099. Epub 2020/02/23. doi: 10.1016/j.gep.2020.119099. PubMed PMID: 32081718.

63. Klein C, Mikutta J, Krueger J, Scholz K, Brinkmann J, Liu D, Veerkamp J, Siegel D, Abdelilah-Seyfried S, le Noble F. Neuron navigator 3a regulates liver organogenesis during zebrafish embryogenesis. Development. 2011;138(10):1935-45. doi: 10.1242/dev.056861. PubMed PMID: 21471154; PMCID: PMC3082300.

64. Lv F, Ge X, Qian P, Lu X, Liu D, Chen C. Neuron navigator 3 (NAV3) is required for heart development in zebrafish. Fish Physiol Biochem. 2022;48(1):173-83. Epub 20220118. doi: 10.1007/s10695-022-01049-5. PubMed PMID: 35039994.

65. Peeters PJ, Baker A, Goris I, Daneels G, Verhasselt P, Luyten WH, Geysen JJ, Kass SU, Moechars DW. Sensory deficits in mice hypomorphic for a mammalian homologue of unc-53. Brain Res Dev Brain Res. 2004;150(2):89-101. doi: 10.1016/j.devbrainres.2004.03.004. PubMed PMID: 15158073.

66. McNeill EM, Roos KP, Moechars D, Clagett-Dame M. Nav2 is necessary for cranial nerve development and blood pressure regulation. Neural Dev. 2010;5:6. doi: 10.1186/1749-8104-5-6. PubMed PMID: 20184720; PMCID: PMC2843687.

67. McNeill EM, Klockner-Bormann M, Roesler EC, Talton LE, Moechars D, Clagett-Dame M. Nav2 hypomorphic mutant mice are ataxic and exhibit abnormalities in cerebellar development. Dev Biol. 2011;353(2):331-43. doi: 10.1016/j.ydbio.2011.03.008. PubMed PMID: 21419114; PMCID: PMC3250223.

68. Olson HE, Shen Y, Poduri A, Gorman MP, Dies KA, Robbins M, Hundley R, Wu B, Sahin M. Micro-duplications of 1q32.1 associated with neurodevelopmental delay. Eur J Med Genet. 2012;55(2):145-50. Epub 20120102. doi: 10.1016/j.ejmg.2011.12.008. PubMed PMID: 22266072; PMCID: PMC3288188.

69. Carter J, Zombor M, Máté A, Sztriha L, Waters JJ. De Novo Interstitial Microdeletion at 1q32.1 in a 10-Year-Old Boy with Developmental Delay and Dysmorphism. Case Rep Genet. 2016;2016:2501741. Epub 20160203. doi: 10.1155/2016/2501741. PubMed PMID: 26955491; PMCID: PMC4756132.

70. Asselin L, Rivera Alvarez J, Heide S, Bonnet CS, Tilly P, Vitet H, Weber C, Bacino CA, Baranaño K, Chassevent A, Dameron A, Faivre L, Hanchard NA, Mahida S, McWalter K, Mignot C, Nava C, Rastetter A, Streff H, Thauvin-Robinet C, Weiss MM, Zapata G, Zwijnenburg PJG, Saudou F, Depienne C, Golzio C, Héron D, Godin JD. Mutations in the KIF21B kinesin gene cause neurodevelopmental disorders through imbalanced canonical motor activity. Nat Commun. 2020;11(1):2441. Epub 20200515. doi: 10.1038/s41467-020-16294-6. PubMed PMID: 32415109; PMCID: PMC7229210.

71. Shi Y. Histone lysine demethylases: emerging roles in development, physiology and disease. Nat Rev Genet. 2007;8(11):829-33. doi: 10.1038/nrg2218. PubMed PMID: 17909537.

72. Accogli A, Lu S, Musante I, Scudieri P, Rosenfeld JA, Severino M, Baldassari S, Iacomino M, Riva A, Balagura G, Piccolo G, Minetti C, Roberto D, Xia F, Razak R, Lawrence E, Hussein M, Chang EY, Holick M, Calì E, Aliberto E, De-Sarro R, Gambardella A, Network UD, Group SS, Emrick L, McCaffery PJA, Clagett-Dame M, Marcogliese PC, Bellen HJ, Lalani SR, Zara F, Striano P, Salpietro V. Loss of Neuron Navigator 2 Impairs Brain and Cerebellar Development. Cerebellum. 2022. Epub 20220226. doi: 10.1007/s12311-022-01379-3. PubMed PMID: 35218524.

73. Brenner S. The genetics of Caenorhabditis elegans. Genetics. 1974;77(1):71-94. Epub 1974/05/01. PubMed PMID: 4366476; PMCID: PMC1213120.

74. Pandey A, Yadav V, Sharma A, Khurana JP, Pandey GK. The unc-53 gene negatively regulates rac GTPases to inhibit unc-5 activity during Distal tip cell migrations in C. elegans. Cell Adh Migr. 2018;12(3):195-203. doi: 10.1080/19336918.2017.1345413. PubMed PMID: 28678595; PMCID: PMC6149439.

75. Rohatgi R, Ma L, Miki H, Lopez M, Kirchhausen T, Takenawa T, Kirschner MW. The interaction between N-WASP and the Arp2/3 complex links Cdc42-dependent signals to actin assembly. Cell. 1999;97(2):221-31. doi: 10.1016/s0092-8674(00)80732-1. PubMed PMID: 10219243.

76. Ober EA, Verkade H, Field HA, Stainier DY. Mesodermal Wnt2b signalling positively regulates liver specification. Nature. 2006;442(7103):688-91. Epub 20060621. doi: 10.1038/nature04888. PubMed PMID: 16799568.

77. Marín O, Valiente M, Ge X, Tsai LH. Guiding neuronal cell migrations. Cold Spring Harb Perspect Biol. 2010;2(2):a001834. doi: 10.1101/cshperspect.a001834. PubMed PMID: 20182622; PMCID: PMC2828271.

78. Stradal T, Courtney KD, Rottner K, Hahne P, Small JV, Pendergast AM. The Abl interactor proteins localize to sites of actin polymerization at the tips of lamellipodia and filopodia. Curr Biol. 2001;11(11):891-5. doi: 10.1016/s0960-9822(01)00239-1. PubMed PMID: 11516653.

79. Woodring PJ, Litwack ED, O'Leary DD, Lucero GR, Wang JY, Hunter T. Modulation of the F-actin cytoskeleton by c-Abl tyrosine kinase in cell spreading and neurite extension. J Cell Biol. 2002;156(5):879-92. Epub 20020225. doi: 10.1083/jcb.200110014. PubMed PMID: 11864995; PMCID: PMC2173320.

80. Innocenti M, Frittoli E, Ponzanelli I, Falck JR, Brachmann SM, Di Fiore PP, Scita G. Phosphoinositide 3-kinase activates Rac by entering in a complex with Eps8, Abi1, and Sos-1. J Cell Biol. 2003;160(1):17-23. Epub 20030106. doi: 10.1083/jcb.200206079. PubMed PMID: 12515821; PMCID: PMC2172734.

81. Kotula L. Abi1, a critical molecule coordinating actin cytoskeleton reorganization with PI-3 kinase and growth signaling. FEBS Lett. 2012;586(17):2790-4. Epub 20120519. doi: 10.1016/j.febslet.2012.05.015. PubMed PMID: 22617151; PMCID: PMC4521604.

82. Marzinke MA, Mavencamp T, Duratinsky J, Clagett-Dame M. 14-3-3epsilon and NAV2 interact to regulate neurite outgrowth and axon elongation. Arch Biochem Biophys. 2013;540(1-2):94-100. doi: 10.1016/j.abb.2013.10.012. PubMed PMID: 24161943; PMCID: PMC4120646.

83. Toyo-oka K, Wachi T, Hunt RF, Baraban SC, Taya S, Ramshaw H, Kaibuchi K, Schwarz QP, Lopez AF, Wynshaw-Boris A. 14-3-3ε and ζ regulate neurogenesis and differentiation of neuronal progenitor cells in the developing brain. J Neurosci. 2014;34(36):12168-81. doi: 10.1523/JNEUROSCI.2513-13.2014. PubMed PMID: 25186760; PMCID: PMC4152612.

84. Ridley AJ, Paterson HF, Johnston CL, Diekmann D, Hall A. The small GTP-binding protein rac regulates growth factor-induced membrane ruffling. Cell. 1992;70(3):401-10. doi: 10.1016/0092-8674(92)90164-8. PubMed PMID: 1643658.

85. Radhakrishna H, Al-Awar O, Khachikian Z, Donaldson JG. ARF6 requirement for Rac ruffling suggests a role for membrane trafficking in cortical actin rearrangements. J Cell Sci. 1999;112 (Pt 6):855-66. PubMed PMID: 10036235.

86. Borm B, Requardt RP, Herzog V, Kirfel G. Membrane ruffles in cell migration: indicators of inefficient lamellipodia adhesion and compartments of actin filament reorganization. Exp Cell Res. 2005;302(1):83-95. doi: 10.1016/j.yexcr.2004.08.034. PubMed PMID: 15541728.

87. Bonanomi D, Fornasiero EF, Valdez G, Halegoua S, Benfenati F, Menegon A, Valtorta F. Identification of a developmentally regulated pathway of membrane retrieval in neuronal growth cones. J Cell Sci. 2008;121(Pt 22):3757-69. doi: 10.1242/jcs.033803. PubMed PMID: 18940911; PMCID: PMC2731302.

88. Xu C, Fu X, Zhu S, Liu JJ. Retrolinkin recruits the WAVE1 protein complex to facilitate BDNF-induced TrkB endocytosis and dendrite outgrowth. Mol Biol Cell. 2016;27(21):3342-56. Epub 20160907. doi: 10.1091/mbc.E16-05-0326. PubMed PMID: 27605705; PMCID: PMC5170866.

89. Cheung ZH, Chin WH, Chen Y, Ng YP, Ip NY. Cdk5 is involved in BDNF-stimulated dendritic growth in hippocampal neurons. PLoS Biol. 2007;5(4):e63. doi: 10.1371/journal.pbio.0050063. PubMed PMID: 17341134; PMCID: PMC1808488.

90. Zheng J, Shen WH, Lu TJ, Zhou Y, Chen Q, Wang Z, Xiang T, Zhu YC, Zhang C, Duan S, Xiong ZQ. Clathrin-dependent endocytosis is required for TrkB-dependent Akt-mediated neuronal protection and dendritic growth. J Biol Chem. 2008;283(19):13280-8. Epub 20080319. doi: 10.1074/jbc.M709930200. PubMed PMID: 18353779.

91. Zhou P, Porcionatto M, Pilapil M, Chen Y, Choi Y, Tolias KF, Bikoff JB, Hong EJ, Greenberg ME, Segal RA. Polarized signaling endosomes coordinate BDNF-induced chemotaxis of cerebellar precursors. Neuron. 2007;55(1):53-68. doi: 10.1016/j.neuron.2007.05.030. PubMed PMID: 17610817; PMCID: PMC2661852.

92. King JS, Kay RR. The origins and evolution of macropinocytosis. Philos Trans R Soc Lond B Biol Sci. 2019;374(1765):20180158. doi: 10.1098/rstb.2018.0158. PubMed PMID: 30967007; PMCID: PMC6304743.

93. Marinović M, Mijanović L, Šoštar M, Vizovišek M, Junemann A, Fonović M, Turk B, Weber I, Faix J, Filić V. IQGAP-related protein IqgC suppresses Ras signaling during large-scale endocytosis. Proc Natl Acad Sci U S A. 2019;116(4):1289-98. Epub 20190108. doi: 10.1073/pnas.1810268116. PubMed PMID: 30622175; PMCID: PMC6347711.

94. Arpino G, Somasundaram A, Shin W, Ge L, Villareal S, Chan CY, Ashery U, Shupliakov O, Taraska JW, Wu LG. Clathrin-mediated endocytosis cooperates with bulk endocytosis to generate vesicles. iScience. 2022;25(2):103809. Epub 20220124. doi: 10.1016/j.isci.2022.103809. PubMed PMID: 35198874; PMCID: PMC8841809.

95. Joset A, Dodd DA, Halegoua S, Schwab ME. Pincher-generated Nogo-A endosomes mediate growth cone collapse and retrograde signaling. J Cell Biol. 2010;188(2):271-85. Epub 20100118. doi: 10.1083/jcb.200906089. PubMed PMID: 20083601; PMCID: PMC2812518.

96. Valdez G, Akmentin W, Philippidou P, Kuruvilla R, Ginty DD, Halegoua S. Pincher-mediated macroendocytosis underlies retrograde signaling by neurotrophin receptors. J Neurosci. 2005;25(21):5236-47. doi: 10.1523/JNEUROSCI.5104-04.2005. PubMed PMID: 15917464; PMCID: PMC6724820.

97. Kay RR. Macropinocytosis: Biology and mechanisms. Cells Dev. 2021:203713. Epub 20210624. doi: 10.1016/j.cdev.2021.203713. PubMed PMID: 34175511.

98. Swanson JA. Shaping cups into phagosomes and macropinosomes. Nat Rev Mol Cell Biol. 2008;9(8):639-49. Epub 20080709. doi: 10.1038/nrm2447. PubMed PMID: 18612320; PMCID: PMC2851551.

99. Diefenbach TJ, Guthrie PB, Stier H, Billups B, Kater SB. Membrane recycling in the neuronal growth cone revealed by FM1-43 labeling. J Neurosci. 1999;19(21):9436-44. PubMed PMID: 10531447; PMCID: PMC6782927.

100. Clayton EL, Cousin MA. Differential labelling of bulk endocytosis in nerve terminals by FM dyes. Neurochem Int. 2008;53(3-4):51-5. Epub 20080611. doi: 10.1016/j.neuint.2008.06.002. PubMed PMID: 18586059.

101. Wang R, Hosaka M, Han L, Yokota-Hashimoto H, Suda M, Mitsushima D, Torii S, Takeuchi T. Molecular probes for sensing the cholesterol composition of subcellular organelle membranes. Biochim Biophys Acta. 2006;1761(10):1169-81. Epub 20060830. doi: 10.1016/j.bbalip.2006.06.016. PubMed PMID: 17011819.

102. Kirkham M, Parton RG. Clathrin-independent endocytosis: new insights into caveolae and non-caveolar lipid raft carriers. Biochim Biophys Acta. 2005;1746(3):349-63. doi: 10.1016/j.bbamcr.2005.11.007. PubMed PMID: 16440447.

103. Orth JD, Krueger EW, Weller SG, McNiven MA. A novel endocytic mechanism of epidermal growth factor receptor sequestration and internalization. Cancer Res. 2006;66(7):3603-10. doi: 10.1158/0008-5472.CAN-05-2916. PubMed PMID: 16585185.

104. Buccione R, Orth JD, McNiven MA. Foot and mouth: podosomes, invadopodia and circular dorsal ruffles. Nat Rev Mol Cell Biol. 2004;5(8):647-57. doi: 10.1038/nrm1436. PubMed PMID: 15366708.

105. Li L, Wan T, Wan M, Liu B, Cheng R, Zhang R. The effect of the size of fluorescent dextran on its endocytic pathway. Cell Biol Int. 2015;39(5):531-9. Epub 20150126. doi: 10.1002/cbin.10424. PubMed PMID: 25623938.

106. Innocenti M, Gerboth S, Rottner K, Lai FP, Hertzog M, Stradal TE, Frittoli E, Didry D, Polo S, Disanza A, Benesch S, Di Fiore PP, Carlier MF, Scita G. Abi1 regulates the activity of N-WASP and WAVE in distinct actin-based processes. Nat Cell Biol. 2005;7(10):969-76. Epub 20050911. doi: 10.1038/ncb1304. PubMed PMID: 16155590.

107. Fares H, Greenwald I. Genetic analysis of endocytosis in Caenorhabditis elegans: coelomocyte uptake defective mutants. Genetics. 2001;159(1):133-45. doi: 10.1093/genetics/159.1.133. PubMed PMID: 11560892; PMCID: PMC1461804.

108. Chen L, Cheng D, Chu J, Zhang T, Dong Z, Lou H, Zhu L, Liu Y. A Novel Method to Image Macropinocytosis. Front Neurosci. 2018;12:324. Epub 20180515. doi: 10.3389/fnins.2018.00324. PubMed PMID: 29867333; PMCID: PMC5962816.

109. von Delwig A, Hilkens CM, Altmann DM, Holmdahl R, Isaacs JD, Harding CV, Robertson H, McKie N, Robinson JH. Inhibition of macropinocytosis blocks antigen presentation of type II collagen in vitro and in vivo in HLA-DR1 transgenic mice. Arthritis Res Ther. 2006;8(4):R93. doi: 10.1186/ar1964. PubMed PMID: 16704744; PMCID: PMC1779380.

110. Kerr MC, Teasdale RD. Defining macropinocytosis. Traffic. 2009;10(4):364-71. Epub 20090124. doi: 10.1111/j.1600-0854.2009.00878.x. PubMed PMID: 19192253.

111. Lim JP, Gleeson PA. Macropinocytosis: an endocytic pathway for internalising large gulps. Immunol Cell Biol. 2011;89(8):836-43. Epub 20110322. doi: 10.1038/icb.2011.20. PubMed PMID: 21423264.

112. West MA, Bretscher MS, Watts C. Distinct endocytotic pathways in epidermal growth factor-stimulated human carcinoma A431 cells. J Cell Biol. 1989;109(6 Pt 1):2731-9. doi: 10.1083/jcb.109.6.2731. PubMed PMID: 2556406; PMCID: PMC2115909.

113. Fujii M, Kawai K, Egami Y, Araki N. Dissecting the roles of Rac1 activation and deactivation in macropinocytosis using microscopic photo-manipulation. Sci Rep. 2013;3:2385. doi: 10.1038/srep02385. PubMed PMID: 23924974; PMCID: PMC3737501.

114. Masereel B, Pochet L, Laeckmann D. An overview of inhibitors of Na(+)/H(+) exchanger. Eur J Med Chem. 2003;38(6):547-54. doi: 10.1016/s0223-5234(03)00100-4. PubMed PMID: 12832126.

115. Koivusalo M, Welch C, Hayashi H, Scott CC, Kim M, Alexander T, Touret N, Hahn KM, Grinstein S. Amiloride inhibits macropinocytosis by lowering submembranous pH and

preventing Rac1 and Cdc42 signaling. J Cell Biol. 2010;188(4):547-63. Epub 20100215. doi: 10.1083/jcb.200908086. PubMed PMID: 20156964; PMCID: PMC2828922.

116. Sabharanjak S, Sharma P, Parton RG, Mayor S. GPI-anchored proteins are delivered to recycling endosomes via a distinct cdc42-regulated, clathrin-independent pinocytic pathway. Dev Cell. 2002;2(4):411-23. doi: 10.1016/s1534-5807(02)00145-4. PubMed PMID: 11970892.

117. Grassart A, Dujeancourt A, Lazarow PB, Dautry-Varsat A, Sauvonnet N. Clathrin-independent endocytosis used by the IL-2 receptor is regulated by Rac1, Pak1 and Pak2. EMBO Rep. 2008;9(4):356-62. Epub 20080314. doi: 10.1038/embor.2008.28. PubMed PMID: 18344974; PMCID: PMC2288760.

118. Araki N, Johnson MT, Swanson JA. A role for phosphoinositide 3-kinase in the completion of macropinocytosis and phagocytosis by macrophages. J Cell Biol. 1996;135(5):1249-60. doi: 10.1083/jcb.135.5.1249. PubMed PMID: 8947549; PMCID: PMC2121091.

119. Takenawa T, Suetsugu S. The WASP-WAVE protein network: connecting the membrane to the cytoskeleton. Nat Rev Mol Cell Biol. 2007;8(1):37-48. doi: 10.1038/nrm2069. PubMed PMID: 17183359.

120. Williamson CD, Donaldson JG. Arf6, JIP3, and dynein shape and mediate macropinocytosis. Mol Biol Cell. 2019;30(12):1477-89. Epub 20190410. doi: 10.1091/mbc.E19-01-0022. PubMed PMID: 30969891; PMCID: PMC6724687.

121. Orth JD, Krueger EW, Cao H, McNiven MA. The large GTPase dynamin regulates actin comet formation and movement in living cells. Proc Natl Acad Sci U S A. 2002;99(1):167-72. doi: 10.1073/pnas.012607899. PubMed PMID: 11782546; PMCID: PMC117533.

122. Kim N, Kim S, Nahm M, Kopke D, Kim J, Cho E, Lee MJ, Lee M, Kim SH, Broadie K, Lee S. BMP-dependent synaptic development requires Abi-Abl-Rac signaling of BMP receptor macropinocytosis. Nat Commun. 2019;10(1):684. Epub 20190208. doi: 10.1038/s41467-019-08533-2. PubMed PMID: 30737382; PMCID: PMC6368546.

123. Kabayama H, Nakamura T, Takeuchi M, Iwasaki H, Taniguchi M, Tokushige N, Mikoshiba K. Ca2+ induces macropinocytosis via F-actin depolymerization during growth cone collapse. Mol Cell Neurosci. 2009;40(1):27-38. Epub 20080911. doi: 10.1016/j.mcn.2008.08.009. PubMed PMID: 18848894.

124. Kabayama H, Takeuchi M, Taniguchi M, Tokushige N, Kozaki S, Mizutani A, Nakamura T, Mikoshiba K. Syntaxin 1B suppresses macropinocytosis and semaphorin 3A-induced growth cone collapse. J Neurosci. 2011;31(20):7357-64. doi: 10.1523/JNEUROSCI.2718-10.2011. PubMed PMID: 21593320; PMCID: PMC6622584.

125. Kolpak AL, Jiang J, Guo D, Standley C, Bellve K, Fogarty K, Bao ZZ. Negative guidance factor-induced macropinocytosis in the growth cone plays a critical role in repulsive axon turning. J Neurosci. 2009;29(34):10488-98. doi: 10.1523/JNEUROSCI.2355-09.2009. PubMed PMID: 19710302; PMCID: PMC2748960.

126. Marqués G, Zhang B. Retrograde signaling that regulates synaptic development and function at the Drosophila neuromuscular junction. Int Rev Neurobiol. 2006;75:267-85. doi: 10.1016/S0074-7742(06)75012-7. PubMed PMID: 17137932.

127. Dhamodharan R, Jordan MA, Thrower D, Wilson L, Wadsworth P. Vinblastine suppresses dynamics of individual microtubules in living interphase cells. Mol Biol Cell. 1995;6(9):1215-29. doi: 10.1091/mbc.6.9.1215. PubMed PMID: 8534917; PMCID: PMC301278.

128. Tojima T, Kamiguchi H. Exocytic and endocytic membrane trafficking in axon development. Dev Growth Differ. 2015;57(4):291-304. Epub 20150513. doi: 10.1111/dgd.12218. PubMed PMID: 25966925.

129. Tojima T, Itofusa R, Kamiguchi H. Steering neuronal growth cones by shifting the imbalance between exocytosis and endocytosis. J Neurosci. 2014;34(21):7165-78. doi: 10.1523/JNEUROSCI.5261-13.2014. PubMed PMID: 24849351; PMCID: PMC6608195.

130. Akhmanova A, Steinmetz MO. Tracking the ends: a dynamic protein network controls the fate of microtubule tips. Nat Rev Mol Cell Biol. 2008;9(4):309-22. Epub 2008/03/07. doi: 10.1038/nrm2369. PubMed PMID: 18322465.

131. Preciado Lopez M, Huber F, Grigoriev I, Steinmetz MO, Akhmanova A, Koenderink GH, Dogterom M. Actin-microtubule coordination at growing microtubule ends. Nat Commun. 2014;5:4778. doi: 10.1038/ncomms5778. PubMed PMID: 25159196; PMCID: PMC4365169.

132. Henty-Ridilla JL, Rankova A, Eskin JA, Kenny K, Goode BL. Accelerated actin filament polymerization from microtubule plus ends. Science. 2016;352(6288):1004-9. Epub 2016/05/21. doi: 10.1126/science.aaf1709. PubMed PMID: 27199431; PMCID: PMC5179141.

133. Dehmelt L, Halpain S. Actin and microtubules in neurite initiation: are MAPs the missing link? J Neurobiol. 2004;58(1):18-33. Epub 2003/11/05. doi: 10.1002/neu.10284. PubMed PMID: 14598367.

134. Pacheco A, Gallo G. Actin filament-microtubule interactions in axon initiation and branching. Brain Res Bull. 2016;126(Pt 3):300-10. doi: 10.1016/j.brainresbull.2016.07.013. PubMed PMID: 27491623; PMCID: PMC5518172.

135. Dent EW, Gupton SL, Gertler FB. The growth cone cytoskeleton in axon outgrowth and guidance. Cold Spring Harb Perspect Biol. 2011;3(3). doi: 10.1101/cshperspect.a001800. PubMed PMID: 21106647; PMCID: PMC3039926.

136. Suter DM, Forscher P. Substrate-cytoskeletal coupling as a mechanism for the regulation of growth cone motility and guidance. J Neurobiol. 2000;44(2):97-113. PubMed PMID: 10934315.

137. Lin CH, Forscher P. Growth cone advance is inversely proportional to retrograde F-actin flow. Neuron. 1995;14(4):763-71. doi: 10.1016/0896-6273(95)90220-1. PubMed PMID: 7536426.

138. McCormick LE, Gupton SL. Mechanistic advances in axon pathfinding. Curr Opin Cell Biol. 2020;63:11-9. Epub 20200108. doi: 10.1016/j.ceb.2019.12.003. PubMed PMID: 31927278; PMCID: PMC7247931.

139. Mitchison TJ, Cramer LP. Actin-based cell motility and cell locomotion. Cell. 1996;84(3):371-9. doi: 10.1016/s0092-8674(00)81281-7. PubMed PMID: 8608590.

140. Garcia-Del-Muro X, Lopez-Pousa A, Maurel J, Martin J, Martinez-Trufero J, Casado A, Gomez-Espana A, Fra J, Cruz J, Poveda A, Meana A, Pericay C, Cubedo R, Rubio J, De Juan A, Lainez N, Carrasco JA, de Andres R, Buesa JM, Spanish Group for Research on S. Randomized phase II study comparing gemcitabine plus dacarbazine versus dacarbazine alone in patients with previously treated soft tissue sarcoma: a Spanish Group for Research on Sarcomas study. J Clin Oncol. 2011;29(18):2528-33. Epub 2011/05/25. doi: 10.1200/JCO.2010.33.6107. PubMed PMID: 21606430.

141. Visel A, Thaller C, Eichele G. GenePaint.org: an atlas of gene expression patterns in the mouse embryo. Nucleic Acids Res. 2004;32(Database issue):D552-6. doi: 10.1093/nar/gkh029. PubMed PMID: 14681479; PMCID: PMC308763.

142. Binder LI, Frankfurter A, Rebhun LI. The distribution of tau in the mammalian central nervous system. J Cell Biol. 1985;101(4):1371-8. doi: 10.1083/jcb.101.4.1371. PubMed PMID: 3930508; PMCID: PMC2113928.

143. Agholme L, Lindström T, Kågedal K, Marcusson J, Hallbeck M. An in vitro model for neuroscience: differentiation of SH-SY5Y cells into cells with morphological and biochemical characteristics of mature neurons. J Alzheimers Dis. 2010;20(4):1069-82. doi: 10.3233/JAD-2010-091363. PubMed PMID: 20413890.

144. Dehmelt L, Nalbant P, Steffen W, Halpain S. A microtubule-based, dynein-dependent force induces local cell protrusions: Implications for neurite initiation. Brain Cell Biol. 2006;35(1):39-56. Epub 2007/10/18. doi: 10.1007/s11068-006-9001-0. PubMed PMID: 17940912.

145. Janke C, Bulinski JC. Post-translational regulation of the microtubule cytoskeleton: mechanisms and functions. Nat Rev Mol Cell Biol. 2011;12(12):773-86. Epub 20111116. doi: 10.1038/nrm3227. PubMed PMID: 22086369.

146. Encinas M, Iglesias M, Liu Y, Wang H, Muhaisen A, Ceña V, Gallego C, Comella JX. Sequential treatment of SH-SY5Y cells with retinoic acid and brain-derived neurotrophic factor gives rise to fully differentiated, neurotrophic factor-dependent, human neuron-like cells. J Neurochem. 2000;75(3):991-1003. doi: 10.1046/j.1471-4159.2000.0750991.x. PubMed PMID: 10936180.

147. Dotti CG, Sullivan CA, Banker GA. The establishment of polarity by hippocampal neurons in culture. J Neurosci. 1988;8(4):1454-68. Epub 1988/04/01. PubMed PMID: 3282038; PMCID: PMC6569279.

148. Schaefer AW, Kabir N, Forscher P. Filopodia and actin arcs guide the assembly and transport of two populations of microtubules with unique dynamic parameters in neuronal growth cones. J Cell Biol. 2002;158(1):139-52. doi: 10.1083/jcb.200203038. PubMed PMID: 12105186; PMCID: PMC2173029.

149. Perez F, Diamantopoulos GS, Stalder R, Kreis TE. CLIP-170 highlights growing microtubule ends in vivo. Cell. 1999;96(4):517-27. doi: 10.1016/s0092-8674(00)80656-x. PubMed PMID: 10052454.

150. Charras GT, Coughlin M, Mitchison TJ, Mahadevan L. Life and times of a cellular bleb. Biophys J. 2008;94(5):1836-53. Epub 2007/10/05. doi: 10.1529/biophysj.107.113605. PubMed PMID: 17921219; PMCID: PMC2242777.

151. Cunningham CC. Actin polymerization and intracellular solvent flow in cell surface blebbing. J Cell Biol. 1995;129(6):1589-99. doi: 10.1083/jcb.129.6.1589. PubMed PMID: 7790356; PMCID: PMC2291187.

152. Fackler OT, Grosse R. Cell motility through plasma membrane blebbing. J Cell Biol. 2008;181(6):879-84. doi: 10.1083/jcb.200802081. PubMed PMID: 18541702; PMCID: PMC2426937.

153. Chauhan BK, Lou M, Zheng Y, Lang RA. Balanced Rac1 and RhoA activities regulate cell shape and drive invagination morphogenesis in epithelia. Proc Natl Acad Sci U S A. 2011;108(45):18289-94. Epub 2011/10/20. doi: 10.1073/pnas.1108993108. PubMed PMID: 22021442; PMCID: PMC3215052.

154. Bang J, Jang M, Huh JH, Na JW, Shim M, Carlson BA, Tobe R, Tsuji PA, Gladyshev VN, Hatfield DL, Lee BJ. Deficiency of the 15-kDa selenoprotein led to cytoskeleton remodeling and non-apoptotic membrane blebbing through a RhoA/ROCK pathway. Biochem Biophys Res Commun. 2015;456(4):884-90. doi: 10.1016/j.bbrc.2014.12.059. PubMed PMID: 25529450; PMCID: PMC4758352.

155. Bridgman PC, Kachar B, Reese TS. The structure of cytoplasm in directly frozen cultured cells. II. Cytoplasmic domains associated with organelle movements. J Cell Biol. 1986;102(4):1510-21. doi: 10.1083/jcb.102.4.1510. PubMed PMID: 3514635; PMCID: PMC2114159.

156. Forscher P, Kaczmarek LK, Buchanan JA, Smith SJ. Cyclic AMP induces changes in distribution and transport of organelles within growth cones of Aplysia bag cell neurons. J Neurosci. 1987;7(11):3600-11. PubMed PMID: 2824715; PMCID: PMC6569040.

157. Weed SA, Du Y, Parsons JT. Translocation of cortactin to the cell periphery is mediated by the small GTPase Rac1. J Cell Sci. 1998;111 (Pt 16):2433-43. Epub 1998/07/31. PubMed PMID: 9683637.

158. Mizui T, Kojima N, Yamazaki H, Katayama M, Hanamura K, Shirao T. Drebrin E is involved in the regulation of axonal growth through actin-myosin interactions. J Neurochem. 2009;109(2):611-22. Epub 20090213. doi: 10.1111/j.1471-4159.2009.05993.x. PubMed PMID: 19222710.

159. Buck KB, Schaefer AW, Schoonderwoert VT, Creamer MS, Dufresne ER, Forscher P. Local Arp2/3-dependent actin assembly modulates applied traction force during apCAM adhesion site maturation. Mol Biol Cell. 2017;28(1):98-110. Epub 20161116. doi: 10.1091/mbc.E16-04-0228. PubMed PMID: 27852899; PMCID: PMC5221634.

160. Thompson C, Lin CH, Forscher P. An Aplysia cell adhesion molecule associated with site-directed actin filament assembly in neuronal growth cones. J Cell Sci. 1996;109 (Pt 12):2843-54. PubMed PMID: 9013332.

161. Rochlin MW, Dailey ME, Bridgman PC. Polymerizing microtubules activate site-directed F-actin assembly in nerve growth cones. Mol Biol Cell. 1999;10(7):2309-27. doi: 10.1091/mbc.10.7.2309. PubMed PMID: 10397767; PMCID: PMC25445.

162. Betz WJ, Mao F, Smith CB. Imaging exocytosis and endocytosis. Curr Opin Neurobiol. 1996;6(3):365-71. doi: 10.1016/s0959-4388(96)80121-8. PubMed PMID: 8794083.

163. Hinrichsen L, Harborth J, Andrees L, Weber K, Ungewickell EJ. Effect of clathrin heavy chain- and alpha-adaptin-specific small inhibitory RNAs on endocytic accessory proteins and receptor trafficking in HeLa cells. J Biol Chem. 2003;278(46):45160-70. doi: 10.1074/jbc.M307290200. PubMed PMID: 12960147.

164. Falcone S, Cocucci E, Podini P, Kirchhausen T, Clementi E, Meldolesi J. Macropinocytosis: regulated coordination of endocytic and exocytic membrane traffic events. J Cell Sci. 2006;119(Pt 22):4758-69. Epub 20061031. doi: 10.1242/jcs.03238. PubMed PMID: 17077125.

165. Rupper A, Lee K, Knecht D, Cardelli J. Sequential activities of phosphoinositide 3-kinase, PKB/Aakt, and Rab7 during macropinosome formation in Dictyostelium. Mol Biol Cell. 2001;12(9):2813-24. doi: 10.1091/mbc.12.9.2813. PubMed PMID: 11553719; PMCID: PMC59715.

166. Winckler B, Yap CC. Endocytosis and endosomes at the crossroads of regulating trafficking of axon outgrowth-modifying receptors. Traffic. 2011;12(9):1099-108. Epub 2011/05/23. doi: 10.1111/j.1600-0854.2011.01213.x. PubMed PMID: 21535338; PMCID: PMC3155643.

167. Scott-Solomon E, Kuruvilla R. Mechanisms of neurotrophin trafficking via Trk receptors. Mol Cell Neurosci. 2018;91:25-33. Epub 20180327. doi: 10.1016/j.mcn.2018.03.013. PubMed PMID: 29596897; PMCID: PMC6128733.

168. Bai Y, Xu J, Brahimi F, Zhuo Y, Sarunic MV, Saragovi HU. An agonistic TrkB mAb causes sustained TrkB activation, delays RGC death, and protects the retinal structure in optic nerve axotomy and in glaucoma. Invest Ophthalmol Vis Sci. 2010;51(9):4722-31. Epub 20100331. doi: 10.1167/iovs.09-5032. PubMed PMID: 20357199.

169. Bamba Y, Shofuda T, Kato M, Pooh RK, Tateishi Y, Takanashi J, Utsunomiya H, Sumida M, Kanematsu D, Suemizu H, Higuchi Y, Akamatsu W, Gallagher D, Miller FD, Yamasaki M, Kanemura Y, Okano H. In vitro characterization of neurite extension using induced pluripotent stem cells derived from lissencephaly patients with TUBA1A missense mutations. Mol Brain. 2016;9(1):70. Epub 2016/07/20. doi: 10.1186/s13041-016-0246-y. PubMed PMID: 27431206; PMCID: PMC4950778.

170. Kannan M, Bayam E, Wagner C, Rinaldi B, Kretz PF, Tilly P, Roos M, McGillewie L, Bar S, Minocha S, Chevalier C, Po C, Sanger Mouse Genetics P, Chelly J, Mandel JL, Borgatti R, Piton A, Kinnear C, Loos B, Adams DJ, Herault Y, Collins SC, Friant S, Godin JD, Yalcin B. WD40-repeat 47, a microtubule-associated protein, is essential for brain development and autophagy. Proc Natl Acad Sci U S A. 2017;114(44):E9308-E17. Epub 2017/10/29. doi: 10.1073/pnas.1713625114. PubMed PMID: 29078390; PMCID: PMC5676932.

171. Sadybekov A, Tian C, Arnesano C, Katritch V, Herring BE. An autism spectrum disorder-related de novo mutation hotspot discovered in the GEF1 domain of Trio. Nat Commun. 2017;8(1):601. Epub 20170919. doi: 10.1038/s41467-017-00472-0. PubMed PMID: 28928363; PMCID: PMC5605661.

172. Da Silva JS, Medina M, Zuliani C, Di Nardo A, Witke W, Dotti CG. RhoA/ROCK regulation of neuritogenesis via profilin IIa-mediated control of actin stability. J Cell Biol. 2003;162(7):1267-79. Epub 2003/10/01. doi: 10.1083/jcb.200304021. PubMed PMID: 14517206; PMCID: PMC2173969.

173. Hodge RG, Ridley AJ. Regulating Rho GTPases and their regulators. Nat Rev Mol Cell Biol. 2016;17(8):496-510. Epub 2016/06/15. doi: 10.1038/nrm.2016.67. PubMed PMID: 27301673.

174. Symons M, Rusk N. Control of vesicular trafficking by Rho GTPases. Curr Biol. 2003;13(10):R409-18. doi: 10.1016/s0960-9822(03)00324-5. PubMed PMID: 12747855.

175. Wilkinson S, Paterson HF, Marshall CJ. Cdc42-MRCK and Rho-ROCK signalling cooperate in myosin phosphorylation and cell invasion. Nat Cell Biol. 2005;7(3):255-61. Epub 2005/02/20. doi: 10.1038/ncb1230. PubMed PMID: 15723050.

176. Sanz-Moreno V, Gadea G, Ahn J, Paterson H, Marra P, Pinner S, Sahai E, Marshall CJ. Rac activation and inactivation control plasticity of tumor cell movement. Cell. 2008;135(3):510-23. doi: 10.1016/j.cell.2008.09.043. PubMed PMID: 18984162.

177. Catlett TS, Onesto MM, McCann AJ, Rempel SK, Glass J, Franz DN, Gómez TM. RHOA signaling defects result in impaired axon guidance in iPSC-derived neurons from patients

with tuberous sclerosis complex. Nat Commun. 2021;12(1):2589. Epub 20210510. doi: 10.1038/s41467-021-22770-4. PubMed PMID: 33972524; PMCID: PMC8110792.

178. Williamson T, Gordon-Weeks PR, Schachner M, Taylor J. Microtubule reorganization is obligatory for growth cone turning. Proc Natl Acad Sci U S A. 1996;93(26):15221-6. doi: 10.1073/pnas.93.26.15221. PubMed PMID: 8986791; PMCID: PMC26384.

179. Delcroix JD, Valletta JS, Wu C, Hunt SJ, Kowal AS, Mobley WC. NGF signaling in sensory neurons: evidence that early endosomes carry NGF retrograde signals. Neuron. 2003;39(1):69-84. doi: 10.1016/s0896-6273(03)00397-0. PubMed PMID: 12848933.

180. Medeiros NA, Burnette DT, Forscher P. Myosin II functions in actin-bundle turnover in neuronal growth cones. Nat Cell Biol. 2006;8(3):215-26. doi: 10.1038/ncb1367. PubMed PMID: 16501565.

181. Innocenti M. New insights into the formation and the function of lamellipodia and ruffles in mesenchymal cell migration. Cell Adh Migr. 2018;12(5):401-16. Epub 20180508. doi: 10.1080/19336918.2018.1448352. PubMed PMID: 29513145; PMCID: PMC6363039.

182. Schnoor M, Stradal TE, Rottner K. Cortactin: Cell Functions of A Multifaceted Actin-Binding Protein. Trends Cell Biol. 2018;28(2):79-98. Epub 20171120. doi: 10.1016/j.tcb.2017.10.009. PubMed PMID: 29162307.

183. Beattie EC, Howe CL, Wilde A, Brodsky FM, Mobley WC. NGF signals through TrkA to increase clathrin at the plasma membrane and enhance clathrin-mediated membrane trafficking. J Neurosci. 2000;20(19):7325-33. PubMed PMID: 11007890; PMCID: PMC6772792.

184. Middlemas DS, Meisenhelder J, Hunter T. Identification of TrkB autophosphorylation sites and evidence that phospholipase C-gamma 1 is a substrate of the TrkB receptor. J Biol Chem. 1994;269(7):5458-66. PubMed PMID: 8106527.

185. Kaplan DR, Miller FD. Neurotrophin signal transduction in the nervous system. Curr Opin Neurobiol. 2000;10(3):381-91. doi: 10.1016/s0959-4388(00)00092-1. PubMed PMID: 10851172.

186. Lai KO, Wong AS, Cheung MC, Xu P, Liang Z, Lok KC, Xie H, Palko ME, Yung WH, Tessarollo L, Cheung ZH, Ip NY. TrkB phosphorylation by Cdk5 is required for activity-dependent structural plasticity and spatial memory. Nat Neurosci. 2012;15(11):1506-15. Epub 20121014. doi: 10.1038/nn.3237. PubMed PMID: 23064382; PMCID: PMC7511999.

187. Calabrese B, Halpain S. Essential role for the PKC target MARCKS in maintaining dendritic spine morphology. Neuron. 2005;48(1):77-90. doi: 10.1016/j.neuron.2005.08.027. PubMed PMID: 16202710.

188. Hand R, Polleux F. Neurogenin2 regulates the initial axon guidance of cortical pyramidal neurons projecting medially to the corpus callosum. Neural Dev. 2011;6:30. Epub 20110824. doi: 10.1186/1749-8104-6-30. PubMed PMID: 21864333; PMCID: PMC3174110.

189. Calabrese B, Halpain S. Lithium prevents aberrant NMDA-induced F-actin reorganization in neurons. Neuroreport. 2014;25(17):1331-7. doi: 10.1097/WNR.0000000000000268. PubMed PMID: 25304495; PMCID: PMC4213241.

190. Courchet J, Lewis TL, Lee S, Courchet V, Liou DY, Aizawa S, Polleux F. Terminal axon branching is regulated by the LKB1-NUAK1 kinase pathway via presynaptic mitochondrial capture. Cell. 2013;153(7):1510-25. doi: 10.1016/j.cell.2013.05.021. PubMed PMID: 23791179; PMCID: PMC3729210.